

ROLE OF CHOLESTEROL 24-HYDROXYLASE IN HIPPOCAMPAL
LONG-TERM POTENTIATION

APPROVED BY SUPERVISORY COMMITTEE

David W. Russell, Ph. D.

Shmuel Muallem, Ph. D.

Kimberly M. Huber, Ph. D.

Steven G. Kernie, M. D.

Helen L. Yin, Ph. D.

DEDICATION

I would like to thank first and foremost my mentor, David Russell, for his unconditional support and guidance and for providing a superb environment for graduate study. Thanks also to my dissertation committee members for their helpful suggestions and discussions regarding my experiments as well as my career. I am incredibly grateful to my entire family for encouraging and supporting me throughout my education, but especially to my parents, Bob and Donna O'Donnell, who instilled in me the value of a good education and to always do my best. Finally, to my husband, Patrick – thanks for always being there for me, during college, graduate school, and in the future.

ROLE OF CHOLESTEROL 24-HYDROXYLASE IN HIPPOCAMPAL
LONG-TERM POTENTIATION

by

DENISE MARIE O'DONNELL RAMIREZ

DISSERTATION

Presented to the Faculty of the Graduate School of Biomedical Sciences

The University of Texas Southwestern Medical Center at Dallas

In Partial Fulfillment of the Requirements

For the Degree of

DOCTOR OF PHILOSOPHY

The University of Texas Southwestern Medical Center at Dallas

Dallas, Texas

April, 2009

ROLE OF CHOLESTEROL 24-HYDROXYLASE IN HIPPOCAMPAL
LONG-TERM POTENTIATION

Denise Marie O'Donnell Ramirez, Ph. D.

The University of Texas Southwestern Medical Center at Dallas, 2009

Supervising Professor: David W. Russell, Ph. D.

The mammalian brain contains a disproportionately large percentage of the body's cholesterol, steady-state levels of which are maintained within a narrow range to preserve membrane function. The brain is denied access to circulating lipoproteins by the blood-brain barrier and therefore relies on *de novo* cholesterol synthesis through the mevalonate pathway to meet the tissue's requirement for this essential lipid. A small amount of brain cholesterol is turned over daily in select neurons by cholesterol 24-hydroxylase, which catalyzes the production of the membrane-permeable oxysterol

24(*S*)-hydroxycholesterol and represents the major pathway of cholesterol catabolism in this organ. Mice lacking 24-hydroxylase have a decreased rate of brain cholesterol synthesis and exhibit deficiencies in spatial, associative, and motor learning. Hippocampal slices prepared from these mice are unable to support the induction of long-term potentiation, a type of synaptic strengthening thought to underlie learning and memory. The ability of 24-hydroxylase knockout slices to exhibit long-term potentiation can be restored by treatment with geranylgeraniol, an isoprenoid end-product of the mevalonate pathway. Mechanistic insight into the role of geranylgeraniol in long-term potentiation has been revealed by calcium imaging studies in neurons cultured from wild-type and 24-hydroxylase knockout embryos. Neurons from mice lacking 24-hydroxylase have specific defects in *N*-methyl-D-aspartate (NMDA) receptor function, a subtype of ionotropic glutamate receptor essential for long-term potentiation. The subunit composition of NMDA receptors located in various functional pools is normal in 24-hydroxylase knockout hippocampus, suggesting that geranylgeraniol does not affect expression of NMDA receptors. Localization studies of 24-hydroxylase show the enzyme is predominantly expressed in the endoplasmic reticulum throughout the soma and dendrites of selected hippocampal, cerebellar, and cortical neurons, consistent with a postsynaptic need for cholesterol turnover in neurons of brain regions important for learning and memory. These findings reveal that cholesterol turnover is important to produce a constant supply of geranylgeraniol, which in turn is necessary for the induction of long-term potentiation and presumably learning in mice.

TABLE OF CONTENTS

ABSTRACT	iv
TABLE OF CONTENTS	vi
PRIOR PUBLICATIONS	viii
LIST OF FIGURES AND TABLES	ix
LIST OF ABBREVIATIONS	xii
CHAPTER 1 INTRODUCTION	1
CHAPTER 2 NEURONAL EXPRESSION AND SUBCELLULAR LOCALIZATION OF CHOLESTEROL 24-HYDROXYLASE IN THE MOUSE BRAIN	27
A. INTRODUCTION	
B. MATERIALS AND METHODS	
C. RESULTS	
D. DISCUSSION	
E. TABLES AND FIGURES	
CHAPTER 3 BRAIN CHOLESTEROL TURNOVER REQUIRED FOR GERANYLGERANIOL PRODUCTION AND LEARNING IN MICE	93
A. INTRODUCTION	
B. MATERIALS AND METHODS	
C. RESULTS	
D. DISCUSSION	
E. FIGURES	
CHAPTER 4 ROLE OF GERANYLGERANIOL IN <i>N</i> -METHYL-D-ASPARTATE RECEPTOR FUNCTION	131
A. INTRODUCTION	
B. MATERIALS AND METHODS	
C. RESULTS	
D. DISCUSSION	
E. FIGURES	
CHAPTER 5 CONCLUDING REMARKS	171

BIBLIOGRAPHY 178

PRIOR PUBLICATIONS

Jo M, Thomas KS, **O'Donnell DM**, Gonias SL. (2003) Epidermal growth factor receptor-dependent and -independent cell-signaling pathways originating from the urokinase receptor. J Biol Chem 278:1642-6.

Kotti TJ, **Ramirez DM**, Pfeiffer BE, Huber KM, Russell DW. (2006) Brain cholesterol turnover required for geranylgeraniol production and learning in mice. PNAS 103:3869-74.

Yildiz Y, Matern H, Thompson B, Allegood JC, Warren RL, **Ramirez DM**, Hammer RE, Hamra FK, Matern S, Russell DW. (2006) Mutation of mouse bile acid β -glucosidase gene (*Gba2*) causes glycolipid storage disease and impaired male fertility. J Clin Invest 116: 2985-94.

Ramirez DM, Andersson S, Russell DW. (2008) Neuronal expression and subcellular localization of cholesterol 24-hydroxylase in the mouse brain. J Comp Neurol 507: 1676-93.

Russell DW, Halford RW, **Ramirez DM**, Shah R, Kotti T. (2009) Cholesterol 24-hydroxylase: an enzyme of cholesterol turnover in the brain. Annu Rev Biochem 78: in press.

LIST OF FIGURES AND TABLES

CHAPTER 1

FIGURE 1 – Schematic of the mevalonate pathway	18
FIGURE 2 – Ontogeny of brain cholesterol synthesis and accumulation in the mouse ..	20
FIGURE 3 – Conversion of cholesterol to 24(<i>S</i>)-hydroxycholesterol by cholesterol 24-hydroxylase (CYP46A1)	22
FIGURE 4 – Examples of <i>N</i> -methyl-D-aspartate receptor heterotetramer assembly.....	24
FIGURE 5 – Molecular processes involved in long-term potentiation of excitatory synaptic transmission	26

CHAPTER 2

TABLE 1 – Antibodies used in this study	64
TABLE 2 – Average Pearson correlation coefficients.....	68
FIGURE 1 – Assessment of monoclonal antibody specificity.....	70
FIGURE 2 – Assessment of anti-P450 reductase antiserum specificity and P450 reductase distribution in wild-type and 24-hydroxylase knockout brain ...	72
FIGURE 3 – Localization of 24-hydroxylase in transfected cells by immunofluorescence	74
FIGURE 4 – Localization of 24-hydroxylase in cultured neurons by immunofluorescence	76
FIGURE 5 – Coexpression of 24-hydroxylase with dendritic MAP2 but not presynaptic Rab3A in cultured neurons	78

FIGURE 6 – Colocalization of 24-hydroxylase with a known endoplasmic reticulum protein in cultured neurons	80
FIGURE 7 – 24-hydroxylase is expressed in the endoplasmic reticulum	82
FIGURE 8 – Expression of 24-hydroxylase in the hippocampus	84
FIGURE 9 – Expression of 24-hydroxylase in the cerebellum.....	86
FIGURE 10 – Expression of P450 reductase in the cerebellum	88
FIGURE 11 – Expression of 24-hydroxylase in the cortex	90
FIGURE 12 – Expression of 24-hydroxylase in the retina	92

CHAPTER 3

FIGURE 1 – Schematic of the mevalonate pathway	114
FIGURE 2 – Assessment of behavioral learning	116
FIGURE 3 – Histology and protein expression in the hippocampus	118
FIGURE 4 – Synaptic transmission in wild-type and 24-hydroxylase knockout mice .	120
FIGURE 5 – Impaired hippocampal LTP and normal LTD in 24-hydroxylase knockout mice.....	122
FIGURE 6 – Restoration of LTP by mevalonate and isoprenoids.....	124
FIGURE 7 – LTP deficit persists in the absence of γ -aminobutyric acid type A (GABA _A) receptor-mediated inhibition	126
FIGURE 8 – Absence of liver X receptor (LXR) effects in LTP	128
FIGURE 9 – Quantitation of statin, mevalonate, and geranylgeraniol effects on LTP .	130

CHAPTER 4

FIGURE 1 – Calcium channel activity in neurons cultured from wild-type and 24-hydroxylase knockout embryos	158
FIGURE 2 – 24-hydroxylase knockout neurons exhibit subtype-specific defects in NMDAR function	160
FIGURE 3 – Geranylgeraniol treatment normalizes functional NR2A/NR2B ratio in 24-hydroxylase knockout neurons	162
FIGURE 4 – Calcium influx through NMDA receptor has an extracellular origin	164
FIGURE 5 – Measurement of synaptic NMDAR levels in wild-type and 24-hydroxylase knockout hippocampal synaptoneurosome.....	166
FIGURE 6 – Measurement of synaptic NMDAR levels in wild-type and 24-hydroxylase knockout hippocampal Triton X-100-soluble and –insoluble fractions...	168
FIGURE 7 – Surface NMDAR subunit levels in wild-type and 24-hydroxylase knockout hippocampal slices	170

LIST OF ABBREVIATIONS

- 24(*S*)-hydroxycholesterol – 5-cholesten-3 β ,24-diol
- ACSF – artificial cerebrospinal fluid
- AMPA – α -amino-3-hydroxy-5-methyl-4-isoxazole propionic acid
- AMPAR – AMPA receptor
- AP5 – D(-)-2-amino-5-phosphonopentanoic acid
- AraC – cytosine β -D-arabinofuranoside
- ATP – adenosine triphosphate
- b5 reductase – NADPH-cytochrome b5 reductase
- BAPTA – 1,2-bis(*o*-aminophenoxy)ethane-N,N,N',N'-tetraacetic acid
- BCA – bicinchoninic acid
- BLBP – brain lipid binding protein
- BSA – bovine serum albumin
- CA1 – cornu ammonis 1 of the hippocampus
- CA3 – cornu ammonis 3 of the hippocampus
- CHO-K1 – Chinese hamster ovary K1 cells
- Cholesterol – 5-cholesten-3 β -ol
- CNQX – 6-cyano-7-nitroquinoxaline-2,3-dione
- CoA – acyl-coenzyme A
- CYP – cytochrome P450
- CYP7A1 – cholesterol 7 α -hydroxylase
- CYP27A1 – sterol 27-hydroxylase

CYP46A1 – cholesterol 24-hydroxylase

DAB – diaminobenzidine

DAPI – 4',6-diamidino-2-phenylindole

DG – dentate gyrus of the hippocampus

DMEM – Dulbecco's modified Eagle's medium

DNA – deoxyribonucleic acid

E16 – embryonic day 16

EDTA – ethylenediaminetetraacetic acid

ELISA – enzyme-linked immunosorbent assay

EPSP – excitatory postsynaptic potential

ER – endoplasmic reticulum

GABA – γ -aminobutyric acid

GAD67 – glutamic acid decarboxylase of 67 kDa

GCL – ganglion cell layer

GG – geranylgeraniol

GluR – AMPA receptor subunit

GM130 – Golgi matrix protein of 130 kDa

GTP – guanosine triphosphate

HBSS – Hank's balanced salt solution

HEK-293 – human embryonic kidney 293 cells

HEPES – 4-(2-Hydroxyethyl)piperazine-1-ethanesulfonic acid

HMG – 3-hydroxy-3-methylglutaryl

HRP – horseradish peroxidase

INL – inner nuclear layer

IP3R – inositol 1,4,5-trisphosphate receptor

KO – knockout

LTD – long-term depression

LTP – long-term potentiation

LXR – liver X receptor

M6PR – mannose-6-phosphate receptor

MAP2 – microtubule associated protein 2

MnSOD – manganous superoxide dismutase

mRNA – messenger ribonucleic acid

MWM – Morris water maze

NGS – normal goat serum

NMDA – *N*-methyl-D-aspartate

NMDAR – NMDA receptor

NR – NMDA receptor subunit

NVP – NVP-AAM077; NR2A antagonist

OCT – optimal cutting temperature cryopreservation medium

P450 reductase – NADPH-cytochrome P450 oxidoreductase

PBS – phosphate-buffered saline

PDI – protein disulfide isomerase

PCR – polymerase chain reaction

PP – diphosphate

PPF – paired-pulse facilitation

PSD – postsynaptic density

QX-314 – N-(2,6-dimethylphenylcarbamoylmethyl triethylammonium bromide

RPE – retinal pigmented epithelium

RIPA – radioimmune precipitation buffer

SDS – sodium docecyl sulfate

SEM – standard error of the mean

SERCA – sarco-endoplasmic reticulum calcium ATPase

TA – tris-acetate

TBS – theta burst stimulation

TTX – tetrodotoxin

TxS – Triton-X-100 soluble presynaptic fraction

TxP – Triton-X-100 insoluble postsynaptic fraction

VGCC – voltage-gated calcium channel

CHAPTER 1

Introduction

Brain cholesterol metabolism in mammals

Cholesterol is an essential constituent of the plasma membrane in all mammalian cells, and represents about 20-25% of the lipid in this cellular structure (Dietschy and Turley, 2004). Cholesterol regulates the fluidity of the plasma membrane and, in so doing, can affect the activity of membrane-embedded proteins such as ion channels and G-protein coupled receptors (McIntosh and Simon, 2006). For example, channel conductivity of the nicotinic acetylcholine receptor and allosteric modulation of the γ -aminobutyric acid (GABA) type A receptor ion channels are modulated by membrane cholesterol content. Similarly, the activity and stability of rhodopsin as well as various functional properties of β -adrenergic receptors, both of which are G-protein coupled, are affected by cholesterol (Pucadyil and Chattopadhyay, 2006). Interestingly, the fact that many of these proteins are neurotransmitter receptors (Kandel, 1991) is perhaps a function of the unique role of cholesterol in the central nervous system, as will be discussed below.

Mammalian cells obtain cholesterol primarily by *de novo* synthesis from acetate, or by receptor-mediated endocytosis of extracellular cholesterol contained in circulating lipoproteins. The pathway by which cells produce sterols as well as various nonsterol isoprenoids is known as the mevalonate pathway and is comprised of ~35 enzymes (Figure 1). This pathway is regulated by feedback inhibition at multiple levels of the rate-limiting step, the conversion of 3-hydroxy-3-methylglutaryl (HMG)-CoA to

mevalonate (Espenshade and Hughes, 2007; Goldstein and Brown, 1990; Horton et al., 2002). This reaction is catalyzed by the enzyme HMG-CoA reductase, which is competitively inhibited by the statin class of cholesterol-lowering drugs (Endo, 1992). Multiple tightly controlled regulatory processes ensure continuous availability of nonsterol isoprenoids, which are necessary for a variety of cellular processes, and prevent the excess accumulation of sterols, which can be toxic to cells (Goldstein and Brown, 1990).

The brain contains the highest cholesterol concentration of any mammalian organ; a trend which is evolutionarily conserved from mice to humans. Brain cholesterol is predominantly unesterified and forms two functionally distinct pools (Dietschy and Turley, 2004). The majority of brain cholesterol (~70% in rodents) is found in the myelin sheaths that surround and insulate neuronal axons, whereas a smaller fraction (~30%) is found in the plasma membranes of neurons and glial cells (Davidson, 1965). Proper brain cholesterol levels are crucial to maintain the insulatory properties of myelin; therefore, the brain has evolved specialized mechanisms to keep the cholesterol pool size constant (Bjorkhem, 2006; Dietschy and Turley, 2004). To this end, brain cholesterol is isolated from other pools of cholesterol in the body by the blood-brain barrier, which prevents access to circulating lipoproteins. In contrast to other organs in the periphery, the brain obtains cholesterol solely from *de novo* synthesis through the mevalonate pathway (Bjorkhem, 2006; Dietschy and Turley, 2004).

The ontogeny of brain cholesterol metabolism has been studied in the mouse; steady-state cholesterol levels rise quickly during the transition from neonates to young mice, especially during the first 1-4 weeks of life when myelin is formed. Cholesterol

levels reach a peak by about 13 weeks of age and are maintained in the adult animal. Conversely, rates of cholesterol synthesis exhibit a sharp peak between 1-4 weeks of age, presumably to accommodate myelin formation, and then level off in adult animals, although a low level of cholesterol synthesis continues (Figure 2) (Quan et al., 2003). The fact that continued cholesterol synthesis in the brains of adult animals does not cause an increase in steady-state cholesterol levels in this organ suggests that a mechanism for brain cholesterol excretion must exist (Bjorkhem, 2006; Dietschy and Turley, 2004).

Available evidence implicated the production of oxysterols, oxygenated cholesterol metabolites, as a means of cholesterol excretion from the central nervous system. In particular, the side-chain oxidized compound 24(*S*)-hydroxycholesterol was thought to be involved for several reasons. First, cholesterol 24-hydroxylase activity had been demonstrated in the brain and cultured neurons (Bjorkhem et al., 1997; Zhang et al., 1997). Second, 24(*S*)-hydroxycholesterol was detected in human and mouse brains at levels higher than in any other organ (Lund et al., 2003; Lutjohann et al., 1996; Smith et al., 1972). Third, side-chain oxidized oxysterols including 24(*S*)-hydroxycholesterol can pass through lipophilic membranes up to three times faster than cholesterol itself, without the need for energy-dependent transport (Lange et al., 1995; Meaney et al., 2002). Finally, a net efflux of 24(*S*)-hydroxycholesterol from the brain into the circulation was demonstrated in human subjects (Bjorkhem et al., 1998; Lutjohann et al., 1996). These results suggested conversion of cholesterol to 24(*S*)-hydroxycholesterol and its subsequent passage through the blood-brain barrier to the circulation could be an important pathway for brain cholesterol turnover.

Metabolism of cholesterol to 24(*S*)-hydroxycholesterol by cholesterol 24-hydroxylase, a member of the cytochrome P450 family of enzymes (CYP46A1), was confirmed to represent the major pathway by which cholesterol is excreted from the brain by the production of a knockout mouse with constitutive deletion of the *Cyp46a1* gene (Lund et al., 2003). The reaction catalyzed by this enzyme is shown in Figure 3. Earlier studies quantified the relative rates of brain 24(*S*)-hydroxycholesterol and cholesterol synthesis using $^{18}\text{O}_2$ inhalation in rats, and showed that approximately 2/3 of brain cholesterol synthesis is counter-balanced by conversion to 24(*S*)-hydroxycholesterol (Bjorkhem, 2006; Bjorkhem et al., 1997). Consistent with these results, 24-hydroxylase knockout mice display ~50% decreases in rates of brain cholesterol synthesis, but no changes in the steady-state cholesterol pool size in this or any other organ. Therefore, the brains of these mutant animals compensate for a reduced ability to excrete cholesterol by decreasing cholesterol synthesis by a similar amount to maintain the correct pool size, presumably to preserve myelin function (Lund et al., 2003). In accordance with this idea, 24-hydroxylase knockout mice have normal brain development and no defects in myelination (Lund et al., 2003; T. Kotti, unpublished observations). By analogy to previous studies in cultured cells and tissues, localized cholesterol accumulation in the brain cells of 24-hydroxylase knockout mice activates feedback inhibition of HMG-CoA reductase and suppresses the mevalonate pathway (Figure 1) (Espenshade and Hughes, 2007; Horton et al., 2002). This buildup is transient and the associated negative regulation is acute; thus, an increase in cholesterol is not detected in steady-state measurements. These results confirm that approximately half of brain cholesterol turnover is due to formation of 24(*S*)-hydroxycholesterol by 24-hydroxylase. In

agreement with the exclusive expression of this enzyme in the brain (Lund et al., 1999), 24-hydroxylase knockout mice show normal lipoprotein profiles in the plasma and normal fecal sterol excretion (Lund et al., 2003).

In addition to the nearly exclusive presence of 24-hydroxylase in the brain, the enzyme appears to exhibit a specific cellular distribution, with expression in neurons but not in glial cells. Initial studies of the 24-hydroxylase mRNA and protein distribution in mouse brain slices show the enzyme is highly expressed in a subset of neurons, including large, metabolically active neurons such as pyramidal cells of the hippocampus and cortex, and Purkinje cells of the cerebellum (Lund et al., 1999). This pattern has been confirmed by extensive mRNA *in situ* hybridization surveys by the Allen Brain Institute (www.brain-map.org). Therefore, cholesterol excreted from the brain as 24(S)-hydroxycholesterol (0.9 mg/day/kg in the mouse) represents cholesterol turnover in a small subset of highly metabolically active neurons and implies a role for cholesterol metabolism in the functions of these specific neurons. In contrast, although glial cells constitute $\geq 90\%$ of cells in the brain, and together with oligodendrocyte-derived myelin sheaths, their plasma membranes represent the bulk of brain cholesterol, the rate of cholesterol turnover in this pool is calculated to be much lower (Xie et al., 2003). Consistent with these data, decreased rates of regional brain cholesterol turnover are more pronounced in 24-hydroxylase knockout brain regions rich in gray matter, such as the hippocampus and cortex, compared to those rich in myelin, e.g., the spinal cord (Xie et al., 2003 and R. Warren, unpublished observations). Collectively, these data support an important function for cholesterol turnover in specific neurons of the adult brain.

Other cytochromes P450 that metabolize cholesterol (e.g., CYP27A1; sterol 27-hydroxylase and CYP7A1; cholesterol 7 α -hydroxylase) are apparently not involved in brain cholesterol metabolism, as shown by measurements of brain cholesterol levels and synthesis in *Cyp27a1* and *Cyp7a1* knockout mice; these metabolic parameters are identical to those in wild-type animals. These results are consistent with the predominant expression of both CYP27A1 and CYP7A1 mRNA in the liver and their absence from the brain (Xie et al., 2003). The deletion of various genes expressing proteins involved in cholesterol transport across membranes (e.g., ATP-binding cassette A1 transporter, scavenger receptor B1, or low-density lipoprotein receptor) or in the plasma (e.g., apolipoproteins E and A1) also has no effect on either brain cholesterol pool size or synthesis in these mutant mice (Quan et al., 2003). The above-referenced studies eliminate many possibilities for additional pathways of brain cholesterol excretion necessary to fully balance the continued cholesterol synthesis in adult brains. Additional cholesterol metabolites, or perhaps cholesterol itself, may be excreted from the brain by as yet unknown mechanisms and may be derived from glial cells or myelin, in contrast to 24(*S*)-hydroxycholesterol produced by neurons (Dietschy and Turley, 2004; Xie et al., 2003).

Molecular mechanisms of learning and memory

Classic studies of human patients with hippocampal lesions demonstrated that the hippocampus, a part of the limbic system, is an important brain region for learning and memory formation (Kandel, 1991). As exemplified by patient “H. M.”, who underwent complete hippocampal removal for treatment of debilitating seizures, humans with

hippocampal damage suffer loss of the ability to form new declarative memories of facts, names, places, and personal experiences as well as defects in spatial learning. Defective spatial learning has been consistently demonstrated in rodents with hippocampal lesions, which, together with their genetic tractability, suggests that these animals are a good model to study hippocampal-dependent learning and the associated molecular bases in a more detailed manner (Rudy, 2008; Sweatt, 2003).

Spatial learning in rodents is tested by a variety of behavioral learning paradigms, such as the Morris water maze (MWM). Initially described in 1984 (Morris, 1984), this task has now become a preferred method to assess spatial learning in rodents. This task has been shown to depend on the hippocampus in both mice and rats (Schimanski and Nguyen, 2004). The MWM task requires rodents to learn the location of a hidden platform in order to escape a pool of water. The animal is placed into the pool on successive days, and visual cues such as pictures placed at intervals around the pool allow the animal to learn to navigate in the water to reach the hidden platform. A rodent with normal hippocampal function will learn, over a period of several such trials, to swim to the platform and escape the water. A rodent that is unable to utilize the visual cues for spatial navigation due to abnormal hippocampal function will exhibit longer periods of swimming before it reaches the platform, which is known as an increased escape latency (Schimanski and Nguyen, 2004; Sweatt, 2003).

A second type of paradigm used to test learning in rodents is fear conditioning, which is a type of associative learning. These tasks measure the ability of a rodent to learn and remember an association between either a specific environment or an auditory tone and a foot shock, which are referred to as contextual or cued fear conditioning,

respectively. Fear conditioning tasks exploit the natural tendency of rodents to exhibit freezing behavior in the presence of a fearful stimulus. While both contextual and cued fear conditioning tests depend on proper function of the amygdala, contextual fear conditioning is also sensitive to hippocampal lesions. In the contextual fear conditioning test, an animal that has made the connection between a particular environment (context) and a shock will exhibit increased freezing behavior relative to an animal that has not learned that connection due to disruptions in hippocampal or amygdalar function. Similarly, in the cued fear conditioning test, an association learned between a tone (cue) and the shock will produce increased freezing behavior in an animal with normal amygdalar function (Schimanski and Nguyen, 2004; Sweatt, 2003).

In order for memories to be retained briefly in the hippocampus or for long-term storage in the cortex, enduring changes in neuronal function must occur. As postulated in 1949 by Hebb, the cellular basis for learning and memory consists of a “growth process or metabolic change” that occurs in one or both neurons constituting a particular synapse after persistent neuronal activity (Hebb, 1949). The ability of neurons to undergo changes in the strength of synaptic connections is known as synaptic plasticity. While spatial learning tasks are useful to measure rodent hippocampal function, electrophysiological studies are more amenable to analyses of specific changes in neuronal function and thus the identification of potential cellular mechanisms underlying learning and memory (Rudy, 2008; Sweatt, 2003). The idea that synaptic plasticity subsequent to learning-induced neuronal activity could underlie learning and memory formation was reinforced by the seminal work of Bliss and Lomo, who first described a long-lasting form of synaptic plasticity induced by high-frequency stimulation in the

hippocampi of anesthetized rabbits (Bliss and Lomo, 1973). This phenomenon, which they called “long-term potentiation” (LTP) of synaptic transmission met two criteria for a potential mechanism to encode memory formation. First, a long-term change occurred in neuronal function; in their experiments potentiation lasted at least 3 hours. Secondly, the change was elicited by a brief period of unique electrical stimulation, similar to what would be expected when a new memory is formed.

Excitatory neuronal transmission is potentiated during LTP. Glutamate is the major excitatory neurotransmitter in the brain, and binds to both ligand-gated ion channels and metabotropic receptors found on postsynaptic dendritic spines. The major ionotropic glutamate receptors are the α -amino-3-hydroxy-5-methyl-4-isoxazole propionic acid (AMPA) and *N*-methyl-D-aspartate (NMDA) receptors. NMDA and AMPA receptors mediate LTP and other forms of synaptic plasticity such as long-term depression (LTD). Both types of receptor are heterotetrameric complexes formed from the assembly of different pools of subunits. AMPA receptors are composed of subunits designated GluR1-4 and most AMPARs in the adult forebrain are composed of GluR1/GluR2 diheteromers or GluR2/GluR3 diheteromers. NMDA receptors are assembled as dimers of dimers consisting of two obligatory NR1 subunits and either two NR2A-D or two NR3A-B subunits (Genoux and Montgomery, 2007; Kohr, 2006; Lau and Zukin, 2007; Malinow and Malenka, 2002; Rudy, 2008) . A diagram showing typical NMDAR assembly is shown in Figure 4. NMDARs can contain a number of different NR2 subunits, based on developmental time point and tissue distribution. For example, NR1/NR2A and NR1/NR2B diheteromeric receptors are prominently expressed in the adult forebrain, although NR1/NR2A/NR2B triheteromeric receptors have been

reported to constitute a substantial percentage of total NMDARs in this brain region (Al-Hallaq et al., 2007; Stephenson, 2001; Tovar and Westbrook, 1999). A developmental shift in the NR2A/NR2B ratio occurs in rodents, as the low neonatal NR2A/NR2B ratios switch to the higher NR2A/NR2B ratios seen in adult brains. NR2B is highly expressed neonatally, whereas NR2A begins to be expressed at about 1-2 weeks of age and continues to be highly expressed in the adult (Petralia et al., 2005; Sheng et al., 1994; Tovar and Westbrook, 1999). NR2C containing receptors are restricted to the cerebellum, and the NR2D subunit is predominantly expressed during early developmental stages (Ritter et al., 2002; Stephenson, 2001). The subunit composition of both AMPARs and NMDARs has profound consequences on the biophysical properties and subcellular localization of these receptors and is exploited during LTP, as discussed below.

A large body of literature dating from Bliss and Lomo's original work up to the present describes LTP and related forms of synaptic plasticity such as LTD in the hippocampus and other brain regions including the cortex and amygdala (Nakazawa et al., 2006; Yashiro and Philpot, 2008). Perhaps the most widely studied hippocampal synaptic connections are those between the Schaffer collateral axons emanating from area CA3 and their postsynaptic targets, the pyramidal cells of area CA1 (Sweatt, 2003). LTP and LTD induction at CA3-CA1 synapses are known to be dependent on the NMDA subtype of ionotropic glutamate receptors, whereas the mechanism by which LTP is maintained after induction requires increased function of AMPA receptors. In contrast, LTD results in a weakening of synaptic strength mediated by decreased function of AMPARs. Briefly, LTP is a multi-step process that occurs when 1) presynaptically

released glutamate binds postsynaptic NMDA and AMPA receptors, 2) AMPARs mediate postsynaptic depolarization by allowing influx of sodium ions, 3) the magnesium blockade of NMDARs at resting potential is relieved by depolarization, 4) calcium enters through NMDARs and acts as a second messenger, and 5) AMPAR function is increased, thereby potentiating responses at stimulated synapses (Rudy, 2008; Sweatt, 2003). This process is shown in schematic form in Figure 5. The well-supported hypothesis that LTP is mediated by postsynaptic mechanisms and ultimately by increased AMPAR function (the “silent synapse” hypothesis) has taken precedence over earlier work suggesting the possibility of presynaptic mechanisms and is now essentially universally accepted (Kerchner and Nicoll, 2008).

NMDARs are required for LTP induction by virtue of an ability to coincidentally detect presynaptic glutamate release and postsynaptic depolarization due to a complete magnesium block at resting membrane potentials, as well as a high permeability to calcium, increased levels of which are essential for the generation of LTP (Kohr, 2006; Rudy, 2008; Sweatt, 2003; Yashiro and Philpot, 2008). NMDARs of different subunit composition possess unique biophysical, pharmacological, developmental expression and possibly subcellular localization properties that are important for determining the direction of synaptic plasticity (LTP or LTD) (Erreger et al., 2005; Sheng et al., 1994; Tovar and Westbrook, 1999; Yashiro and Philpot, 2008). NR2A containing receptors have faster channel kinetics, higher open probabilities, and higher peak currents, whereas the presence of NR2B subunits confers slower channel kinetics, lower open probabilities, and lower peak currents. In general, since NR2B containing receptors deactivate more slowly, this subtype allows for a greater charge transfer of calcium compared to NR2A

containing receptors. Therefore, a predominance of NR2B-containing receptors at the synapse is postulated to promote induction of LTP (Yashiro and Philpot, 2008). Indeed, many studies show that NR2B is required or involved in LTP, but not necessary for LTD (Barria and Malinow, 2005; Bartlett et al., 2007; Gardoni et al., 2009; Morishita et al., 2007). Furthermore, mice overexpressing NR2B have increased hippocampal LTP (Tang et al., 1999). However, a patch-clamp study of recombinant NR1/NR2A and NR1/NR2B receptors shows that simulated high-frequency stimulation patterns used to produce LTP should result in greater charge transfer through NR2A. In contrast, simulated low-frequency stimulation used to induce LTD should allow greater charge transfer through NR2B. These data suggest NR2A may promote LTP and NR2B may promote LTD under physiological conditions (Erreger et al., 2005). Many electrophysiological studies using subtype-specific pharmacological agents and mutant mice support this alternative idea (Kutsuwada et al., 1996; Liu et al., 2004; Massey et al., 2004; Sakimura et al., 1995; Sprengel et al., 1998), which is consistent with the developmental regulation of NR2A subunit expression (Sheng et al., 1994). Finally, although earlier studies proposed that NR2A subunits predominate at synapses while NR2Bs are predominantly extrasynaptic (Li et al., 2002; Tovar and Westbrook, 1999), more recent work has shown the presence of similarly composed receptors in both subcellular compartments (Harris and Pettit, 2007). The surface mobility of NR2B subunits is greater than NR2As, which would be expected to influence their relative synaptic contribution (Groc et al., 2006) and presumably the expression of synaptic plasticity. It seems likely that eventually both hippocampal NMDAR subtypes will be shown to be involved in both types of synaptic plasticity.

Calcium is the master regulator of LTP induction and maintenance. Postsynaptic calcium influx through NMDAR triggers downstream processes such as kinase activation and AMPAR phosphorylation, resulting in increased AMPAR function and the expression of LTP, most notably through insertion of GluR1/2 heteromeric AMPARs into postsynaptic membranes (Malinow and Malenka, 2002; Man et al., 2007; Oh et al., 2006), but increased AMPAR channel conductance as a result of phosphorylation may also contribute to this process (Derkach, 2003; Rudy, 2008). Further increases in postsynaptic calcium during LTP result from the temporary insertion of calcium-permeable GluR1 homomeric AMPARs into the postsynaptic membrane, increases in voltage-gated calcium channel (VGCC) activity, and the release of calcium from ER stores (Biou et al., 2008; Plant et al., 2006; Raymond and Redman, 2002; 2006). In addition to the well-established role of AMPAR insertion into the postsynaptic membrane as a means to increase synaptic strength during LTP, activity-dependent NMDAR membrane insertion or redistribution to the synapse from extrasynaptic sites and changes in NMDAR subunit composition are implicated in this process (Bellone and Nicoll, 2007; Grosshans et al., 2002; Harris and Pettit, 2008; Lan et al., 2001; Lau and Zukin, 2007; Quinlan et al., 1999; Tovar and Westbrook, 2002; Yashiro and Philpot, 2008). Other processes downstream of LTP induction that are thought to be involved in the expression of this form of synaptic plasticity include changes in spine morphology and size (Kopec and Malinow, 2006; Kopec et al., 2006; Park et al., 2006).

Although LTP and other forms of synaptic plasticity have emerged as probable mechanisms involved in learning and memory formation, we must remember that LTP measurements are generally conducted in artificial preparations of brain slices maintained

in vitro. These slices are subjected to various patterns of high-frequency electrical stimulation that may or may not recapitulate endogenous patterns of neural activity produced by learning in an intact animal (Rudy, 2008; Sweatt, 2003). The use of theta-burst stimulation (TBS) may better reflect physiological activity in the hippocampus, as this protocol is based on the increased rate of firing exhibited by hippocampal pyramidal neurons that occurs when a rodent is exploring a novel environment, known as the theta rhythm (Rudy, 2008; Sweatt, 2003; Winston, 1978). Decades after the phenomenon's discovery, LTP has now been demonstrated to occur as a result of actual learning. Recent studies show that behavioral learning produces LTP of synaptic transmission in the hippocampus of both mice and rats (Gruart et al., 2006; Whitlock et al., 2006). Furthermore, *in vivo* studies of learning-induced glutamate receptor phosphorylation and trafficking show that biochemical changes which occur in the hippocampus are similar to those documented after LTP induction *in vitro* (Shukla et al., 2007; Whitlock et al., 2006; Williams et al., 2007). These results confirm a fundamental role of LTP in at least some types of hippocampal-dependent learning.

Role of cholesterol in synaptic transmission and LTP

Cholesterol is implicated in a variety of processes, both pre- and postsynaptic, relating to synaptic transmission and therefore potentially involved in LTP. Many studies focus on the role of cholesterol in lipid raft formation, where the sterol is known to be an essential constituent of these membrane microdomains. Lipid rafts are abundant in both neurons and glia and are important for many brain functions, including membrane trafficking, regulated intermembrane proteolysis, and signal transduction (Korade and

Kenworthy, 2008). Lipid rafts appear to be important for controlling neurotransmission due to an ability to cluster postsynaptic receptors. Both NMDARs and AMPARs are known to associate with lipid rafts on postsynaptic dendrites. Acute cholesterol depletion disrupts lipid rafts and surface glutamate receptor stability, which causes removal of the receptors from rafts and, in the case of NMDARs, protects neurons from excitotoxicity (Hering et al., 2003; Ponce et al., 2008). On the presynaptic side, cholesterol modulates the balance between evoked and spontaneous synaptic vesicle recycling and serves to prevent spontaneous neurotransmitter vesicle fusion when neurons are at rest (Wasser et al., 2007). This role is consistent with a report of altered paired-pulse facilitation (PPF) ratios in hippocampal slices treated with cyclodextrin, a water-soluble oligosaccharide capable of extracting a majority of cholesterol from plasma membranes (Koudinov and Koudinova, 2001); however, other more recent studies describe no effect of cyclodextrin treatment on PPF (Frank et al., 2008). Several studies describe defective LTP after acute cholesterol depletion with cyclodextrin (Frank et al., 2008; Koudinov and Koudinova, 2001) or inhibition of the mevalonate pathway (Matthies et al., 1997), which may be due to presynaptic and/or postsynaptic mechanisms as described above.

An assessment of the roles of cholesterol 24-hydroxylase and brain cholesterol turnover in learning and memory are reported here. I find that postsynaptic brain cholesterol turnover in hippocampal neurons is necessary to supply constant levels of the nonsterol isoprenoid, geranylgeraniol, which in turn is necessary for synaptic plasticity in mice. Geranylgeraniol acts to modulate the function of a subtype of ionotropic glutamate receptor, the NMDAR, which is essential for hippocampal LTP and learning. While constant brain cholesterol levels are of vital importance for basic neural transmission as a

function of myelin maintenance, cholesterol turnover has a crucial role in neuronal synaptic plasticity in the adult brain and is required for normal learning ability in the whole animal.

Figure 1. Schematic of the mevalonate pathway. Arrows indicate the flow of intermediates, and brakes indicate pharmacologic and genetic inhibition of the indicated steps. PP, diphosphate.

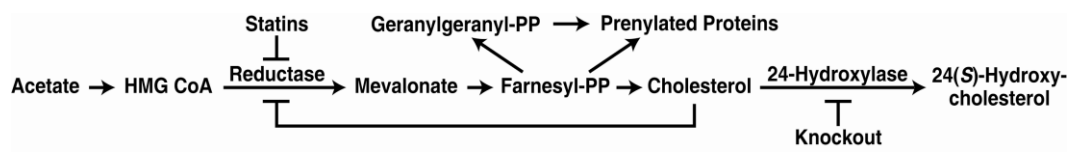


Figure 2. Ontogeny of brain cholesterol synthesis and accumulation in the mouse.

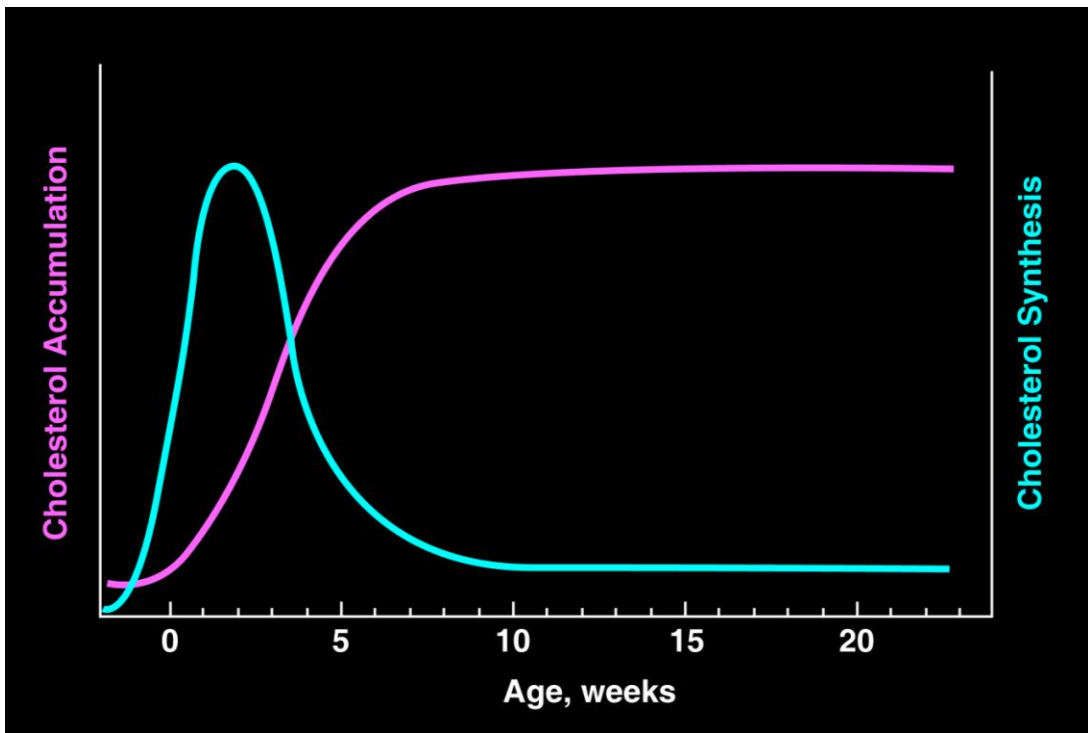


Figure 3. Conversion of cholesterol to 24(*S*)-hydroxycholesterol by cholesterol 24-hydroxylase (CYP46A1).

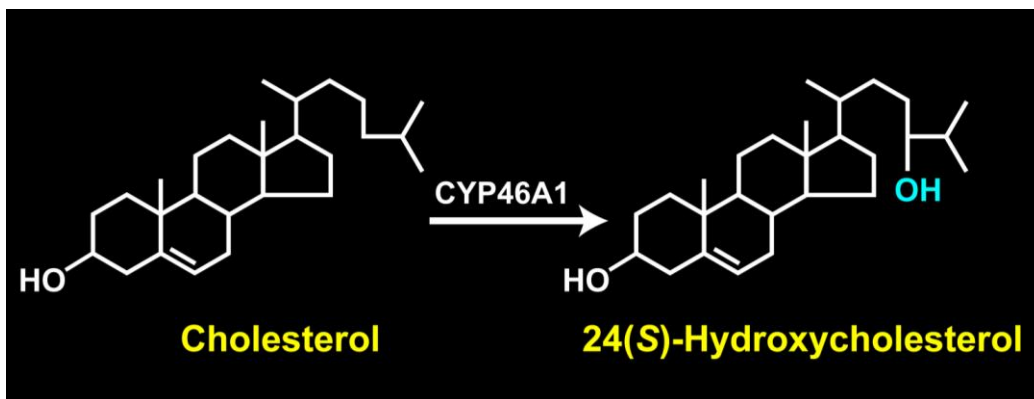


Figure 4. Examples of *N*-methyl-D-aspartate receptor heterotetramer assembly. NR1/NR2A and NR1/NR2B diheteromers, the predominant species in the forebrain, are shown in schematic form.

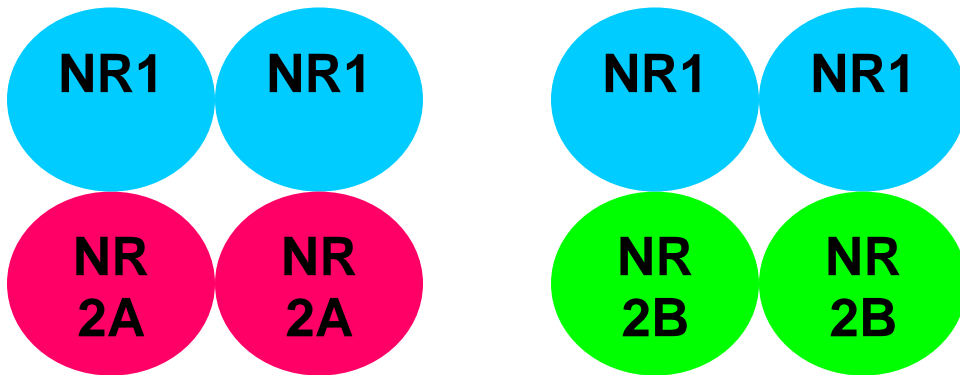
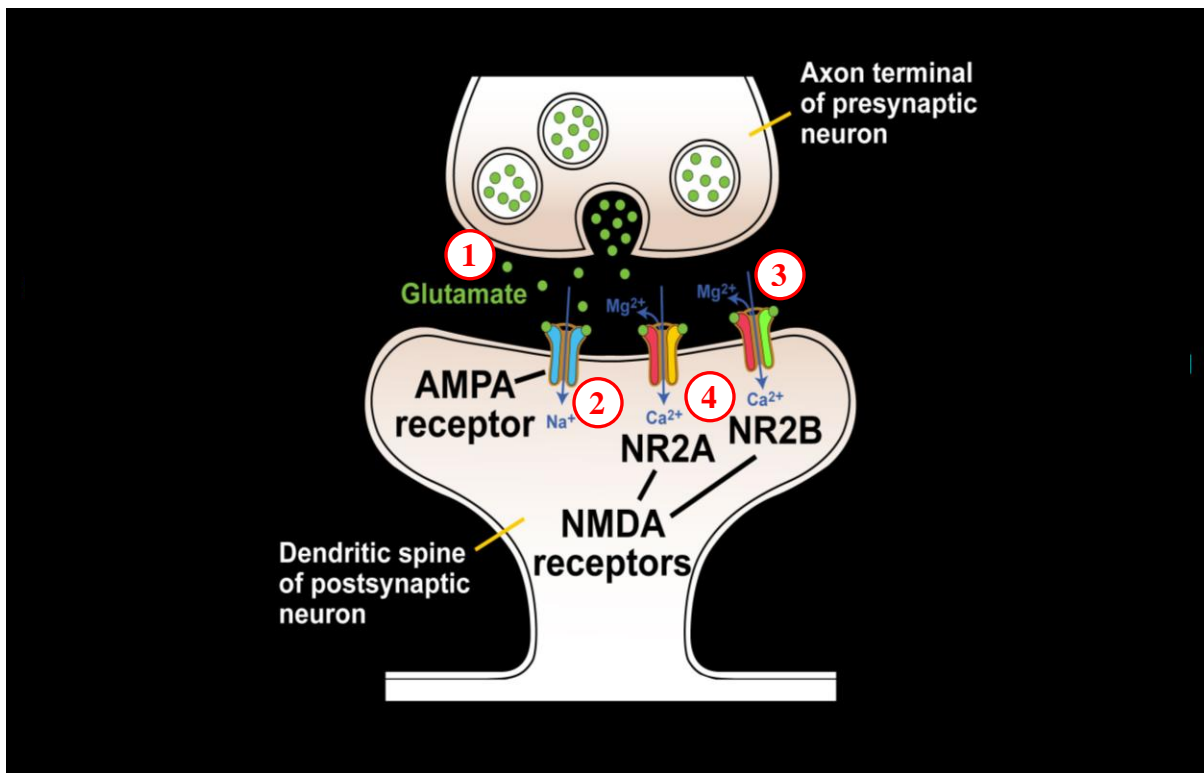


Figure 5. Molecular processes involved in long-term potentiation of excitatory synaptic transmission. 1) Presynaptically released glutamate binds postsynaptic *N*-methyl-D-aspartate (NMDA) and α -amino-3-hydroxy-5-methyl-4-isoxazole propionic acid (AMPA) ionotropic glutamate receptors. 2) AMPARs allow sodium ions to enter, depolarizing the postsynaptic neuron. 3) Postsynaptic depolarization relieves the magnesium blockade of NMDARs that is present at resting potential. 4) Calcium enters through NMDARs. Not depicted are the many actions of calcium as a second messenger, which results in increased AMPAR function and potentiates the responses at stimulated synapses.



CHAPTER TWO

Neuronal Expression and Subcellular Localization of Cholesterol 24-Hydroxylase in the Mouse Brain

Introduction

The human brain contains ~25% of the total body cholesterol pool but represents only a small percentage of body mass (~2%) (Bjorkhem, 2006; Dietschy and Turley, 2004). The majority of brain cholesterol is contained within myelin sheaths elaborated by oligodendrocytes that surround and insulate neuronal axons, whereas smaller amounts are found in the plasma membranes of neurons and glial cells. Unvarying cholesterol levels are essential for oligodendrocytes to maintain the insulatory properties of their myelin sheaths (Bjorkhem, 2006; Dietschy and Turley, 2004). In contrast, the continued synthesis and turnover of cholesterol is necessary in neurons for learning and the production of long-term potentiation (LTP), an electrophysiological correlate of learning (Kotti et al., 2006). The adult brain meets these seemingly disparate needs by exactly balancing cholesterol synthesis and catabolism (Quan et al., 2003).

To these ends, small amounts of cholesterol are synthesized and broken down daily within select neurons of the central nervous system. Synthesis involves the conversion of acetyl-CoA into cholesterol by ≥ 20 enzymes, whereas a majority of catabolism is accomplished by a single enzyme, cholesterol 24-hydroxylase, which converts cholesterol into 24(*S*)-hydroxycholesterol (Bjorkhem and Meaney, 2004; Lund et al., 1999). Cholesterol 24-hydroxylase is a cytochrome P450 and therefore requires the activity of its obligate redox partner, NADPH-cytochrome P450 oxidoreductase (P450 reductase) (Pikuleva, 2006; Shen et al., 2002). 24(*S*)-hydroxycholesterol is membrane-

permeable, and once synthesized crosses the cellular membrane and the blood-brain barrier and enters the peripheral circulation from which it is cleared by the liver (Bjorkhem et al., 2001; Li-Hawkins et al., 2000). The metabolism of cholesterol to 24(*S*)-hydroxycholesterol is offset by an equal amount of synthesis ensuring that steady state levels of cholesterol do not vary within the tissue. The equilibrium between synthesis and breakdown is illustrated in 24-hydroxylase knockout mice, in which an ~50% reduction in catabolism is balanced by a similar reduction in *de novo* cholesterol synthesis, thus maintaining wild-type levels of cholesterol in the brains of the mutant animals (Lund et al., 2003). Accordingly, these mice have no observed defects in brain anatomy or myelination; however, the mutant mice do exhibit severe deficiencies in behavioral learning and hippocampal LTP (Kotti et al., 2006) (see also Chapter 3).

Expression of 24-hydroxylase has been documented in multiple regions of the brain, including the hippocampus, cortex, and cerebellum by immunohistochemistry using a polyclonal antiserum raised against a peptide antigen and by *in situ* mRNA hybridization (Lund et al., 2003). These regions of the brain, especially area CA1 of the hippocampus, are involved in learning and memory (Sweatt, 2003; Whitlock et al., 2006). The enzyme appears to be expressed in only a subset of neurons, suggesting that constant cholesterol synthesis and turnover is crucial for the specific functions of these select cells. One of these functions is long-term potentiation of synaptic transmission at Schaffer collateral-CA1 synapses, as shown by the deficit in LTP production at these synapses in 24-hydroxylase knockout mice. The metabolic basis of this defect was traced to the lack of adequate amounts of newly synthesized geranylgeranyl-pyrophosphate, a nonsterol

end-product of the cholesterol biosynthetic pathway (Kotti et al., 2006) (see also Chapter 3).

It is currently unknown what roles the cellular distribution and subcellular localization of 24-hydroxylase have in cholesterol turnover and higher order brain functions. To gain insight into these roles, we generated three monoclonal antibodies that recognize 24-hydroxylase and used these probes to determine the enzyme's cell type-specific expression patterns and subcellular localizations within individual neurons. The data confirm and extend the exclusive neuronal expression of 24-hydroxylase reported previously and show that within neurons, the protein is localized throughout the endoplasmic reticulum (ER) of the soma and dendrites.

Materials and Methods

Production of mouse monoclonal antibodies recognizing 24-hydroxylase

Partially purified, recombinant human 24-hydroxylase protein (H Δ 46A1) was prepared as described (Mast et al., 2003). This protein contained four histidine residues at the amino terminus and lacked the membrane anchor region of the protein (amino acids 3-27). Four 8-week-old female BALB/c mice (Harlan Sprague Dawley, Inc., Indianapolis, IN) were each injected with 75 μ g of H Δ 46A1 emulsified in an equal volume of RIBI Adjuvant R-700 (Corixa, Hamilton, MT). These and all other experiments involving mice in this study followed protocols approved by the UT Southwestern Institutional Animal Care and Use Committee. The mice each received three priming injections of 25 μ g H Δ 46A1 consisting of two dorsal subcutaneous injections and one intraperitoneal injection. After four weeks, one mouse received a

booster intraperitoneal injection of 100 μg H Δ 46A1 mixed with an equal volume of phosphate-buffered saline (PBS), pH 7.4. Three days later, this mouse was killed, the spleen was dissected under sterile conditions, and the tissue dissociated into a single-cell suspension using a 150 mesh sieve (#CD-1, Sigma-Aldrich, Inc., St. Louis, MO). Spleenocytes and Sp 2/0 myeloma cells were washed separately in PBS three times, collected by centrifugation for 10 minutes at 228 x g, and then combined ($\sim 10^8$ spleenocytes: 2.5×10^6 myeloma cells) and pelleted in the same tube. The cells were resuspended in 1-ml of 50% (w/v) polyethylene glycol 1500 (#10783641001, Roche Applied Science, Indianapolis, IN) and allowed to fuse for 1 minute. Treated cells were collected by centrifugation at 100 x g for 8 minutes and resuspended in complete medium (Dulbecco's modified Eagle's medium (DMEM) containing 4.5 g/L glucose supplemented with 10% (v/v) fetal calf serum, 10 mM HEPES pH 7.0, 50 μM β -mercaptoethanol, 100 units/ml penicillin, 100 $\mu\text{g}/\text{ml}$ streptomycin sulfate, and 1% (v/v) mouse interleukin-6 (mIL-6, #11444581001, Roche Applied Science)) to approximately 2.5×10^6 cells/ml, and then plated (100 $\mu\text{l}/\text{well}$) into five 96-well flat-bottom tissue-culture plates. The plates were transferred to an incubator maintained at 37°C in a 5% CO₂ atmosphere. After 24 hours, the cultures were supplemented with 100 μl of 2X HAT (#H0262, Sigma-Aldrich, Inc.) in complete medium containing IL-6 to achieve a final concentration of 100 μM hypoxanthine (H), 0.4 μM aminopterin (A), and 16 μM thymidine (T). Replacements of 1X HAT medium were performed every second day. As soon as hybridoma growth became macroscopically visible (\sim day 11), supernatants were screened for relevant antibodies by ELISA (see below).

ELISA-positive clones were expanded to 24-well tissue culture plates in 1X HT medium (#H0137, Sigma-Aldrich, Inc.) containing 100 μ M H and 16 μ M T. Twenty-two hybridomas out of 100 macroscopically visible clones produced antibodies against the antigen as determined by ELISA. These 22 hybridoma supernatants were further subjected to secondary screening by immunocytochemistry of Chinese hamster ovary (CHO)-K1 cells expressing the mouse 24-hydroxylase (see below) when hybridoma growth reached appropriate levels (~days 13-14). Immunocytochemical-positive clones were expanded to 10-ml culture volumes in T-25 tissue culture flasks in 1X HT medium. Three hybridoma supernatants (designated 1A7, 1F11, and 1F4) out of 22 specifically stained expressing CHO-K1 cells and were subjected to tertiary screening by immunoblotting of brain homogenates from wild-type and 24-hydroxylase knockout (Lund et al., 2003) mice as described below. Two of the three hybridoma supernatants (1A7 and 1F11) detected a single protein of the predicted molecular weight (~50,000) of 24-hydroxylase that was absent in samples from 24-hydroxylase knockout animals. Sub-cloning of the three positive hybridoma lines (1A7, 1F11, and 1F4) was performed by limiting dilution as follows: 100, 10, and 1 cells/well were seeded into 96-well flat-bottom tissue-culture plates. When growth was macroscopically visible, hybridoma supernatants were screened by ELISA. All wells of the 100 cells/well and 10 cells/well plates were ELISA-positive, indicating the stability of the hybridoma lines. The culture well with the highest optical density at 450 nm from the 1 cell/well plate was expanded and sub-cloning was repeated as above for a total of four rounds. The immunoglobulin subtypes of the final hybridoma clones were determined with an ELISA-based isotyping kit according to the manufacturer's instructions (#172-2051, Bio-Rad, Hercules, CA).

All experiments were performed with monoclonal antibodies produced by the hybridomas arising from the 4th round of sub-cloning. Hybridomas were maintained in complete medium without IL-6, HAT, or HT.

ELISA

96-well microtiter plates (MaxiSorp #442404, Nunc, Rochester, NY) were coated overnight at 4°C with 50 µl/well of HΔ46A1 protein at 5 µg/ml in 50 mM Tris-acetate buffer, pH 7.4 containing 20% (v/v) glycerol. Plates were washed two times with phosphate-buffered saline (PBS) containing 0.05% (v/v) Tween 20 (PBS-T). Tissue culture supernatants were diluted with an equal volume of PBS containing 0.1% (v/v) Tween 20, added to the wells, and incubated for 2-3 hours at 37°C. Plates were then washed three times with PBS-T. Horseradish peroxidase-conjugated goat anti-mouse IgG (#170-6516, Bio-Rad) was diluted 1:2000 in PBS-T, added to the wells, and incubated for 5 minutes at room temperature. Plates were then washed four times with PBS-T. A fresh mixture of peroxidase substrates containing 1 volume of 20 mM tetramethylbenzidine in acetone/methanol (1:9) and 20 volumes of 2 mM H₂O₂ in 0.1 M potassium citrate buffer, pH 4.25, was prepared and 0.2 ml was added to each well. The reaction was incubated for 5 minutes at room temperature and stopped with 0.1 ml of 1 M H₂SO₄. The absorbance at 450 nm was measured on a microtiter plate reader (Opsys MR, Dynex Technologies, Chantilly, VA).

Transfection

For immunocytochemistry, CHO-K1 cells (American Type Culture Collection, Manassas, VA) were plated at a density of 9×10^3 cells/well in 24-well tissue culture plates containing 22 mm² glass coverslips in DMEM and Ham's F12 (50:50 mix) medium supplemented with 5% (v/v) fetal calf serum, 100 units/ml penicillin, and 100 µg/ml streptomycin sulfate. The following day, cells were transfected with 0.5 µg of plasmid DNA per well encoding no protein (pCMV6), the mouse 24-hydroxylase (pCMV6-mc24), the human 24-hydroxylase (pCMV6-hc24), and/or the rat NADPH cytochrome P450 reductase (pCMV6-ratCP450Red) using Fugene 6 reagent (#11988387001, Roche Applied Science), and incubated at 37°C in a 5% CO₂ atmosphere for approximately 18 hours prior to fixation as described below.

For immunoblotting of transfected cell lysates, human embryonic kidney-293 (HEK-293, American Type Culture Collection) cells were plated in 60 mm dishes at a density of 4×10^5 cells/dish in DMEM containing 1 g/L glucose supplemented with 10% (v/v) fetal calf serum, 100 units/ml penicillin, and 100 µg/ml streptomycin sulfate. Two days after plating, cells were transfected with 3 µg plasmid DNA per well (pCMV6, pCMV6-mc24, pCMV6-hc24, or pCMV6-ratCP450Red) using Fugene 6 reagent and incubated at 37°C in an 8.8% CO₂ atmosphere for approximately 18 hours. Cells were washed once with ice-cold PBS and scraped into ice-cold RIPA buffer (50 mM Tris-HCl pH 8.0, 150 mM NaCl, 1% (v/v) NP-40, 0.5% (w/v) sodium deoxycholate, and 0.1% (w/v) sodium dodecyl sulfate, #R0278, Sigma-Aldrich, Inc.) containing Complete Protease Inhibitor tablets (EDTA-free, #11836170001, Roche Applied Science). The cells were lysed by passage through a 23-gauge needle 10-15 times. Cellular debris was

removed by centrifugation at 2000 x g for 5 minutes at 4°C, and the resulting supernatant was removed to a fresh tube, aliquoted, and stored at -20°C. The protein concentration of the cell lysate was determined by bicinchoninic acid assay (BCA Assay, #23225, Pierce Biotechnology, Rockford, IL).

Preparation of tissue homogenates and microsomes

Brain homogenates were prepared from adult wild-type and 24-hydroxylase knockout mice (mixed strain background, C57Bl/6J;129S6/SvEv), as well as from adult rats and one adult rabbit. Whole brains were minced with a scalpel and then homogenized in a glass-Teflon homogenizer in ice-cold Tris-acetate buffer (50 mM Tris-acetate pH 7.4, 2 mM CaCl₂, 10% (w/v) sucrose) containing Complete Protease Inhibitor tablets (EDTA-free, Roche Applied Science). Samples were further homogenized by passage through a 23-gauge needle and clarified by centrifugation at 1500 x g for 15 minutes at 4°C in a desktop microcentrifuge. The resulting supernatant was removed to a fresh tube, aliquoted, and stored at -80°C. The protein concentration of the homogenate was determined by BCA assay.

Homogenates and microsomes from embryonic day 16 mouse cortex and hippocampus and from mature primary cell cultures derived from the cortex and hippocampus were prepared. Embryonic cortices and hippocampi from one litter (4-8 embryos) of wild-type or 24-hydroxylase knockout mice were dissected into ice-cold Tris-acetate buffer as described for the preparation of primary cell cultures below. Similarly, primary cells grown for 14 days *in vitro* were washed once in PBS and scraped into ice-cold Tris-acetate buffer. The samples were homogenized by sequential

trituration with P1000 and P200 micropipettors, followed by passage through a 23-gauge needle. The cell debris and nuclei were removed by centrifugation at 1500 x *g* for 15 minutes at 4°C to yield a crude homogenate, which was further centrifuged at 100,000 x *g* for 30 minutes at 4°C to yield a microsomal pellet. The pellet was resuspended in a small volume of Buffer A (50 mM Tris-HCl pH 7.4, 1 mM EDTA, 20% (v/v) glycerol) containing Complete Protease Inhibitors (EDTA-free, Roche Applied Science). The protein concentrations of the homogenates and microsomes were determined by BCA assay.

Immunoblotting procedures

To assess the reactivity and specificity of monoclonal antibodies (Fig. 1A), 30 µg of wild-type and knockout total brain homogenates were subjected to SDS-PAGE. For assessment of monoclonal antibody reactivity against the mouse versus human recombinant 24-hydroxylase proteins (Fig. 1B), increasing amounts (2 to 10 µg) of pCMV6-mc24- or pCMV6-hc24-transfected cell lysate and 10 µg of pCMV6-transfected lysate were subjected to SDS-PAGE. To determine monoclonal antibody reactivity against the mouse, rat, and rabbit 24-hydroxylase proteins (Fig. 1C), 40 µg of total brain homogenates and 1 µg of transfected cell lysates were subjected to SDS-PAGE. To examine 24-hydroxylase expression in mouse embryonic cortex and hippocampus and primary cells (Fig. 1D), 75 µg of embryonic brain and 25 µg of cell microsomal fractions were subjected to SDS-PAGE.

All protein samples were diluted 1:1 with 2X Laemmli sample buffer (#161-0737, Bio-Rad) containing 5% (v/v) β -mercaptoethanol and boiled at 95°C for 10 minutes. Samples were loaded onto 10% Ready Gel Tris-HCl polyacrylamide gels (#161-1155, Bio-Rad) with Kaleidoscope and Precision Plus Blue (#161-0324 and #161-0373, Bio-Rad) molecular weight markers. Gels were electrophoresed at 100 volts for approximately 1.5 hours in 1X Tris-Glycine-SDS (TGS, #161-0772, Bio-Rad) running buffer followed by electrophoretic transfer to nitrocellulose membranes (Hybond-C Extra, GE Healthcare Biosciences, Piscataway, NJ) for 1.25 hours in a tank transfer apparatus (Hoefer TE 22, San Francisco, CA) at 100 volts. Protein transfer was verified by staining with Ponceau S (#P7170, Sigma-Aldrich Inc.) and membranes were incubated for at least 1 hour at room temperature in 10% (w/v) milk dissolved in PBS-T. Primary antibodies were incubated overnight at 4°C. Monoclonal antibodies were used as neat hybridoma tissue culture supernatants (20-25 μ g/ml antibody) supplemented with Tween 20 to 0.05% (v/v). The membranes were washed three times for 10 minutes each with PBS-T. Horseradish peroxidase-conjugated goat-anti-mouse secondary antibody (#115-035-003, Jackson ImmunoResearch, West Grove, PA) was diluted 1:10,000 in 10% (w/v) milk-PBS-T and incubated for 1 hour at room temperature. The membranes were washed three times for 10 minutes each with PBS-T, blotted briefly on paper towels, and incubated for 2 minutes in ECL reagent (#RPN2106, GE Healthcare Biosciences), or 5 minutes in SuperSignal West Pico chemiluminescent substrate (#34080, Pierce Biotechnology), and exposed to film (X-Omat Blue, Kodak, New Haven, CT). For the detection of proteins that served as loading controls, membranes were stripped for 35 minutes at room temperature with Restore Western Blot Stripping Buffer (#21059, Pierce

Biotechnology), washed twice in PBS-T, and incubated for 1 hour in 10% (w/v) milk. Mouse anti- β III tubulin, mouse anti- α tubulin, and rabbit anti-NADPH cytochrome P450 reductase antibodies were obtained and diluted (Table 1) in 10% (w/v) milk-PBS-T and then incubated with the filter overnight at 4°C. Washing, secondary antibody incubation, and chemiluminescence detection were repeated as described above. Films were scanned and imported into Adobe Illustrator for figure preparation.

Primary cell culture

Primary cells from wild-type and 24-hydroxylase knockout mice were prepared using a modification of a protocol described for rat neurons (Banker and Goslin, 2002). A pregnant mouse at 15-17 days gestation was anesthetized with isoflurane and killed by cervical dislocation. The uterus was dissected, male and female fetuses were decapitated, and heads removed to ice-cold Hank's Balanced Salt Solution (HBSS, calcium and magnesium free, #14175-079, Invitrogen, Carlsbad, CA). Brains were extricated and cortical lobes placed in ice-cold HBSS. The meninges were removed and the hippocampus and cortex were dissected free of the thalamic regions under a dissecting microscope (Leica Wild MZ8). Trypsin-EDTA (#15400-054, Invitrogen) was added to the tissue from a 10X stock for a final concentration of 0.05% (v/v) and incubated at 37°C for 15 minutes. The digestion was stopped by the addition of 200 μ l fetal bovine serum and tissue was collected by centrifugation at 800 x *g* for 2 minutes. The supernatant was decanted and 900 μ l of dissociation medium (HBSS containing 12 mM Mg^{2+} , 0.025% (w/v) deoxyribonuclease, 0.4 mg/ml trypsin inhibitor, and 2 mg/ml bovine serum albumin) was added to the pellet and incubated for 5 minutes at 37°C. The tissue

was dissociated by trituration 40 times with a P200 micropipettor or until no clumps remained. Dissociated cells were diluted with 5 ml of Neurobasal medium (#21103-049, Invitrogen, Brewer et al. 1993) supplemented with 100 units/ml penicillin, 100 µg/ml streptomycin sulfate, 1 mM L-glutamine, and 2% (v/v) B27 (#17504-044, Invitrogen) and collected by centrifugation at 800 x g for 3 minutes. Supernatant was decanted; the cell pellet was resuspended in 5-ml of Neurobasal medium supplemented as above, and the cells collected by centrifugation. The final cell pellet was resuspended in a volume (in ml) of supplemented Neurobasal medium equal to the number of brains dissected, resulting in a cell suspension containing approximately 8×10^6 cells/ml. Cells were plated onto poly-D-lysine (50 µg/ml, #P7280, Sigma-Aldrich, Inc.) coated 6-well tissue culture plates for biochemical experiments at a density of 1.3×10^6 cells/well, or onto poly-D-lysine coated 24-well plates containing pre-washed 12 mm diameter #0 round German glass coverslips (#63-3009, Carolina Biological Supply, Burlington, NC) for immunocytochemical experiments at a density of 5×10^5 cells/well. On day 4 after plating, one half of the medium volume was removed and replaced with fresh supplemented Neurobasal medium. Neurons were grown in a 37°C, 5% CO₂ incubator and analyzed after 14 days in culture.

Immunocytochemistry

CHO-K1 cells and primary cells grown on coverslips were processed for immunocytochemistry in the same manner. Cells were washed once with 37°C PBS and fixed in 4% (w/v) paraformaldehyde (PFA, #19200, Electron Microscopy Sciences, Hatfield, PA) in PBS at room temperature for 15 minutes. Cells were then rinsed four

times with PBS and either processed for immunocytochemistry immediately or stored in PBS at 4°C for up to 2 weeks prior to staining. The cells were incubated for 10 minutes at room temperature in 1% (w/v) glycine in PBS to reduce fixative-induced autofluorescence. Next, cells were permeabilized with 0.2% (v/v) Triton X-100 (Surfact-Amps X-100, #28314, Pierce Biotechnology) in PBS for 10 minutes at room temperature, and then treated to reduce non-specific staining by incubation for at least one hour in a solution of 10% (v/v) normal goat serum (#G9023, Sigma-Aldrich, Inc.), 5% (v/v) bovine serum albumin (#37525, Pierce Biotechnology), and 0.025% (v/v) Triton X-100 in PBS (NGS blocking solution). Primary antibody incubation was overnight at 4°C. Staining with anti-24-hydroxylase monoclonal antibodies 1A7, 1F4, and 1F11 was performed using neat hybridoma culture supernatants containing 20-25 µg/ml antibody and supplemented with 0.025% (v/v) Triton X-100. For double staining of 24-hydroxylase and subcellular markers, the second antibody (see below) was added directly to the hybridoma supernatant solution containing 0.025% Triton X-100 and the mixture was then transferred to cells.

The primary antibodies used in this study are described in Table 1. They were directed against NADPH-cytochrome P450 reductase, protein disulfide isomerase (PDI) (Colombo et al., 2005; Mezgrahani et al., 2000), brain lipid binding protein (Feng et al., 1994; Rousselot et al., 1997), calnexin, NADPH-cytochrome b5 reductase (Colombo et al., 2005; Zhu et al., 2004), manganous superoxide dismutase (MnSOD) (Beltran-Parrazal et al., 2006; Chang and Reynolds, 2006), prohibitin (Ikonen et al., 1995), mannose-6-phosphate receptor (M6PR), Golgi matrix protein of 130 kDa (GM130) (Sannerud et al., 2006), glutamic acid decarboxylase of 67 kDa (GAD67) (Fong et al.,

2005), synaptophysin (Johnston et al., 1989), synapsin (Rosahl et al., 1993), Rab3A (Fischer von Mollard et al., 1990), β III-tubulin (Flajollet et al., 2006; Lee et al., 1990), α -tubulin (Berasi et al., 2006), microtubule associated protein 2 (MAP2) (Kosik and Finch, 1987; Longart et al., 2004), brain spectrin (Riederer et al., 1986), and phosphorylated neurofilament protein (Goldstein et al., 1983; Sternberger and Sternberger, 1983). The specificity of each antiserum was tested in immunoblots of total cell lysate protein prepared from wild-type primary neurons cultured for 14 days as described above. All antisera detected a single protein of the expected molecular weight except for the GM130 antiserum, which also weakly bound two additional proteins, the synaptophysin antiserum, which weakly bound one other protein, and the brain spectrin antiserum, which weakly detected one additional protein and possibly aggregates of spectrin. Antisera against brain lipid binding protein and the M6PR did not recognize any proteins in immunoblotting experiments performed as described above.

For detection of lysosomes using LysoTracker® Red, cells were incubated with 60 nM LysoTracker® Red in Neurobasal complete medium for 45 minutes at 37°C, washed once, fixed in 4% PFA, and processed for 1A7 immunocytochemistry in the dark.

Following primary antibody incubation, coverslips were washed three times in PBS-T for 10 minutes at room temperature. Goat anti-mouse secondary antibodies conjugated to Alexa Fluor 488 and goat anti-rabbit secondary antibodies conjugated to Alexa Fluor 594 (highly cross adsorbed against other species; #A-11029 and #A-11037, Invitrogen) were diluted 1:1000 in NGS blocking solution and incubated with coverslips for 1 hour in the dark. In experiments using 1A7 and the M6PR or GAD67 primary antibodies, subtype-specific goat anti-mouse IgG₁ conjugated to Alexa Fluor 488 and

goat anti-mouse IgG_{2a} conjugated to Alexa Fluor 594 secondary antibodies were used (#A-21121 and #A-21135, Invitrogen). The coverslips were washed 3 times with PBS-T for 10 minutes. After the last wash, coverslips were mounted using ProLong Gold Antifade reagent (#P-36931, Invitrogen) containing 4',6-diamidino-2-phenylindole (DAPI) and allowed to cure overnight at room temperature in the dark before imaging. Each batch of secondary antibody used in these studies was tested in control experiments to ensure that when applied to cells or sections in the absence of primary antibody, no background staining was observed.

Immunocytochemistry experiments were imaged on an Applied Precision Deltavision RT wide-field epifluorescence deconvolution microscope equipped with a Photometrics CoolSNAP_{HQ} monochromatic digital camera using the associated SoftWorx image acquisition software. Images were subjected to 10 iterations of constrained deconvolution using the enhanced aggressive method. The objectives used consisted of an Olympus U Apo 40X, 1.35 NA and an Olympus U Plan Apo 100X, 1.35 NA. Exposure times were held constant for images comparing transfected and untransfected or wild-type versus knockout samples. Images presented in Figures 2-5 represent a single *z* slice from the stack, selected for the best focus using Image J (National Institutes of Health) software. Image J was also used to adjust the brightness and contrast of the images, levels of which were again held constant for comparison of different samples. For colocalization analysis (Figs. 2-6, and Table 2), 100X image stacks of 1A7 and subcellular marker double-stained neurons were rendered in three dimensions using Imaris 3D (Bitplane) software. Background was subtracted from all three channels using a filter width of 16.112249 μm . The images were filtered with an edge preserving filter

of width 0.063 μm . The images were thresholded and intensity was adjusted to further reduce background and to highlight the region of interest (the subcellular structures of the neuron) using the blend feature of the volume projection. The image stack was cropped in the x and y dimensions to remove parts of the image that did not contain the neuron and out of focus slices were deleted from the top and bottom of the stack as necessary. The “coloc” feature, with automatically detected thresholds, was then employed to obtain the Pearson correlation coefficient of colocalization between green (24-hydroxylase) and red (subcellular markers) staining. A Pearson correlation coefficient of greater than 0.5 was considered to indicate significant colocalization. A minimum of three images from two independent experiments ($n = 6$ neurons) was analyzed in this fashion to determine the average Pearson correlation coefficients shown in Table 2. The colocalized pixels were displayed in white as the coloc channel. To obtain 3D renderings of the images as shown in Figure 6, the volume for the red, green, and white (colocalized) channels was displayed as an Iso Surface projection. The opacity of the red and green channels was adjusted to 75% in the enlarged images (Fig. 5,D,I,E,J) to allow for better visualization of the colocalized pixels. For final figure preparation, TIF files obtained as described above were imported into Adobe Illustrator.

Immunohistochemistry

For preparation of brain cryosections, 3- month-old (Fig. 7A-D, Fig. 8, Fig. 9) or 14-month-old (Fig. 7E,F) female wild-type and 24-hydroxylase knockout mice (C57Bl/6J background) were overdosed with isoflurane and perfused through the heart with PBS followed by 4% PFA in PBS. The brains were removed and postfixed overnight at 4°C in

4% PFA in PBS. The brains were cryoprotected with three 24 hour incubations at 4°C in graded sucrose solutions of 10%, 18%, and 30% (all w/v) in PBS. After 24 hours of incubation in 30% sucrose, the brains were embedded in Optimal Cutting Temperature (OCT) compound (Sakura Finetek, Torrance, CA) and frozen by immersion of the block in a dry ice/isopentane bath and stored at -80°C until cryosectioning. Various sagittal sections (10 µm) were collected onto positively charged slides, allowed to dry overnight, and stored at -80°C until processed for immunohistochemistry. For preparation of retinal and optic nerve cryosections, 3-month-old male albino wild-type (C57Bl/6J; 129S6/SvEv; SJL/J background) and 24-hydroxylase knockout mice (C57Bl/6J background) were anesthetized with isoflurane and killed by cervical dislocation. The eyes were removed and the posterior eyecups or dissected optic nerves were immersion-fixed in 4% PFA in PBS at 4°C for 30 minutes. The tissues were cryoprotected with 20 minute incubations at 4°C in graded sucrose solutions of 10%, 18%, and 30% (all w/v) in PBS, and then embedded in OCT as described above. Transverse sections (6 µm) were collected onto positively charged slides, allowed to dry overnight, and stored at -80°C until processed for immunohistochemistry.

The same procedures were followed to immunostain brain, retinal, and optic nerve cryosections. Slides were allowed to warm to room temperature for 30 minutes. Antigen retrieval was performed in sodium citrate buffer (10 mM sodium citrate, pH 6.0, 0.05% (v/v) Tween 20) at 90°C for 30 minutes in a water bath. The holder containing the citrate buffer and slides was allowed to cool to room temperature. The sections were then permeabilized with 0.2% (v/v) Triton X-100 (Surfact Amps X-100, #28314, Pierce Biotechnology) in PBS for 15 minutes at room temperature. The sections were blocked

for at least 1 hour with NGS blocking solution as described for immunocytochemistry above. Primary antibody incubation was overnight at 4°C in a humidified chamber. Neat hybridoma culture supernatants containing 20-25 µg/ml antibody and supplemented with Triton X-100 to 0.025% were used as primary antibodies. Slides were washed three times for 10 minutes with PBS containing 0.025% Triton X-100 (PBS-T). Secondary goat anti-mouse biotin-conjugated antibody (#115-065-003, Jackson ImmunoResearch) was diluted 1:4000 in NGS blocking and incubated for 1 hour at room temperature. The slides were washed three times for 10 minutes in PBS-T. Streptavidin-horseradish peroxidase conjugate (#S911, Invitrogen) was diluted 1:4000 in 0.5X NGS blocking and incubated for 20 minutes at room temperature. The slides were washed three times for 10 minutes in PBS-T. A fresh mixture (1:10) of metal-enhanced diaminobenzidine (DAB) and stable peroxide buffer (#34065, Pierce Biotechnology) was prepared and incubated on the slides for 3-5 minutes.

For fluorescent detection of double immunohistochemical staining of P450 reductase with other cellular markers, the sections were prepared as described above and immunostained using a similar protocol. The primary antibodies were diluted as shown in Table 1 in NGS blocking. Secondary antibody incubation and slide mounting was performed as described above for immunocytochemical experiments.

All slides stained with the same primary antibody were incubated with the substrate for the same amount of time. The reaction was stopped by extensive washing of the slides in PBS. The slides were counterstained with hematoxylin 1 (#7221, Richard-Allan Scientific, Kalamazoo, MI) according to the manufacturer's instructions and mounted using GelMount (#G0918, Sigma-Aldrich, Inc.). All DAB

immunohistochemistry experiments were imaged on a Nikon E1000 brightfield microscope equipped with a Nikon DMX1200F color digital camera using 10X Plan Apo, 0.45 NA or 20X Plan Apo, 0.75 NA, or 40X Plan Fluor 0.75 NA objectives and ACT-1 image acquisition software. Fluorescent immunohistochemistry experiments were imaged either on the Applied Precision Deltavision Deconvolution system using the 40X objective as described for immunocytochemistry above, or on a Zeiss Axioplan 2 fluorescence microscope using a 20X Plan-Apochromat, 0.75 NA objective. Exposure times were held constant for wild-type and knockout sections in the same experiment. The images were processed in Adobe Photoshop, including cropping and adjustment of brightness and contrast of the complete image. Brightness and contrast were adjusted to the same level when comparing wild-type and knockout images. For final figure preparation, TIF files were imported into Adobe Illustrator.

Results

Assessment of monoclonal antibody specificity

To facilitate detection and localization of 24-hydroxylase in cells and tissues, monoclonal antibodies that recognize the protein were generated as described in Materials and Methods. Multiple immunizations and screenings yielded three hybridomas (1A7, immunoglobulin G₁; 1F4, immunoglobulin G_{2b}, and 1F11, immunoglobulin G₁) that secreted monoclonal antibodies of high titer which consistently recognized the protein as judged by ELISA. To further characterize the specificity of each antibody, a series of immunoblotting experiments was performed. In Figure 1A, total brain homogenates from wild-type and 24-hydroxylase knockout mice were

resolved by SDS-PAGE, transferred to nitrocellulose filters, and incubated with hybridoma supernatants derived from the 1A7, 1F4, and 1F11 clones. A single protein with the predicted molecular weight of 24-hydroxylase (~50,000) was detected by the 1A7 and 1F11 antibodies in homogenates derived from wild-type brains but not those prepared from knockout brains. The 1F4 antibody did not detect any proteins in the brain homogenates. To ensure that equal amounts of protein were examined in these experiments, immunocomplexes formed with the monoclonal antibodies were stripped from the membranes and the filters were reprobed with an antibody that recognized β III tubulin. As indicated in the bottom panels of Figure 1A, the β III tubulin signal was equivalent in all lanes.

The abilities of the 1A7 and 1F11 antibodies to recognize mouse and human 24-hydroxylase expressed in transfected HEK 293 cells were determined next. As shown in Figure 1B, when increasing amounts of cell lysates (2 to 10 μ g) containing either the mouse (lanes 2-6) or human (lanes 7-11) recombinant 24-hydroxylase were resolved by SDS-PAGE, transferred to nitrocellulose membranes, and incubated with antibodies 1A7 or 1F11, a single protein with the predicted molecular weight of the enzyme was detected. In contrast, no protein was detected in lysates prepared from mock-transfected cells (lane 1). The 1A7 antibody produced a stronger signal than the 1F11 antibody for a given amount of lysate containing either the mouse or human protein, and both antibodies produced a stronger signal against the mouse protein than the human protein. Whether these apparent differences in reactivity were due to unequal expression of the two transfected proteins or to the better recognition of epitopes on the mouse versus the human protein by these antibodies was not determined.

To establish whether the monoclonal antibodies recognized 24-hydroxylase in other species, homogenates from mouse, rat, and rabbit brain, as well as homogenates from transfected cells expressing mouse 24-hydroxylase or mock-transfected cells were subjected to SDS-PAGE and immunoblotting with 1A7 and 1F11 (Fig. 1C, upper panels). Both antibodies detected 24-hydroxylase from mouse, rat, and rabbit. The blots were stripped and reprobed with an antibody against α -tubulin to demonstrate that equal amounts of protein were present in the lanes containing transfected cell lysate or brain homogenates (Fig. 1C, lower panel).

24-hydroxylase expression was next assessed in microsomal fractions from embryonic mouse cortex and hippocampus and in cultured cells (neurons and astrocytes, see below) derived from these tissues (Fig. 1D, upper panels). A low level of 24-hydroxylase was detected with antibodies 1A7 and 1F11 in microsomes prepared from wild-type E16 brain samples but not in those from 24-hydroxylase knockout mice. A larger amount of protein was present in primary cells from wild-type brains that had been cultured for 14 days. Equal amounts of protein were present in each pair of lanes as judged by subsequent blotting with an antibody that recognized NADPH-cytochrome P450 reductase (Fig. 1D, lower panel).

To confirm the specificity of the polyclonal antiserum used to detect P450 reductase, additional immunoblotting experiments were performed. Brain and cerebellar microsomes and lysates of transfected HEK-293 cells expressing recombinant rat P450 reductase were subjected to immunoblotting with this antiserum. (Fig. 2A) A single protein was recognized by the antiserum in the brain preparations and transfected cells, which was absent from mock-transfected cells. A second, lower molecular weight

protein seen only in the transfected cells likely corresponded to a truncated protein produced from an internal methionine start codon under overexpression conditions. Furthermore, the putative P450 reductase protein was enriched in microsomal fractions compared to total homogenates as expected. The expression and microsomal localization of the P450 reductase enzyme were not affected in whole brain and cerebellar samples from 24-hydroxylase knockout mice (Fig. 2B). Stripping and reprobing these blots with a monoclonal antibody recognizing α -tubulin revealed that equal amounts of protein were analyzed.

Immunocytochemical detection of 24-hydroxylase in cultured cells

Two types of experiments were performed to assess the abilities of the 1A7, 1F11, and 1F4 monoclonal antibodies to detect 24-hydroxylase within cultured cells. In the first, CHO-K1 cells were transfected with a plasmid vector encoding mouse 24-hydroxylase and after a period of expression (18 hours), the cells were permeabilized and stained with these antibodies and with an irrelevant monoclonal antibody (3C11) isolated during the production process (Fig. 3A-D). A reticular pattern of 24-hydroxylase staining was observed with all three specific monoclonal antibodies suggestive of an ER localization. Similar results were obtained with CHO cells expressing the human 24-hydroxylase (data not shown). No staining was detected with these antibodies in non-expressing cells or in transfected cells incubated with the 3C11 control antibody (Fig. 3A).

To more precisely define the subcellular localization of 24-hydroxylase in transfected cells, double staining was performed with antibody 1A7 and other antisera

that recognize known ER markers. To generate the data shown in Figure 3D-F, CHO-K1 cells were transfected with expression constructs encoding the mouse 24-hydroxylase and the rat NADPH-cytochrome P450 reductase and after 18 hours of expression, fixed and subsequently incubated with 1A7 and a rabbit polyclonal antibody against the P450 reductase. Substantial colocalization between the two over-expressed proteins as indicated by a yellow color in the merged image (Fig. 3F) was observed. To determine whether expressed 24-hydroxylase colocalized with an endogenous ER protein, transfected CHO-K1 cells were stained with the 1A7 monoclonal antibody and a polyclonal antibody that recognized protein disulfide isomerase (PDI) (Fig. 3G-I). The merged image in Figure 3I revealed extensive colocalization between 1A7 and endogenous PDI staining. Similar colocalization results were obtained in CHO-K1 cells after 24 and 41 hour expression periods (data not shown).

In the second type of experiment, primary cells from the cortex and hippocampus of embryonic wild-type and 24-hydroxylase knockout mice were cultured for 14 days and then subjected to immunostaining (Fig. 4). 24-hydroxylase expression was detected in the cell bodies and processes of wild-type neurons by the 1A7, 1F4, and 1F11 antibodies (Fig. 4A,C,E). No staining was observed when the monoclonal antibodies were incubated with cells cultured from knockout embryos (Fig. 4B,D,F). Double staining of cell cultures with monoclonal antibody 1A7 and a rabbit polyclonal antibody that recognized the brain lipid binding protein (BLBP), an astrocyte marker, showed that 24-hydroxylase expression was confined to wild-type neurons and was not present in BLBP-expressing astrocytes (Fig. 4G,H). Furthermore, astrocyte proliferation and morphology in cell cultures established from the knockout mice appeared normal.

Localization of 24-hydroxylase within neuronal processes

To determine the subcellular localization of 24-hydroxylase in neuronal processes, cultured neurons from wild-type and 24-hydroxylase knockout embryos were co-stained with monoclonal antibody 1A7 and a rabbit polyclonal antiserum recognizing the dendritic marker microtubule associated protein 2 (MAP2) (Fig. 5A-F). When the two expression patterns from wild-type cells were merged (Fig. 5C), 24-hydroxylase fluorescence was present in MAP2 positive dendrites of the neurons. In contrast, co-staining of wild-type cells for 24-hydroxylase and the presynaptic marker protein Rab3A revealed little or no colocalization in the soma or processes (Fig. 5G-I). Neurons from the knockout mice exhibited no 24-hydroxylase signal but the staining patterns for MAP2 and Rab3A were indistinguishable from those of wild-type neurons (Fig. 5D-F, J-L). We concluded from these experiments that 24-hydroxylase was present in the dendrites of cultured neurons but undetectable in the presynaptic termini formed by these cells.

Immunocytochemical experiments with two axonal markers were performed in an effort to detect 24-hydroxylase expression in this type of process. A polyclonal antiserum raised against brain spectrin (Table 1) preferentially stained the initial segments of axons but no colocalization with the 1A7 monoclonal antibody against 24-hydroxylase was detected (data not shown). Similarly, a monoclonal antibody that recognized phosphorylated neurofilaments (SMI-31, Table 1) stained entire axons but the pattern did not overlap with that produced with the 1F4 antibody. Antisera against two other ER resident proteins (P450 reductase, calnexin) also failed to co-localize with these axonal markers. We concluded from these experiments that 24-hydroxylase was either

not present in axons or axonal ER was present in amounts too small to be detected by the light microscopy methods employed.

Localization of 24-hydroxylase in the dendritic ER

The photomicrographs of Figure 6 show double staining for 24-hydroxylase and P450 reductase in neurons cultured from the hippocampus and cortex of E16 wild-type and 24-hydroxylase knockout mouse brains. The merged image from the wild-type neurons (Fig. 6C) demonstrated a high degree of colocalization between the two staining patterns, especially in the cell body. Neurons from 24-hydroxylase knockout mice did not express 24-hydroxylase but did show a normal pattern of P450 reductase staining and a normal neuronal morphology (Fig. 6D-F). At the level of resolution afforded by the photomicrographs of Figure 6A-C, the 24-hydroxylase and P450 reductase proteins appeared to be colocalized in vesicle-like structures distributed throughout the cell bodies and dendrites of the cultured neurons. To explore further this apparent distribution, deconvolved z -stacks of doubly-stained wild-type neurons were enlarged and examined by three-dimensional reconstruction. Figure 7 shows a proximal dendrite stained with 1A7 (panel A) and P450 reductase (B) antibodies and photographed at 100x magnification. In these single z -slices, the vesicular nature of the two staining patterns and their frequent colocalization (Fig. 7C) was still apparent but the images revealed a faint background staining reminiscent of an interconnected reticular network. When the merged image was rendered three-dimensional by computer-assisted assembly and presentation of the entire z -stack, the contiguous nature of the subcellular membrane in which the proteins were located was revealed (Fig. 7D,E). A substantial portion of the

24-hydroxylase staining colocalized with that of P450 reductase as indicated by the white regions in the three-dimensional images. The data of Figure 7F-J from an experiment of similar design show staining for 24-hydroxylase and synaptophysin, a marker of the presynaptic terminal. No colocalization was observed in the merged single *z*-slice image (Fig. 7H) or in the rendered three-dimensional images (Fig. 7I,J).

In additional experiments for which the photomicrographs are not shown, semi-quantitative analyses of rendered three-dimensional images of cultured neurons using Bitplane Imaris software revealed that the staining generated with antisera recognizing four different ER markers had significant Pearson correlation coefficients (>0.5) with 24-hydroxylase staining generated with the 1A7 monoclonal antibody (Table 2). No other subcellular markers tested showed significant colocalization in the merged images or had a Pearson correlation of >0.5 (Table 2, and data not shown).

Cholesterol 24-hydroxylase is expressed in specific neurons of the central nervous system

Immunohistochemical detection of 24-hydroxylase in select subregions of the adult mouse brain was performed next. In the hippocampus, staining of sagittal sections with the 1A7 antibody revealed signal in CA1 pyramidal cell bodies as well as in interneurons of the stratum radiatum (Fig. 8A,C). At higher power, 24-hydroxylase staining was also observed in the dendrites of the pyramidal cells and those of some interneurons in the stratum radiatum (Fig. 8E,F), which confirmed the cellular distribution found in cultured neurons (Fig. 4-7). A lower level of expression was detected in the granule cell layer of the dentate gyrus but hilar interneurons in this sub-region showed strong staining. In agreement with this hippocampal staining pattern,

double immunocytochemistry of wild-type cultured E16 hippocampal and cortical neurons showed strong expression of 24-hydroxylase in γ -aminobutyric acid-positive cells identified by glutamic acid decarboxylase of 67 kDa (GAD67) expression (data not shown). Importantly, no staining was detected in hippocampal sections prepared from animals lacking 24-hydroxylase (Fig. 8B,D). A similar staining pattern was detected in wild-type sections using antibody 1F11, which also showed no staining in knockout sections (data not shown).

Staining of cerebellar sections with the 1A7 antibody revealed robust expression of 24-hydroxylase in the soma and dendritic trees of wild-type Purkinje cells (Fig. 9A,C). In addition, the protein was present in some large cells of the granule cell layer that were provisionally identified as Golgi neurons based on their location and morphology (Crook et al., 2006). Again, no staining was visualized in cerebellar sections from 24-hydroxylase knockout mice (Fig. 9B,D). Antibody 1F11 produced a similar cerebellar staining pattern in the wild-type sections but no staining was observed in knockout sections (data not shown). In these and other immunohistochemical experiments, faint background staining was visible when either antibody was incubated with wild-type sections (e.g., Fig. 9A,C) but not with knockout sections (Fig. 9B,D). We believe this staining may represent 24-hydroxylase in neuropil as it was not detected in knockout sections.

I next determined the cerebellar localization of P450 reductase, the obligate redox partner of 24-hydroxylase and other P450 enzymes, and compared this distribution to that of 24-hydroxylase. As shown in Figure 10A-C, P450 reductase was unexpectedly absent from Purkinje cells, which express calbindin, but was highly expressed in

neighboring cells whose somata were interdigitated among the Purkinje cells and extended processes radially towards the pial surface. The P450 reductase- expressing cells were tentatively identified as Bergmann glia, a cell type known to exist in this location and to exhibit this type of morphology (de Blas, 1984; Sottile et al., 2006). Additional experiments in which cerebellar sections were stained with the anti-P450 reductase antibody and an antibody against a known marker of Bergmann glial cells, S100 (Sottile et al., 2006), showed clear colocalization between these two proteins (Fig.10D-E). In other studies for which the data are not shown, colocalization of P450 reductase in the cerebellum was confirmed with another marker of Bergmann glia, glial fibrillary acidic protein (GFAP) (Custer et al., 2006; de Blas, 1984).

The cortical expression pattern of 24-hydroxylase staining was determined next (Fig. 11A). In sections derived from wild-type mice, strong staining of the somata in Layers II/III, V, and VI was evident whereas little or no enzyme was present in the nonpyramidal cell bodies that comprised Layer IV. Diffuse staining of the neuropil was detected in all cortical layers. The specificity of the antibody was revealed by the absence of staining in cortical sections derived from 24-hydroxylase knockout mice (Fig. 11B). Similar results were obtained in wild-type and knockout cortex using antibody 1F11 (data not shown).

In another series of immunohistochemical experiments, the expression pattern of 24-hydroxylase in the retina was determined using the 1A7 and 1F11 antibodies (Fig. 12A,C). Both antibodies exhibited similar staining patterns in wild-type sections, revealing abundant expression in neurons of the ganglion cell layer and expression in some but not all cells located along one edge of the inner nuclear layer. The 1A7

antibody detected a low level of 24-hydroxylase expression in the retinal pigmented epithelium, whereas this staining was not detected by the 1F11 antibody. No signal was present in retinal sections prepared from 24-hydroxylase knockout mice after incubation with 1A7 or 1F11 (Fig. 12B,D). Nor was 24-hydroxylase staining detected in sections prepared from optic nerve (data not shown).

In additional experiments not shown, the immunohistochemical staining patterns observed for 24-hydroxylase in sagittal sections of the whole brain using the 1A7 and 1F11 antibodies were identical to those for the mRNA established via *in situ* hybridization by the Allen Brain Atlas (<http://www.mouse.brain-map.org>). For this reason, more extensive histochemical surveys were not pursued.

Discussion

The present work describes the preparation of three mouse monoclonal antibodies (1A7, 1F11, 1F4) that recognize 24-hydroxylase and their use in detecting the protein in cultured cells and brain sections. The 1A7 and 1F11 antibodies interact with mouse, rat, rabbit, and human 24-hydroxylase as determined by immunoblotting, while all three antibodies detect recombinant enzyme expressed in transfected CHO-K1 cells and endogenous enzyme present in cultured mouse neurons as judged by immunostaining. Endogenous enzyme was detected immunohistochemically by antibodies 1A7 and 1F11. Within all types of expressing cells, 24-hydroxylase demonstrates a reticular staining pattern that colocalizes with a variety of subcellular markers of the ER. In the soma and dendrites of primary neurons, 24-hydroxylase is present in a contiguous membrane that extends throughout these regions of the cell.

Immunohistochemical detection in brain sections shows high levels of expression in the pyramidal cells of the hippocampus, Purkinje cells of the cerebellum, and neuronal cell bodies in layers II/III, V, and VI of the cortex. Additionally, expression of 24-hydroxylase is found in hippocampal and cerebellar interneurons, in retinal ganglion cells, and in a subset of retinal cells localized to the inner nuclear layer. The enzyme is not detectable using the present procedures in cultured astrocytes or those present in brain sections.

Numerous results presented here confirm the lack of structural abnormalities in the brains of 24-hydroxylase knockout mice (Kotti et al., 2006; Lund et al., 1999), and further substantiate their lack of aberrant brain histology by demonstrating the normal morphologies of cultured embryonic astrocytes and neurons from knockout embryos (Figs. 4,5). The microsomal distribution of P450 reductase, a known ER resident protein, is not altered in brain or cerebellar samples from 24-hydroxylase knockout mice, suggesting the distribution of other ER proteins is normal in these mice. Similarly, the staining pattern of the ER in knockout neurons is indistinguishable from that of wild-type neurons, suggesting again lack of 24-hydroxylase does not affect the generation or morphology of the ER (Fig. 6).

Interestingly, 24-hydroxylase and the enzyme's essential redox partner, P450 reductase, appear to be expressed in different cell types in the mouse cerebellum. Cholesterol 24-hydroxylase is predominantly expressed in Purkinje cells, whereas P450 reductase is localized predominantly to Bergmann glia (Figs. 8 and 9). The physical separation of these two enzymes would seem to preclude 24-hydroxylase enzyme activity in the cerebellum, but two lines of evidence do not support this idea. First, a reduction in

cholesterol synthesis persists, albeit at a lower level, in the isolated cerebella of 24-hydroxylase knockout mice, in which a ~15% reduction in synthesis compared to wild-type mice is measured (Xie et al., 2003); Halford, RW, unpublished observations). Second, 24-hydroxylase knockout mice have modest but statistically significant defects in motor learning (Kotti et al., 2006) (see also Chapter 3), indicative again of a reduction in cholesterol synthesis and a corresponding decrease in geranylgeraniol synthesis. 24-hydroxylase enzyme activity could be explained by the presence of another electron donor in Purkinje cells, such as b5 reductase, which can support cytochrome P450 activity (Finn et al., 2008; Shen et al., 2002); however, b5 reductase does not appear to be highly expressed in Purkinje cells as assessed by histochemical assay and *in situ* mRNA hybridization (Ferri et al., 2005); Allen Brain Atlas, www.brain-map.org). Previous studies have shown cerebellar P450 reductase expression in Purkinje cells alone (Ferri et al., 2005) or in Purkinje cells and Bergmann glia (Norris et al., 1994). Differences in tissue fixation, staining protocols, and species differences between rat and mouse may explain these contrasting results. Furthermore, our studies used a P450 reductase antiserum with documented specificity (Figs. 2 and 3), whereas the above referenced studies provided little or no evidence of antibody specificity. It is interesting to note that the cell-type specific expression patterns of 24-hydroxylase and P450 reductase consistently overlap in other brain regions such as the cortex and hippocampus, which engage in high levels of cholesterol turnover (Figs 6 and 7; Norris et. al., 1994; unpublished observations, Halford, RW and Ramirez, DMO).

The monoclonal antibodies against 24-hydroxylase described here have distinct properties compared to the previously reported rabbit polyclonal anti-peptide antibodies

(Brown et al., 2004; Lund et al., 1999). One monoclonal antibody (1F4) appears to recognize a conformational epitope, whereas the other two (1A7 and 1F11) detect both the denatured and native forms of 24-hydroxylase. These properties suggest that the monoclonal antibodies recognize at least two different epitopes on the 24-hydroxylase protein.

The generation of monoclonal antibodies against 24-hydroxylase was undertaken with two goals in mind. The first objective was to use these more selective probes to confirm and extend preliminary results obtained with a polyclonal antiserum raised against a peptide derived from the sequence of the enzyme. The polyclonal antiserum revealed a neuronal expression pattern for 24-hydroxylase in mouse brain that was substantiated by *in situ* mRNA experiments (Lund et al., 1999); however, this antiserum recognizes two proteins on immunoblots, including 24-hydroxylase and a protein of molecular weight ~53,000, and 24-hydroxylase knockout mice were not available as negative controls at the time this initial expression study was done. Furthermore, many genes that are selectively expressed in the brain shared the same expression pattern as that revealed for 24-hydroxylase by the polyclonal antibody and mRNA hybridization probes, raising the specter of false-positive results. These concerns were eliminated in the current study through the use of multiple monoclonal antibodies and 24-hydroxylase knockout mice, thus meeting the first goal.

The second reason for generating monoclonal antibodies was to more precisely define the subcellular localization of 24-hydroxylase and by doing so provide insight into the enzyme's role in the brain. Subcellular fractionation experiments in this laboratory shown in Chapter Three indicated that 24-hydroxylase was evenly distributed between

presynaptic and postsynaptic membrane fractions (Kotti et al., 2006), suggesting that cholesterol turnover took place in both compartments. This distribution contrasted with results from electrophysiological studies in which presynaptic aspects of neural transmission (miniature synaptic currents, input-output relationships, paired-pulse facilitation ratios) were shown to be normal in hippocampal slices from 24-hydroxylase knockout mice whereas post-synaptic aspects associated with LTP were abnormal (Kotti et al., 2006) (Chapter 3). These data suggested that reduced cholesterol turnover in the post-synaptic compartment caused the impaired LTP observed in the mutant mice.

The current immunocytochemical results clarify these findings by documenting high levels of 24-hydroxylase expression in neuronal cell bodies and dendrites, including those of hippocampal CA1 pyramidal cells in which the electrophysiological measurements were made (Fig. 8A, E). No 24-hydroxylase staining was detected in the axons of primary neurons using the present procedures (data not shown) nor was colocalization observed with presynaptic markers (Fig. 5, 7). Furthermore, 24-hydroxylase was not observed in the axon-rich white matter tracts of the brain or in the optic nerve, which is composed of retinal ganglion cell axons. We now believe that the presynaptic membranes in our earlier study were contaminated with ER based on additional experiments that demonstrated the presence of multiple ER resident proteins in the fraction (Kotti et al., 2006; data not shown), and the extensive subcellular localization data presented here (Table 2). Furthermore, it appears that the amount of ER present in axons is lower than that present in dendrites and thus this subcellular compartment is difficult to detect by light microscopy.

The ER of the neuron as visualized using the 24-hydroxylase monoclonal antibodies is a continuous network that extends throughout the soma and distal dendrites. This picture is consistent with previous ultrastructural observations of the ER in the dendrites and spines of hippocampal pyramidal cells (Spacek and Harris, 1997) and of cerebellar Purkinje neurons (Martone et al., 1993). A morphological study of the ER in these cell types using lipophilic carbocyanine dye (DiI) similarly concluded that the neuronal ER appeared continuous throughout the cell body and dendrites (Terasaki et al., 1994). Recently, an ER-targeted GFP construct was used to visualize the ER in neurons and confirmed the continuous and dynamic nature of neuronal ER (Jones et al., 2008). As an ER resident protein that is present in both the cell body and dendrites, 24-hydroxylase may affect synaptic activity by modulating membrane cholesterol content. The neuronal ER is postulated to serve a number of important functions related to the generation of synaptic transmission, including release of internal calcium stores. The influx of extracellular calcium through the *N*-methyl D-aspartate receptor is an essential mediator of LTP onset; similarly, calcium release from internal stores via ryanodine and inositol (1,4,5)-trisphosphate (IP₃) receptors is required for synaptic plasticity (Berridge, 1998; Raymond, 2007). A functional connection between the somatic and dendritic ER is evident in cultured dopaminergic neurons in which rapid calcium transport occurs between the two compartments, suggesting that dendritic calcium stores are refilled from a somatic reservoir (Choi et al., 2006). Localized changes in membrane cholesterol content mediated by 24-hydroxylase would be expected to change the fluidity of the bilayer and thus perhaps alter calcium flux.

A second major function of the neuronal ER, as in non-neuronal cells, is the synthesis and export of proteins and lipids to the Golgi apparatus. Many secretory organelles have been visualized in dendrites by live-cell imaging, including the ER, exit sites within this organelle, and Golgi “outposts” (Horton and Ehlers, 2003; 2004). Activity-dependent trafficking of α -amino-3-hydroxy-5-methylisoxazole-4-propionic acid (AMPA)-type glutamate receptors to the postsynaptic membrane is necessary for the induction of LTP (Bredt and Nicoll, 2003). The reserve pools of receptors are thought to reside in *trans*-Golgi derived recycling endosomes present in dendritic spines (Ehlers, 2000; Gerges et al., 2004; Gerges et al., 2006; Horton and Ehlers, 2004). Cholesterol turnover mediated by 24-hydroxylase may affect the progress of AMPA receptors through the secretory pathway, thus influencing the availability of these receptors for exocytosis during an LTP-producing stimulus. Alternatively, the regulation of membrane cholesterol content by 24-hydroxylase may affect activity-dependent spine enlargement that depends on lipids delivered by endosomal exocytosis (Kopec and Malinow, 2006; Kopec et al., 2006; Park et al., 2006).

Table 1. Antibodies used in this study.

Antigen	Dilution	Clonality	Species	Immunizing Antigen	References	Source
NADPH-P450 reductase	1:800-1:1000	Poly-clonal	Rabbit	Purified rat liver P450 reductase	Recognizes both native and recombinant protein by immunoblotting and immunofluorescence (Fig 1-3,6) Enriched in microsomal fractions (Fig. 2)	Stressgen Bioreagents, Victoria, BC Canada, #OSA-300
Protein disulfide isomerase	1:500	Poly-clonal	Rabbit	Purified bovine liver PDI	Recognizes a ~58kD protein corresponding to the predicted molecular weight of PDI by immunoblotting (mfr's technical information). See also Mezgrahni et al., 2000; Colombo et al., 2005.	Stressgen Bioreagents, #SPA-890
Brain lipid binding protein	1:1000	Poly-clonal	Rabbit	Recombinant whole BLBP	Recognizes the ~15kD BLBP by immunoblotting (mfr's technical information). BLBP-positive cells exhibit astrocytic morphology and BLBP staining is not present in cultured neurons (Fig 4). See also Feng et al., 1994; Rousselot et al., 1997.	Chemicon, Charlottesville, VA, #AB9558
Calnexin	1:500	Poly-clonal	Rabbit	Synthetic peptide containing amino acids 1-70 of human calnexin	Recognizes a single band at ~90kD, the predicted molecular weight of calnexin (mfr.'s technical information and Kotti et al., 2006). Enriched in microsomal fractions (Ramirez, D., unpublished data).	Santa Cruz Biotechnology, Santa Cruz, CA, #sc-11397
Cytochrome b5 reductase 3	1:100	Poly-clonal	Rabbit	Recombinant human b5 reductase	Recognizes a single band at ~35kD, the predicted molecular weight of b5 reductase (mfr's technical information). Independent antibodies generate ER and mitochondrial staining in a variety of cell types (Colombo et al., 2005; Zhu et al., 2004).	ProteinTech Group, Chicago, IL, #BC004821
Manganous superoxide dismutase	1:100	Poly-clonal	Rabbit	Recombinant human MnSOD	Recognizes the ~24kD MnSOD by immunoblotting (mfr's technical information). Staining pattern is similar to MitoTracker (Invitrogen) staining and recombinant fluorescent mitochondrial targeted protein expression in neurons (Chang and Reynolds, 2006; Beltran-Parrazal et al., 2006).	Upstate Biotechnology, Lake Placid, NY, #06-984
Prohibitin	1:100	Poly-clonal	Rabbit	Synthetic peptide conjugated to KLH derived from within residues 200-300 of human prohibitin	Recognizes a single band at ~30kD representing prohibitin by immunoblotting and produces a mitochondrial staining pattern in HeLa cells by immunofluorescence (mfr's technical information). See also Ikonen et al., 1995.	Abcam, Cambridge, MA, #ab28172

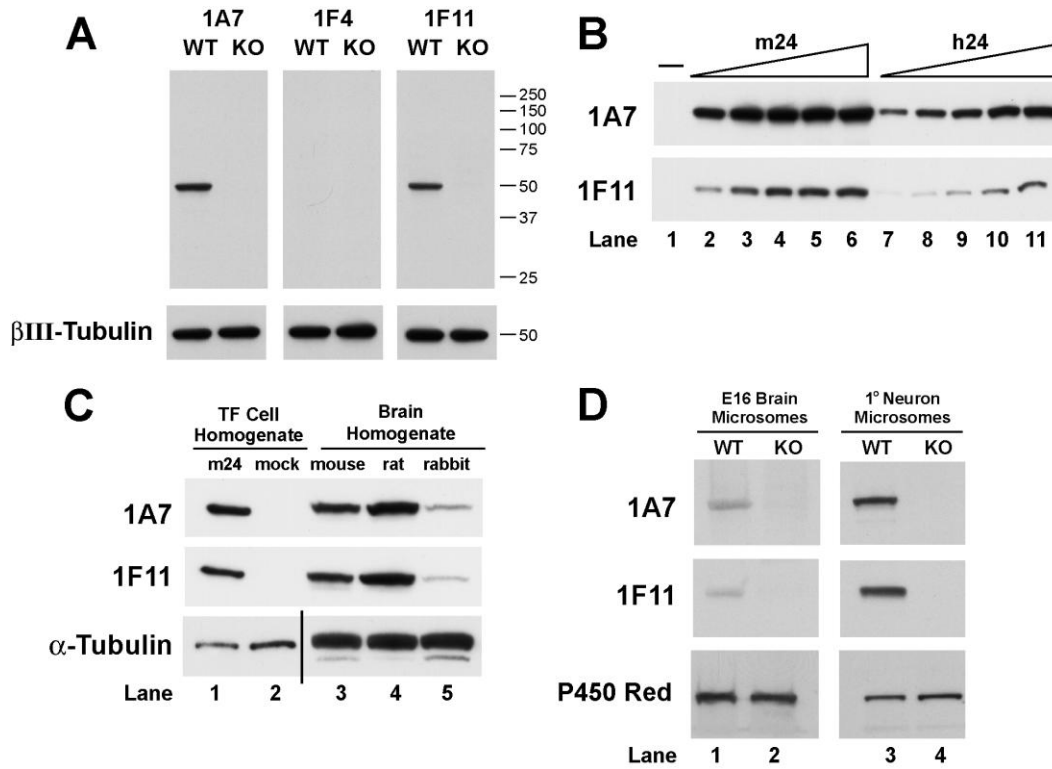
Mannose-6-phosphate receptor	1:500	Monoclonal	Mouse IgG _{2a}	Purified bovine M6PR	Detects a 215kD band representing M6PR under reducing conditions by immunoblotting and immunofluorescence of HeLa cells results in perinuclear vesicular staining (mfr's technical information). Staining pattern in neurons is similar (data not shown).	Abcam, #ab2733
Golgi matrix protein of 130 kDa	1:1500	Polyclonal	Rabbit	Synthetic peptide corresponding to amino acid residues 968-983 of human GM130 with an N-terminal added lysine, conjugated to KLH	Recognizes GM130 (130kD) by immunoblotting. Perinuclear staining concentrated on one side of the nucleus is observed in rat NRK cells (mfr's technical information). An independent antibody produces a similar staining pattern in PC12 cells (data not shown and Sannerud et al., 2006).	Sigma-Aldrich, St. Louis, MO, #G7295
Glutamic acid decarboxylase of 67 kDa	1:600	Monoclonal	Mouse IgG _{2a}	Recombinant fusion protein containing the unique N-terminal regions of GAD67 not shared by GAD65	A single band at ~67kD is detected by western blot of rat cerebellar cortex and mouse brain microsomes (Fong et al., 2005; Kotti et al., 2006). Immunohistochemistry of rat brainstem showed a pattern similar to that previously reported by in situ hybridization (Fong et al., 2005).	Chemicon, #MAB5406
Synaptophysin	1:200	Polyclonal	Rabbit	Synthetic peptide	Detects a single band at the predicted molecular weight of synaptophysin (40kD) in immunoblots of mouse brain microsomes (Ramirez, D., unpublished data). See also Johnston et al., 1989.	Dr. Thomas Sudhof, UT Southwestern Medical Center, #K831
Synapsin	1:200	Polyclonal	Rabbit	Synthetic peptide corresponding to the shared N-terminal regions of synapsins I and II	Detects all four synapsins by immunoblotting (Rosahl et al., 1993).	Dr. Thomas Sudhof, UT Southwestern Medical Center, #E028
Rab3A	1:200	Polyclonal	Rabbit	Synthetic peptide containing the N-terminal sequence of Rab3A (CASCTDSRYGQKE)	Detects a single band at the predicted molecular weight of Rab3A (28kD) in immunoblots of mouse brain microsomes (Kotti et al., 2006). See also Fischer von Mollard et al., 1990.	Dr. Thomas Sudhof, UT Southwestern Medical Center, #P583

β III-Tubulin	1:5000	Monoclonal	Mouse IgG _{2a}	Peptide corresponding to residues 436-450 of neuronal specific β III tubulin; epitope mapped to EAQGPK	Detects a single band at the predicted molecular weight of ~50kD (Fig. 1A). See also Lee et al., 1990; Flajollet et al., 2006, and mfr's technical information.	Upstate Biotechnology, #05-559
α -tubulin	1:2000	Monoclonal	Mouse IgG ₁	Full length native chicken α -tubulin purified from brain; epitope mapped to residues 426-450	Detects a single band at the appropriate molecular weight of ~50kD (Fig. 1C). See also Berasi et al., 2006 and mfr's technical information.	Abcam, #ab7291
Microtubule-associated protein 2	1:500	Polyclonal	Rabbit	Synthetic peptide corresponding to amino acids 1-300 of human MAP-2	Detects a single band at ~70kD, the predicted molecular weight of the low molecular weight isoform of MAP-2 (mfr's technical information). Staining pattern is similar to MAP-2 mAb (Longart et al., 2004; Kosik and Finch, 1987).	Santa Cruz Biotechnology, #sc-20172
S-100	1:100	Monoclonal	Mouse IgG _{2a}	Purified bovine S-100 protein	Specific marker of Bergmann glia in the cerebellum (Sottile et al., 2006) (Fig. 10)	Chemicon, #MAB079-1
Calbindin-D28K	1:3000	Monoclonal	Mouse IgG ₁	Bovine kidney calbindin-D	Specific marker of Purkinje cells in the cerebellum (Custer et al., 2006) (Fig. 10)	Sigma, #C9848

Table 2. Average Pearson correlation coefficients for cholesterol 24-hydroxylase and various subcellular markers as determined by double immunostaining. Wild-type neurons were cultured and immunostained as described in Materials and Methods. Co-localization analysis was performed using Imaris software on a minimum of three neurons from two separate experiments ($n \geq 6$ neurons) to obtain average Pearson correlation coefficients. A Pearson correlation of greater than 0.5 was considered to indicate substantial colocalization between the two proteins. Correlation coefficients between 24-hydroxylase and ER resident proteins were consistently higher than those obtained for proteins found in other subcellular compartments. PDI, protein disulfide isomerase; MnSOD, manganous superoxide dismutase; M6PR, mannose 6-phosphate receptor; GM130, Golgi matrix protein of 130kD; GAD67, glutamic acid decarboxylase of 67kD; ER, endoplasmic reticulum.

Subcellular Marker	Organelle	Average Pearson Coefficient
Calnexin	ER	0.74
PDI	ER	0.71
P450 Reductase	ER	0.68
b5 Reductase	ER	0.6
MnSOD	Mitochondria	0.45
Prohibitin	Mitochondria	0.38
M6PR	Endosome	0.34
Lysotracker	Lysosome	0.27
GM130	Golgi	0.26
GAD67	Presynaptic	0.17
Synapsin	Presynaptic	0.06

Figure 1. Assessment of monoclonal antibody specificity. A. Monoclonal antibodies 1A7, 1F4, and 1F11 were used in immunoblotting experiments of microsomes isolated from whole brain homogenates from wild-type and 24-hydroxylase knockout mice as described in Materials and Methods. 1A7 and 1F11 specifically detected a protein with the predicted molecular weight of 24-hydroxylase (~50,000) whereas 1F4 did not. Immunoblotting with an antiserum recognizing β III tubulin showed that equal amounts of protein were present in each sample. B. Immunoblotting of 24-hydroxylase in transfected CHO-K1 cells. Increasing amounts of total cell homogenate from cells expressing the mouse 24-hydroxylase (m24, lanes 2-6), human 24-hydroxylase (h24, lanes 7-11), and homogenate from mock-transfected cells (lane 1) were separated by SDS-PAGE and subjected to immunoblotting with antibodies 1A7 and 1F11. Both antibodies recognized the mouse and human 24-hydroxylases. C. Cross-species recognition of 24-hydroxylase by monoclonal antibodies 1A7 and 1F11. Transfected (TF) cell homogenates and whole brain homogenates from mouse, rat, and rabbit were subjected to immunoblotting with antibodies 1A7 and 1F11. Both antibodies detect 24-hydroxylase from each of the three species. Immunoblotting with an antiserum recognizing α -tubulin showed that equal amounts of protein were present in each sample. D. Immunodetection of 24-hydroxylase in mouse embryonic brain tissue and cultured neurons. Microsomal membrane proteins were isolated from dissected embryonic day 16 cortex and hippocampal regions or from neurons prepared from these regions and cultured for 14 days *in vitro*. Immunoblotting experiments with 1A7 and 1F11 revealed the 24-hydroxylase protein in both wild-type (WT) preparations, but not in the samples prepared from 24-hydroxylase knockout (KO) mice. Immunoblotting with an antiserum recognizing P450 reductase showed that equal



amounts of protein were present in each sample analyzed. For the detection of 24-hydroxylase, lanes marked *E16 Brain* were exposed to film for 1.5 minutes; those marked *1° Neuron* were exposed to film for 30 seconds.

Figure 2. Assessment of anti-P450 reductase antiserum specificity and P450 reductase distribution in wild-type and 24-hydroxylase knockout brain. A: Homogenates from HEK293 cells expressing either rat P450 reductase or not, wild-type homogenates and microsomal fractions from whole brain and cerebellum were immunoblotted with the P450 reductase polyclonal antibody. A single protein is present in the homogenate and microsomal fractions that corresponds to the predicted molecular weight of P450 reductase, ~78kDa. A protein of the same molecular weight is detected in P450 reductase-expressing HEK293 cells that is absent from the mock-transfected cells. B: Brain and cerebellar homogenates and microsomal fractions from wild-type and 24-hydroxylase knockout mice were subjected to immunoblotting using the P450 reductase polyclonal antibody. Increased levels of P450 reductase were found in the microsomal fraction compared to the homogenate, but no difference was found between wild-type and 24-hydroxylase knockout samples. Analysis of α -tubulin indicated the relative amount of protein present in each lane.

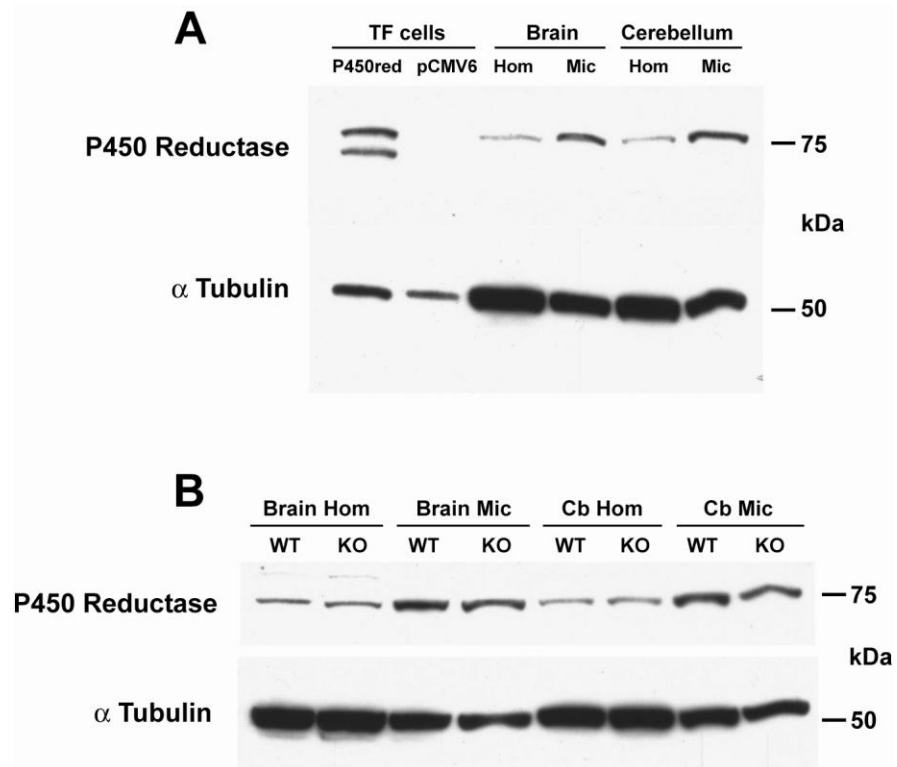


Figure 3. Localization of 24-hydroxylase in transfected cells by immunofluorescence. CHO-K1 cells were transfected with a mouse 24-hydroxylase expression plasmid and stained with the DNA binding dye DAPI and an irrelevant monoclonal antibody, 3C11 (A), or monoclonal antibodies 1F11 (B) or 1F4 (C) that recognize 24-hydroxylase. Green fluorescence represents 24-hydroxylase and nuclear DNA is shown in blue. A reticular staining pattern is observed in expressing cells with 1F11 and 1F4 but not with the irrelevant antibody 3C11. In panels D-F, CHO-K1 cells were co-transfected with mouse 24-hydroxylase and rat NADPH-cytochrome P450 reductase (P450 Red), and then stained with 24-hydroxylase monoclonal antibody 1A7, a rabbit polyclonal antibody recognizing P450 Red, and DAPI. 24-hydroxylase staining is shown in green, P450 reductase staining in red, and DNA staining in blue. The merged image (F) shows strong co-localization, indicated by a yellow color, between exogenously expressed 24-hydroxylase and P450 reductase. In panels G-I, CHO-K1 cells transfected with the mouse 24-hydroxylase plasmid were stained with 1A7, a rabbit polyclonal antiserum recognizing endogenous protein disulfide isomerase (PDI), and DAPI. DNA staining appears in blue, 24-hydroxylase staining in green, and PDI in red. Yellow staining in the merged image (I) indicates that 24-hydroxylase co-localized with endogenous PDI. Scale bar = 5 μm .

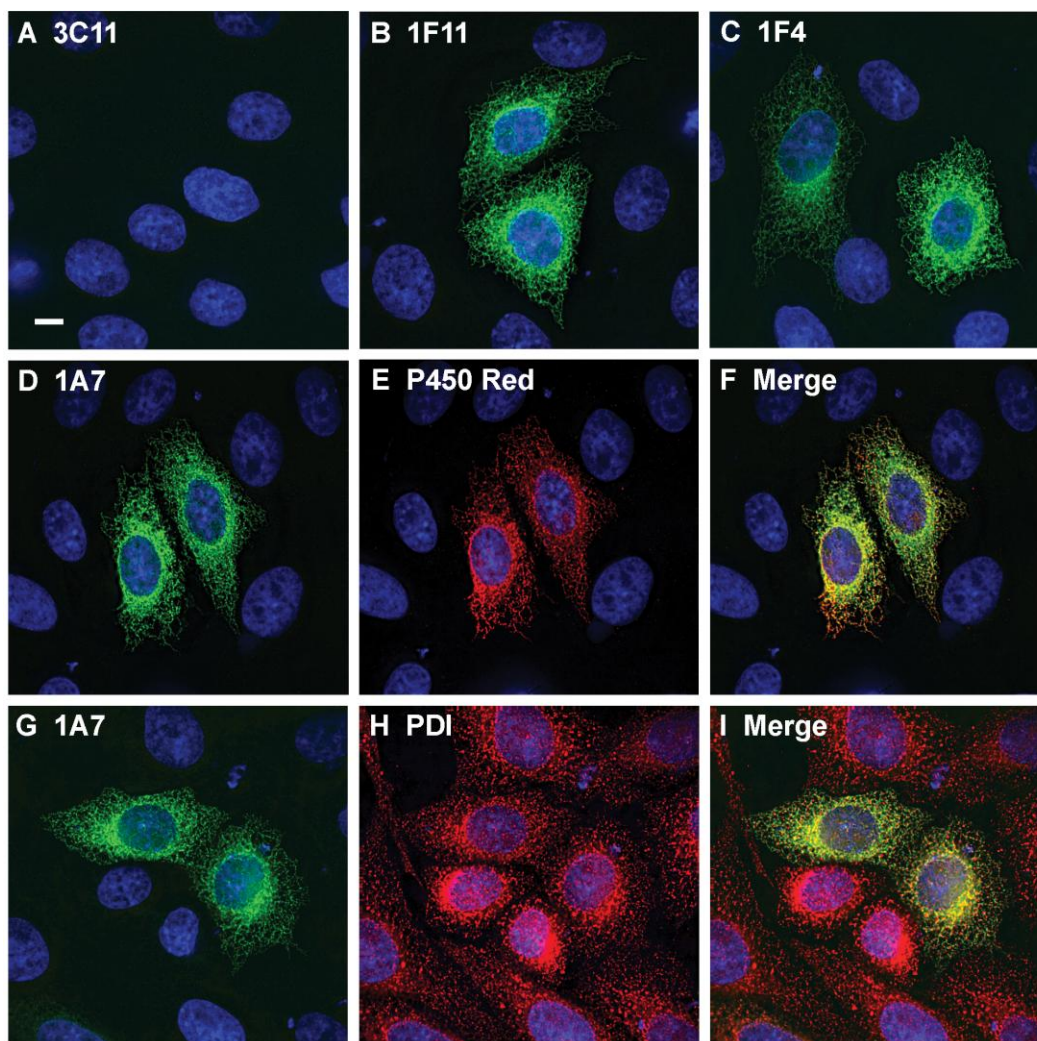


Figure 4. Localization of 24-hydroxylase in cultured neurons by immunofluorescence. Primary neurons prepared as described in Materials and Methods from wild-type (WT) or 24-hydroxylase knockout (KO) mouse embryos as indicated were stained with DAPI and 1A7 (A,B), or 1F4 (C,D), or 1F11 (E,F), or with 1A7 and an antiserum recognizing brain lipid binding protein (BLBP), an astrocyte marker (G,H). DAPI staining appears in blue, 24-hydroxylase staining in green, and BLBP staining in red. 1A7, 1F4, and 1F11 reveal 24-hydroxylase signal in cell bodies and dendrites of cultured wild-type neurons. No 24-hydroxylase staining is detected in neurons from knockout mice. 1A7 staining is present in wild-type neurons but not in BLBP-positive astrocytes. The morphology of astrocytes prepared from knockout mice is indistinguishable from that of wild-type astrocytes as demonstrated by BLBP staining. Scale bar = 10 μ m.

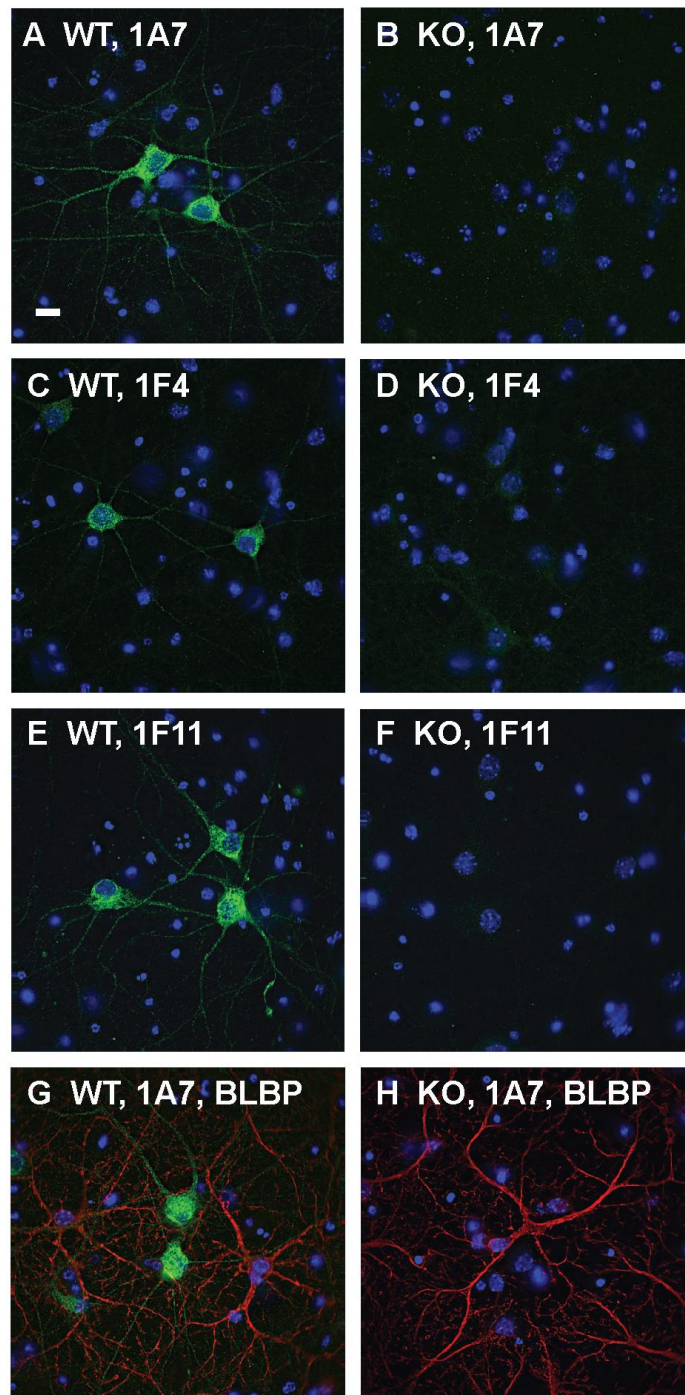


Figure 5. Co-expression of 24-hydroxylase with dendritic MAP2 but not pre-synaptic Rab3A in cultured neurons. Primary neurons prepared as described in Materials and Methods from wild-type (WT) or 24-hydroxylase knockout (KO) mouse embryos were stained with DAPI, 1A7, and a polyclonal antiserum recognizing MAP2 (A-F), or with DAPI, 1A7, and a polyclonal antiserum recognizing Rab3A (G-L). DAPI staining appears in blue, 24-hydroxylase staining in green, and MAP2 and Rab3A staining in red. The merged images from wild-type neurons show overlap between 24-hydroxylase and MAP2 signals (panel C) but no colocalization of 24-hydroxylase and Rab3A (panel I). No 24-hydroxylase staining is detected in neurons from knockout mice (D,J). Neurons from the mutant mice show normal morphology as demonstrated by MAP2 and Rab3A staining (E,K). Scale bar = 5 μ m.

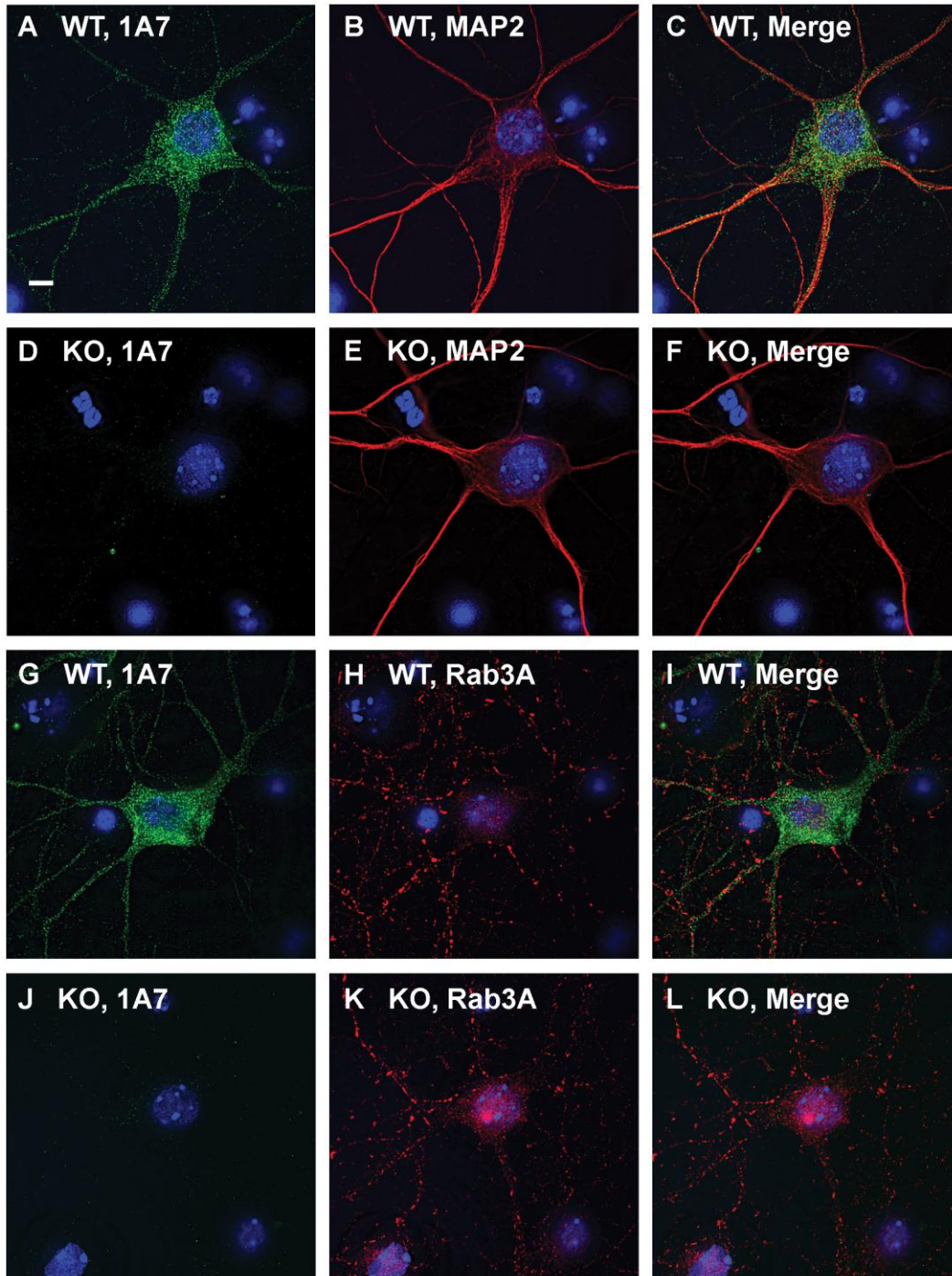


Figure 6. Co-localization of 24-hydroxylase with a known endoplasmic reticulum protein in cultured mouse neurons. A-C: Wild-type (WT) primary neurons were prepared as described in Materials and Methods and stained with DAPI, monoclonal antibody 1A7, and a polyclonal antiserum recognizing the NADPH-cytochrome P450 reductase (P450 Red). 24-hydroxylase staining is shown in green and P450 reductase staining is shown in red. Nuclei are shown in blue. The merged image shows strong colocalization of the two staining patterns in the cell body and somewhat less co-localization in the dendrites. D-F: 24-hydroxylase knockout (KO) neurons were stained with DAPI, 1A7, and P450 reductase antibodies. No staining of 24-hydroxylase (green fluorescence) was detected, although the P450 reductase (red fluorescence) staining pattern was the same as that observed in wild-type neurons. Scale bar = 5 μ m.

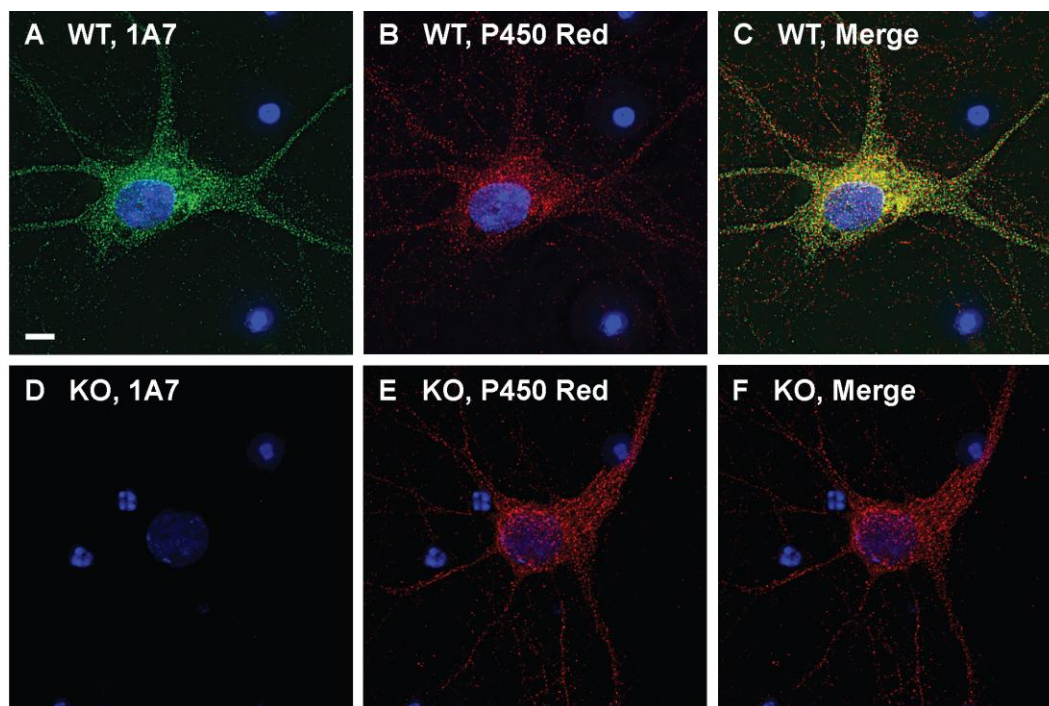


Figure 7. 24-Hydroxylase is expressed in the endoplasmic reticulum, which extends throughout the dendrites of cultured mouse neurons. Wild-type neurons were prepared as described in Materials and Methods and stained with the 1A7 monoclonal antibody recognizing 24-hydroxylase and a polyclonal antiserum recognizing NADPH-cytochrome P450 reductase (P450 Red) (A-E), or 1A7 and a rabbit polyclonal antiserum recognizing synaptophysin (F-J). Sections of proximal dendrites are shown. Merged images on the left (C-E) show many areas of co-localization between 24-hydroxylase and P450 reductase, whereas merged images on the right (H-J) show little or no co-localization between 24-hydroxylase and synaptophysin. Portions of the dendrites (boxed insets C,H) were rendered in three-dimensions, and then enlarged four-times (D,I) and 10-times (E,J). Co-localized pixels are shown in white in these three-dimensional images. The reticular patterns of 24-hydroxylase and P450 reductase are visible. Scale bars = 1 μm in A-H, 0.25 μm in D,I, and 0.1 μm in E,J.

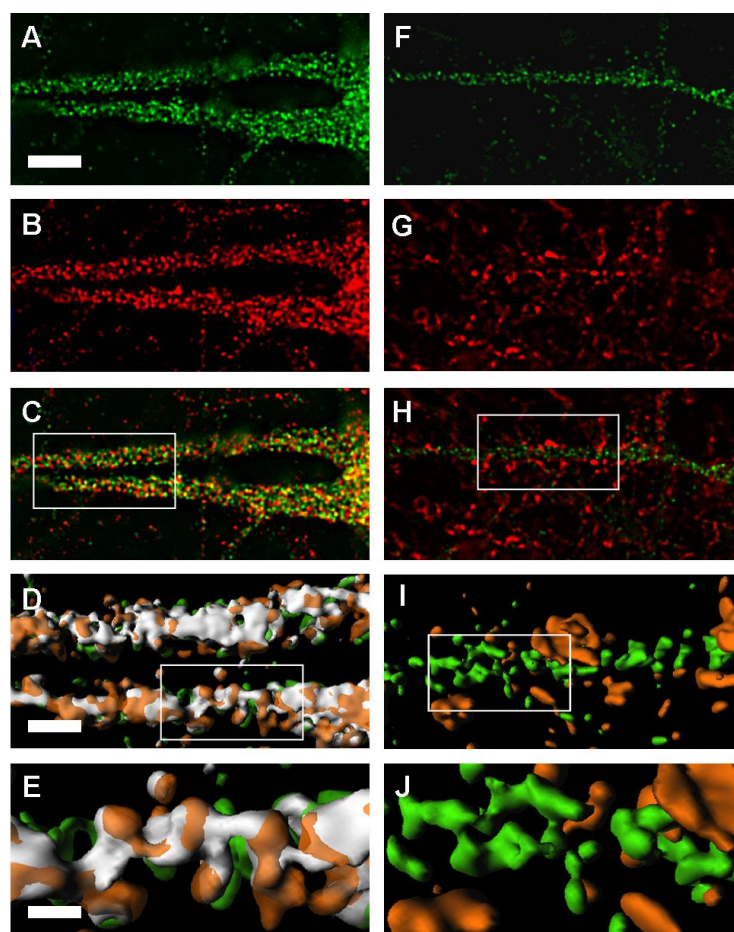


Figure 8. Expression of 24-hydroxylase in the hippocampus. A-F: Cryosections were prepared from female wild-type (WT) and 24-hydroxylase knockout (KO) mouse brains, stained with the monoclonal antibody 1A7, and immunocomplexes visualized by diaminobenzidine-streptavidin-horseradish peroxidase (DAB-HRP) staining. Strong expression was detected in the CA1 region (A), in which 24-hydroxylase staining was visible in the cell bodies and dendrites of pyramidal neurons. Lower levels of expression were detected in the granule neurons of the dentate gyrus, whereas hilar interneurons had high levels of 24-hydroxylase expression (C). No staining was detected in hippocampal sections from knockout mouse brains (B,D). Higher magnification (40X) images of wild-type sections demonstrate 24-hydroxylase staining in CA1 dendrites (E) and those of an interneuron in the stratum radiatum (F). Scale bars = 100 μm in A,B, 50 μm in C,D, and 25 μm in E,F.

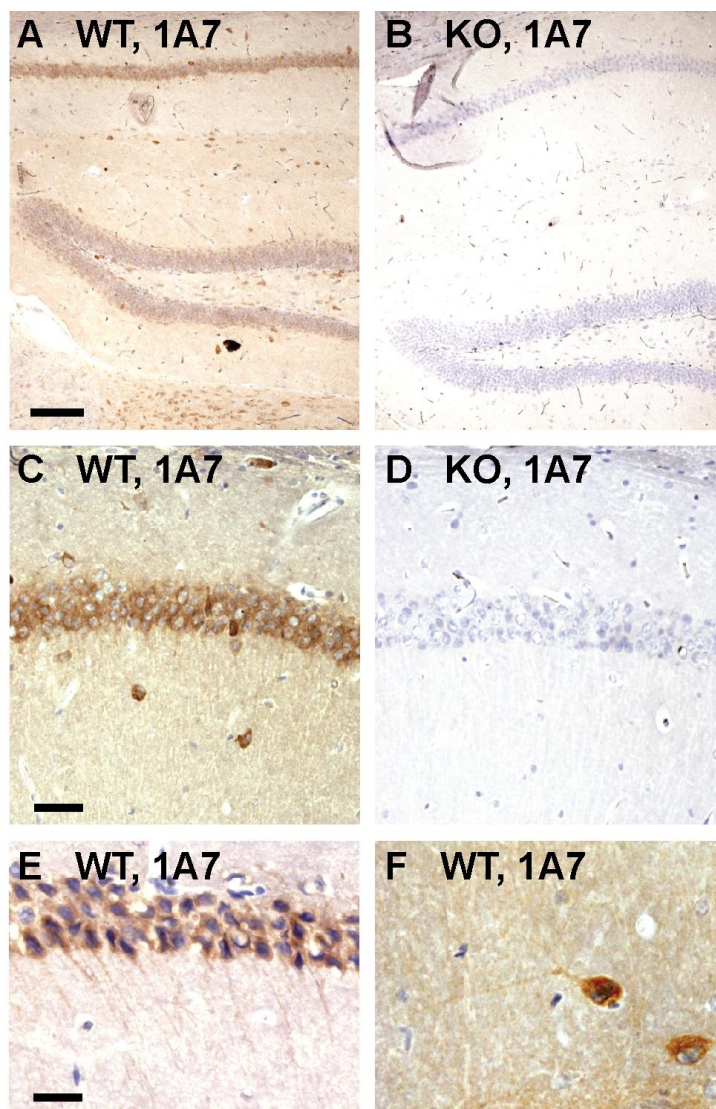


Figure 9. Expression of 24-hydroxylase in the cerebellum. A-D: Cryosections were prepared from female wild-type (A,C) and 24-hydroxylase knockout (B,D) mouse brains, stained with the monoclonal antibody 1A7, and immunocomplexes were visualized by DAB-HRP staining. Strong 24-hydroxylase staining was detected in Purkinje cells and their associated dendritic trees, as well as in some granule cell layer interneurons, which were provisionally identified as Golgi cells (A,C). Cerebellar sections from knockout brains were devoid of 24-hydroxylase staining (B,D). Scale bars = 100 μm in A,B, and 50 μm in C,D.

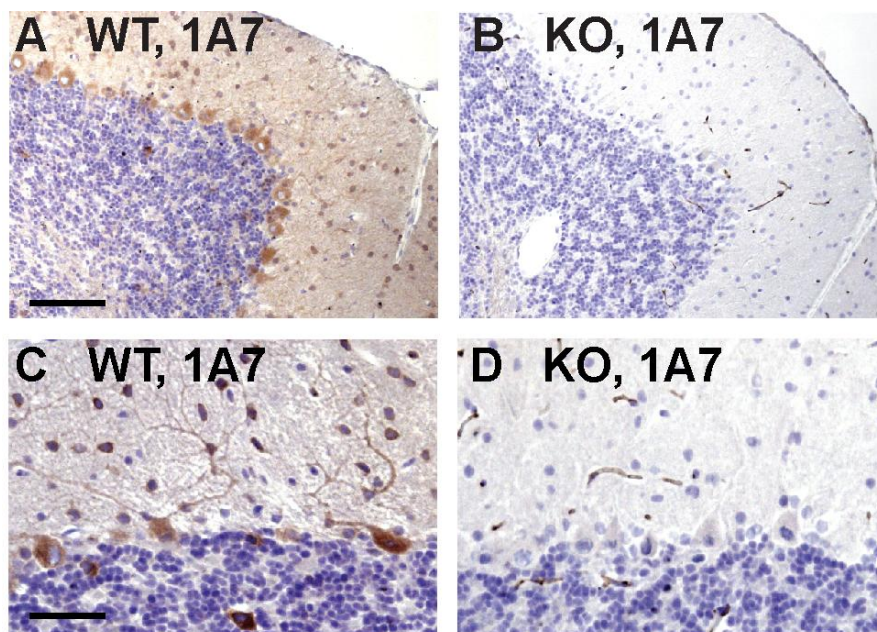


Figure 10. Expression of P450 reductase in the cerebellum. Brain sections were prepared from wild-type mice as described in Materials and Methods, and immunostained with a combination of P450 reductase and calbindin antibodies (A-C), or with a combination of P450 reductase and S100 antibodies (D-F), followed by incubation with Alexa Fluor-conjugated secondary antibodies. All sections were stained with DAPI (blue) as a nuclear marker. P450 reductase staining appears in red, and calbindin or S100 staining appears in green. The merged images show no overlap of P450 reductase and calbindin staining, a marker of Purkinje cells (C), but substantial overlap of P450 reductase and S100 labeling, which marks Bergmann glia (F). Scale bar in C applies to A-C. Scale bar in F applies to D-F.

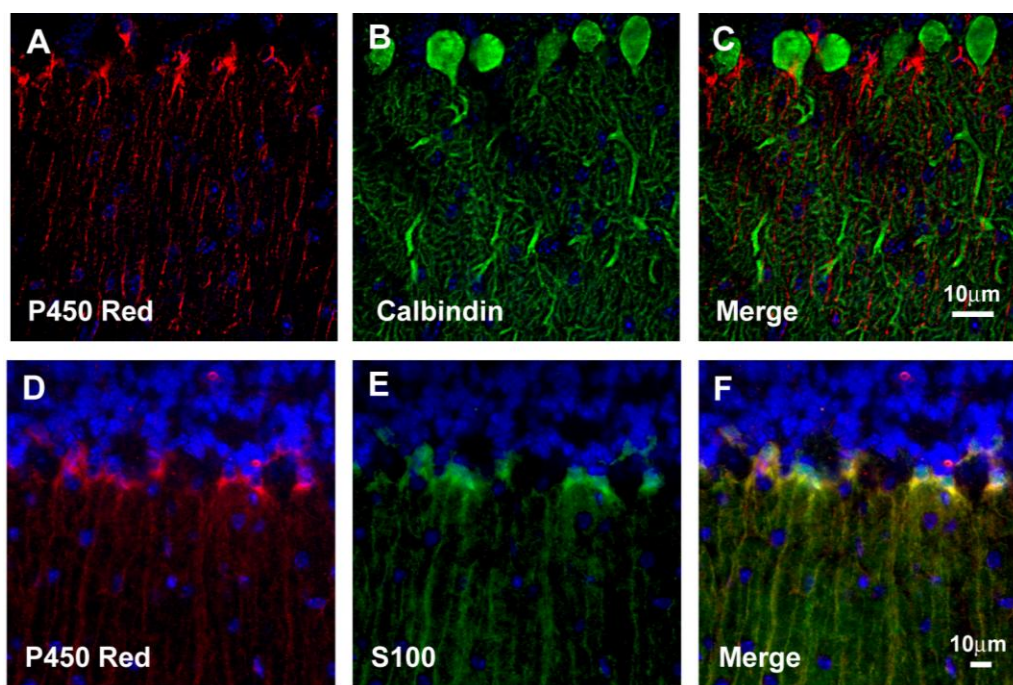


Figure 11. Expression of 24-hydroxylase in the cortex. A,B: Cryosections were prepared from female wild-type (WT) and 24-hydroxylase knockout (KO) mouse brains, stained with the monoclonal antibody 1A7, and immunocomplexes were visualized by DAB-HRP staining. 24-hydroxylase was detected in the somata of cortical neurons within Layers II/III, V, and VI, but not in non-pyramidal neurons of Layer IV or those of Layer I (A). A diffuse staining of the neuropil was present in all layers of the cortex. No staining was visible in cortical sections from knockout brains (B). Scale bar = 100 μm .

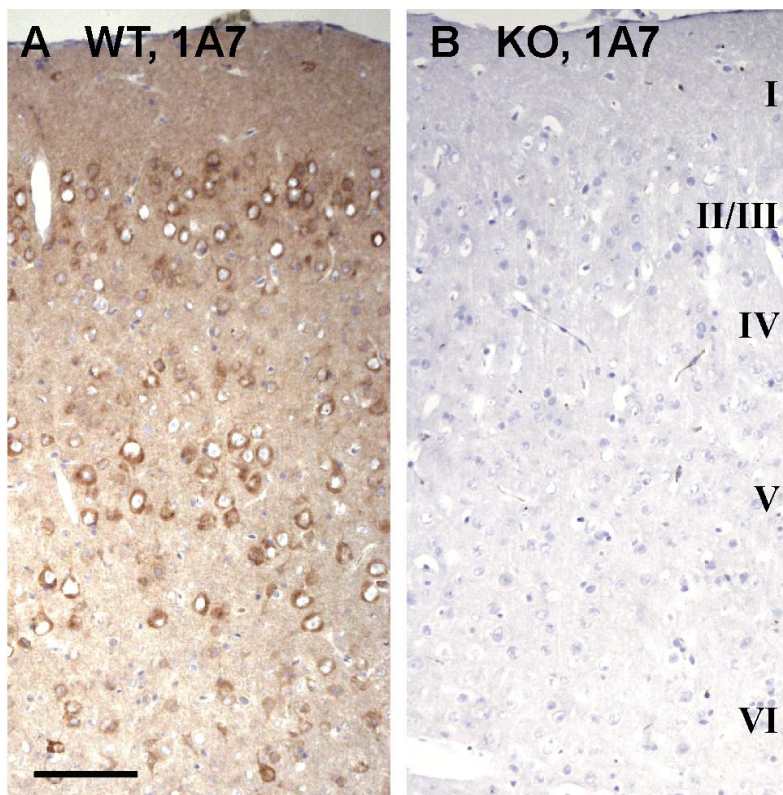
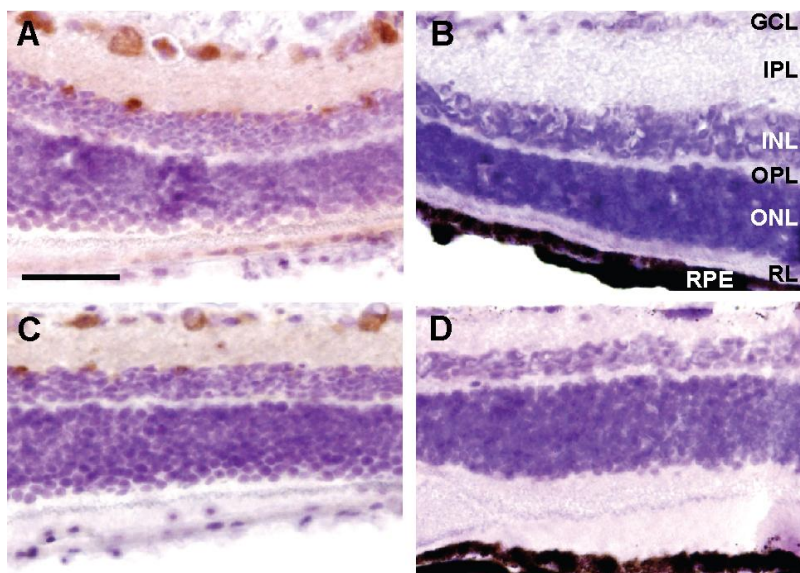


Figure 12. Expression of 24-hydroxylase in the retina. A-D: Cryosections were prepared from male wild-type (WT) and 24-hydroxylase knockout (KO) mouse eyes, stained with monoclonal antibodies 1A7 (A,B) or 1F11 (C,D), and immunocomplexes were visualized by DAB-HRP treatment. Strong 24-hydroxylase staining was observed with both monoclonal antibodies in retinal ganglion cells of the ganglion cell layer (GCL). A lower level of staining was detected with both antibodies in some but not all cells located at the edge of the inner nuclear layer (INL), and by the 1A7 antibody in the retinal pigmented epithelial layer (RPE). No staining was visible in other retinal layers or in retinal sections from knockout eyes. IPL, inner plexiform layer; OPL, outer plexiform layer; ONL, outer nuclear layer; RL, receptor layer. Scale bar = 50 μ m.



CHAPTER THREE

Brain Cholesterol Turnover Required for Geranylgeraniol Production and Learning in Mice

Introduction

The mevalonate pathway is composed of 35 enzymes that synthesize cholesterol and more than a dozen other isoprenoids from mevalonate, the product of 3-hydroxy-3-methylglutaryl CoA reductase (HMG CoA reductase) (Fig. 1, Horton et al., 2002). Among the non-sterol isoprenoids generated by the pathway are farnesyl diphosphate and geranylgeranyl diphosphate, which are covalently linked to a large number of proteins, including GTP binding proteins that play diverse roles within the cell ranging from intracellular signaling to vesicular transport (Pfeffer and Aivazian, 2004). The mevalonate pathway is regulated at multiple levels to prevent the buildup of cholesterol and to ensure a constant supply of non-sterol isoprenoids. The accumulation of cholesterol in membranes activates a negative feedback loop that reduces the levels of transcription factors required for the expression of multiple enzymes in the mevalonate pathway, including HMG CoA reductase (Horton et al., 2002). Cholesterol and isoprenoids also act postranscriptionally to accelerate the degradation of HMG CoA reductase thereby potentially limiting the synthesis of all isoprenoids (Brown and Goldstein, 1980; Goldstein and Brown, 1990; Sever et al., 2003). A class of drugs called statins inhibits HMG CoA reductase directly and therefore has the ability to reduce synthesis of isoprenoids ((Endo, 1992), Fig. 1).

Although the human brain accounts for only a small percentage of body mass (~2%), it contains ~25% of the body's cholesterol. A majority of brain cholesterol is

located in the myelin membranes of oligodendrocytes that surround axons, while smaller amounts are found in the plasma membranes of neurons and other support cells. Cholesterol in the adult brain is largely metabolically inert; however, a small fraction of the pool, estimated to be ~0.02% in humans and somewhat larger in the mouse (~0.4%), turns over each day (Dietschy and Turley, 2004). The major mechanism by which cholesterol is metabolized in the brain is by conversion to 24(*S*)-hydroxycholesterol (Bjorkhem and Meaney, 2004). This reaction is catalyzed by the enzyme cholesterol 24-hydroxylase (24-hydroxylase), a cytochrome P450 (CYP46A1) that is selectively expressed in the brain ((Lund et al., 1999), Fig. 1). The 24(*S*)-hydroxycholesterol diffuses out of cells, crosses the blood brain barrier, and is cleared by the liver (Bjorkhem et al., 2001; Li-Hawkins et al., 2000). Knockout mice lacking 24-hydroxylase have an ~50% reduction in brain cholesterol excretion (Lund et al., 2003). This decrease is compensated for by a reduction in *de novo* synthesis such that steady state levels of cholesterol in the brains of knockout mice are the same as those of wild-type mice. This reduced synthesis is likely to be mediated by a decrease in the activity of HMG CoA reductase.

24-Hydroxylase is expressed in only a small subset of neurons in the brain, including pyramidal cells of the cortex and hippocampus, granule cells of the dentate gyrus, and Purkinje cells of the cerebellum (Lund et al., 1999), but is responsible for a majority of cholesterol turnover in the tissue. When calculated on a per cell basis, 24-hydroxylase expressing neurons turn over cholesterol as fast as any other cell type in the body (Xie et al., 2003), suggesting that cholesterol catabolism in these neurons is of crucial importance. In the current study, we use learning tests in the whole animal and

electrophysiological experiments with hippocampal slices *in vitro* to show that cholesterol turnover via the 24-hydroxylase enzyme ensures activation of the mevalonate pathway and the constant synthesis of geranylgeraniol, which in turn is essential for learning.

Materials and Methods

Animals

Cholesterol 24-hydroxylase knockout (KO) mice harboring a null allele were of mixed strain background (C57Bl/6J;129S6/SvEv) (Lund et al., 2003). LXR $\alpha^{-/-}$, $\beta^{-/-}$ double KO mice on a similar genetic background were from D. Mangelsdorf, UT Southwestern (Repa et al., 2000).

Biochemistry

Presynaptic and postsynaptic membranes were isolated as described (Hell and Jahn, 1998). Synaptic plasma membrane fractionation was performed at 4°C and all buffers contained Complete Protease Inhibitors (EDTA-free, Roche). The hippocampus and cerebral cortex were removed from adult wild-type and 24-hydroxylase knockout mice and homogenized in 15 volumes of ice-cold Tris-acetate (TA) buffer (50 mM Tris pH 7.4, 2 mM CaCl₂, 10% w/v sucrose) with a glass-Teflon homogenizer. Homogenates were centrifuged at 800 x g for 20 minutes to obtain the crude nuclear pellet (P1) and the S1 supernatant. The S1 fraction was centrifuged at 16,000 x g for 30 minutes and the resulting crude mitochondrial pellet (P2) was resuspended in 20 mM HEPES pH 7.4, 2 mM CaCl₂ and centrifuged again at 16,000 x g for 20 minutes. The resulting pellet (P3)

was resuspended in 5 volumes of hypotonic TA buffer (5 mM Tris pH 8.1, 2 mM CaCl₂) and incubated on ice for 45 minutes. Solid sucrose was added to this fraction to 35% w/v and then layered on the bottom of a discontinuous sucrose density gradient. TA buffer containing 20% and 10% w/v sucrose constituted the middle and upper layers, respectively. This gradient was centrifuged for 60,000 x g for 2 hours in a swinging bucket rotor and the synaptosomal fraction was collected from the 35% and 20% sucrose interface. The synaptosomal fraction was diluted with 3 volumes of TA buffer and centrifuged at 30,000 x g for 30 minutes. The resulting synaptosomal pellet was resuspended in TA buffer containing 1% Triton-X-100 and centrifuged at maximum speed in a microcentrifuge for 30 minutes. The supernatant containing the presynaptic membrane fraction was recovered and the pellet containing the postsynaptic membrane fraction was resuspended in TA buffer containing 0.5% v/v SDS.

Microsomal membranes were isolated as previously described (Li-Hawkins et. al, 2000). The procedure was performed at 4°C and all buffers contained Complete Protease Inhibitors (EDTA-free, Roche). Hippocampi were dissected from adult wild-type and 24KO mice and homogenized in 5 volumes of TA buffer (50 mM Tris pH 7.4, 2 mM CaCl₂, 10% w/v sucrose) by trituration with a P200 pipettor followed by passage through a 23 gauge syringe 10-15 times. The homogenates were centrifuged at 600 x g for 10 minutes to obtain the crude nuclear pellet (P1). The S1 fraction was centrifuged at 10,000 x g for 20 minutes to obtain the mitochondrial pellet (P2). The S2 fraction was centrifuged at 130,000 x g for 30 minutes and the resulting pellets containing the microsomal membranes were resuspended in Buffer A (50 mM Tris-acetate pH 7.4, 1 mM EDTA, 20% v/v glycerol, 0.5% v/v SDS).

Immunoblotting

Protein concentration of membrane fractions was determined by BCA Assay (Pierce). 15-30 µg of protein were mixed with 5X SDS sample buffer, boiled for 10 minutes, and separated by SDS-polyacrylamide gel electrophoresis using a 4% stacking/10% separating gel (Bio-rad). Proteins were then transferred to Hybond-C Extra (Amersham) membranes. Primary antibodies were purchased from Upstate Biotechnology except where noted and used at the following dilutions: anti-GluR1 (1:2500), anti-GluR2/3 (1:1000), anti-PSD95 (1:10,000), anti-NR1 C-terminal (1:1000), anti-calnexin (1:1000, Santa Cruz Biotechnology), anti-GAD67 (1:2500, Chemicon International). Presynaptic marker rabbit polyclonal antibodies against synaptophysin, synaptogyrin, synaptotagmin 1, Rab3A, and synaptobrevin 2 were gifts of Dr. T. Sudhof and used at 1:1000 dilution. Hybridoma supernatant containing monoclonal antibodies against cholesterol 24-hydroxylase was also used (Ramirez et al., 2008). Goat anti-mouse (Bio-rad) or donkey anti-rabbit (Amersham) HRP-conjugated secondary antibodies were used and blots were detected by enhanced chemiluminescence (Amersham) and captured on X-ray film (Kodak X-omat blue).

Histology

Mice were perfusion fixed via the heart with 0.9% saline followed by 4% paraformaldehyde in 0.1 M sodium phosphate, pH 7.4. Brains were post-fixed overnight, embedded in paraffin, and coronally sectioned at 10 µm. Immunostaining used primary antibodies from Biodesign and T. Sudhof (UT Southwestern), and Alexa-Fluor-conjugated secondary antibodies from Molecular Probes. For EM, brains were perfusion

fixed with 2% (v/v) glutaraldehyde, 0.1 M cacodylate, pH 8.0. The hippocampus was dehydrated, mounted in resin, and sectioned for transmission electron microscopy.

Behavioral studies

Contextual and cued fear conditioning tests were performed with separate groups of 3-4 mo old male mice (Erbel-Sieller et al., 2004; Garcia et al., 2000). Freezing (total immobilization) was scored at 10 s intervals in real time by an observer and by a video camera running FREEZEFRAME software (Actimetrics). Statistical analyses employed StatView software (SAS Institute) with Mann-Whitney U-parametric and Kolmogorov-Smirnov tests. Threshold tests to determine relative sensitivity to electric shock used a Plexiglas chamber with a metal grid floor (Med Associates). Shock intensity was increased from 0.1 mA to 0.75 mA in four sessions performed at ≥ 1.5 h intervals over a 2-day period.

Morris water maze tests were done on 3-4 mo old male mice. Data were collected in 4 separate experiments with 40 WT and 30 KO mice by 2 experimentalists blinded to mouse genotypes. Latency to reach platform, distance traveled, swim speed, and time along walls were obtained. Probe trials in which the platform was removed were performed as the first trial on days 3, 5, 9, and 12 of each experiment with the same animals. Times spent swimming in target and opposite quadrants were measured together with the number of times mice crossed the former location of the platform. Statistical significance was assessed by Student's t-test.

Motor learning and muscle strength were assessed by rotorod and hanging wire tests (Erbel-Sieller et al., 2004). Mean hang time in the latter test for WT (54.7 ± 1.5 s) and KO mice (42.1 ± 2.2 s) were not significantly different (Student's t-test).

Electrophysiology

Hippocampal slices (400 μ m) were prepared from 5 to 6 wk old mice for LTP experiments, from 20 to 25 day old mice for LTD experiments, and from 14-16 day old mice for single cell recording experiments. LTD and LTP/picrotoxin experiments were done without hippocampal CA3 regions. Artificial cerebrospinal fluid (ACSF) contained 124 mM NaCl, 5 mM KCl, 1.25 mM NaH_2PO_4 , 26 mM NaHCO_3 , 2 mM CaCl_2 , 1 mM MgCl_2 , and 10 mM dextrose, and was equilibrated with 95% O_2 and 5% CO_2 . Field potentials (FPs) were evoked in Schaffer collateral afferents with a concentric bipolar tungsten stimulating electrode (Frederick Haer, Bowdoinham, ME) and recorded from the stratum radiatum of the CA1 region with an extracellular glass capillary electrode. Stimulus intensity was selected as 50–60% of the maximal response (10–30 μ A) and baseline responses were collected every 30 s for 20 min. FPs were filtered at 2 kHz, acquired, and digitized at 10 kHz on a computer using customized LABVIEW software (National Instruments, Austin, TX). The initial slope of the FP was used to measure the stability of synaptic responses and to quantify the magnitude of long-term potentiation (LTP) or long-term depression (LTD). LTP was induced by θ burst stimulation (TBS): four trains, each consisting of ten 100-Hz bursts (four pulses) given at 5 Hz, repeated at 20-s intertrain intervals. LTD was induced by stimuli delivered at 1 Hz for 15 min. After stimulation, signals were recorded for 60 min. Input-output curves were generated by

plotting the mean initial slopes of the excitatory postsynaptic field potentials (fEPSP) versus fiber volley amplitude. Paired pulse facilitation (PPF) experiments used presynaptic stimulations delivered at interpulse intervals of 25, 50, 100, and 200 ms in four trains at 20-s intertrain intervals. Single pulse stimuli were delivered at these time intervals to hippocampal slices from wild-type and knockout mice and fEPSP were measured after each stimulus. The slope values obtained after the second stimulation (S2) were divided by those measured after the first stimulation (S1) to calculate percentage change.

For experiments in which γ -aminobutyric acid type A (GABA_A) receptors were inhibited, ACSF was modified to contain 100 μ M picrotoxin, 119 mM NaCl, 2.5 mM KCl, 1 mM NaH₂PO₄, 26 mM NaHCO₃, 4 mM CaCl₂, 4 mM MgCl₂, and 10 mM dextrose. In the LTP add-back experiments, the ACSF was supplemented with 12.5 μ M compactin (mevastatin/sodium salt; Sigma), 5 μ g/ml cholesterol complexed with methyl- β -cyclodextrin (Cyclodextrin Technologies, High Springs, FL) prepared as described (Adams et al., 2004), 0.2 mM sodium mevalonate, or 0.2 mM geranylgeraniol. For geranylgeraniol supplementation, an aliquot (6.8 μ l) of 100 mM geranylgeraniol (Sigma no. G3278) was first dissolved in 50 μ l of ethanol and then added to the ACSF buffer reservoir. LTP was measured in treated and nontreated hippocampal slices derived from the same brain. Additions were made to the ACSF immediately before baseline measurements and were present through the duration of the experiment. The initial slope of the FP were expressed as percentages of the baseline average and the time-matched, normalized data were averaged across experiments and expressed as means \pm SEM.

Statistical analysis was done with Student's *t* test for the last 10-min interval of measured time.

Single cell recordings were obtained from CA1 pyramidal neurons under visual guidance. Recordings were made at 30°C in a submersion chamber perfused at 3 ml/min with buffer (at pH 7.28 and 320 mOsm) containing 124 mM NaCl, 5 mM KCl, 1.25 mM Na₂PO₄, 26 mM NaHCO₃, 4 mM MgCl₂, 4 mM CaCl₂, 10 mM dextrose, 0.1 mM picrotoxin, and 0.002 mM 2-chloro-adenosine, and saturated with 95% O₂ and 5% CO₂. Whole cell recording pipettes (\approx 2-4 M Ω) were filled with an intracellular solution (at pH 7.2 and 285 mOsm) containing 2.5 mM 1,2-bis(*o*-aminophenoxy)ethane-N,N,N',N'-tetraacetic acid (BAPTA), 125 mM Cs-Meth, 6 mM CsCl, 3 mM NaCl, 10 mM Hepes, 10 mM sucrose, 2 mM N-(2,6-dimethylphenylcarbamoylmethyl) triethylammonium bromide (QX-314), 10 mM tetraethylammonium chloride, 4 mM ATP, 0.4 mM GTP, 14 mM phosphocreatine·Tris.

Results

Behavioral assessment of learning

Spatial learning in 24-hydroxylase knockout mice was assessed in Morris water maze tests (Morris, 1984). As indicated in Fig. 2A, the time required for wild-type mice to find a submerged platform (the latency period) progressively decreased as the animal learned to navigate by visual cues supplied around the tank. In contrast, 24-hydroxylase knockout mice never learned the location of the platform, and instead swam aimlessly until they encountered the platform by chance. When the platform was removed, wild-type mice spent much more time swimming in the area where the platform had been than

did knockout mice (Fig. 2B). Control experiments showed that the knockout mice were not blind and swam normally (data not shown).

Associative learning requires an animal to relate an environmental cue to a mild aversive stimulus such as an electric shock. As shown in the left panels of Fig. 2C, wild-type mice learned to associate a tone with an electric shock and manifest a typical behavior (freezing, or cessation of involuntary movement) upon hearing the sound in the absence of a shock. In contrast, 24-hydroxylase knockout mice were defective in this behavior and stopped moving in response to a tone only half as frequently as did control mice. This defect was manifest at both short (1 h) and long intervals (24 h) after the initial training period. The ability of mice to associate a context (box color and odor) with an electric shock was determined next. When wild-type mice were placed in the scented box in which they had been trained to associate the sound and shock, they froze a high percentage of the time when tested at short and long term intervals after training (Fig. 2C, right panels). The knockout mice were again defective in this form of contextual learning. Control experiments revealed that the mutant mice were not deaf and that their pain thresholds were similar to those of wild-type mice (data not shown).

The cerebellum is associated with motor coordination and learning. The highly innervated Purkinje cells of this tissue express 24-hydroxylase (Lund et al., 1999; Ramirez et al., 2008). The histology and size of the cerebellum is normal in the knockout mice, and they do not exhibit hypotonia, ataxia, or tremor based on observational and open field tests (Lund et al., 2003); however, as indicated by the data of Fig. 2D, the mutant mice displayed defects in motor learning. Whereas wild-type mice were able to double the amount of time they stayed on a rotating rod after a four-day training period,

knockout mice increased their stay times to a lesser extent, and by day three the difference between the two genotypes was significant.

Absence of anatomical defects in knockout mice

Cued, contextual, and associative learning require an intact amygdala and hippocampus (Sweatt, 2003), suggesting that the substandard performance of the 24-hydroxylase knockout mice in the behavioral tests might be due to an anatomical defect in these regions of the brain. To assess this possibility, we performed histological and protein expression analyses. The cellular architecture of the hippocampus and dentate gyrus was indistinguishable between wild-type and knockout mice (Fig. 3A, left panels), as well as in other regions of the brain. Immunohistochemical staining for synaptogyrin, a widely distributed synaptic vesicle protein (Stenius et al., 1995), and for microtubule associated protein 2 (MAP2), a protein expressed in neuronal cell bodies and dendrites (Caceres et al., 1983), were similar in wild-type and knockout mice (Fig. 3A, middle panels). The morphology of the synapse, as examined by electron microscopy, also did not differ between mice of different 24-hydroxylase genotypes (Fig. 3A, right panels).

Immunoblotting of proteins from the hippocampus of wild-type and knockout mice revealed no differences in the levels of several glutamate receptor subunits involved in learning (NR1, GluR1, and GluR2/3), a GTP binding protein involved in synaptic vesicle trafficking (Rab3A), two synaptic vesicle proteins (synaptotagmin and synaptogyrin), an enzyme (glutamic acid decarboxylase, GAD67) involved in the biosynthesis of the neurotransmitter γ -amino butyric acid (GABA), or of calnexin, a chaperone of the endoplasmic reticulum (Fig. 3B).

Synaptic transmission in knockout mice

Changes in synaptic efficacy, or plasticity, are thought to occur during learning and to be required for memory storage. The leading examples of synaptic plasticity are the electrophysiological phenomena termed long-term potentiation (LTP) and long-term depression (LTD), which represent synaptic strengthening and weakening, respectively, in response to electrical stimulation (Bredt and Nicoll, 2003; Malenka and Bear, 2004; Malinow and Malenka, 2002). The neural transmission associated with these processes has both presynaptic and postsynaptic components, and defects in learning can be associated with either of these.

We first examined the subcellular distribution of the 24-hydroxylase at the synapse to determine whether the enzyme acted at the presynaptic or postsynaptic membrane. As indicated in Fig. 4A, 24-hydroxylase was distributed evenly between the presynaptic and postsynaptic membranes from wild-type mice. As expected, the glutamate receptor subunit GluR1 was detected only in postsynaptic membranes, while the synaptic vesicle protein synaptophysin was present only in presynaptic membranes. 24-Hydroxylase was not detected in membranes from knockout mice, and more importantly, the subcellular distributions of GluR1 and synaptophysin were not altered in these membranes (Fig. 4A).

General synaptic transmission was assessed by recording miniature synaptic currents resulting from spontaneous fusion of synaptic vesicles in single pyramidal neurons of the hippocampal CA1 region (Fig. 4B). Measurement of spontaneous currents in wild-type neurons ($n = 11$) from nine hippocampal slices revealed an amplitude of 17.7 ± 1.1 pA (mean \pm SEM) and a frequency of 0.8 ± 0.2 Hz. An amplitude of 19.7 ± 1.5 pA

and a frequency of 1.0 ± 0.1 Hz were recorded in knockout neurons ($n = 14$) from eight hippocampal slices. These values were not significantly different, which suggested that the strength of individual synapses, the number of synapses, and the probability of neurotransmitter release were similar between wild-type and knockout mice.

Consistent with the intracellular measurements of synaptic transmission, excitatory postsynaptic field potentials (fEPSP) recorded at different stimulus intensities in the stratum radiatum of hippocampal slices were similar between animals of different 24-hydroxylase genotypes. No differences were observed between wild-type and knockout slices when the initial slopes of the fEPSP measured in the input-output experiments were plotted against the fiber volley amplitudes (Fig. 4C).

The presynaptic component of plasticity was examined by measuring paired-pulse facilitation in hippocampal slices dissected from 35-40-day old mice. As shown in Fig. 4D, no differences in paired-pulse facilitation responses were detected between wild-type and knockout slices when the interpulse intervals varied between 25 and 200 mS. These data suggested that the presynaptic release probability and short term plasticity were unchanged in the mutant mice.

Defective LTP and normal LTD in knockout mice

We next evaluated LTP and LTD in wild-type and knockout mice. A theta burst stimulation protocol was used to induce LTP in the CA1 region of the hippocampus. Baseline responses recorded in wild-type slices in response to monophasic stimulation were stable, and the application of high frequency stimulation resulted in a robust and long lasting potentiation of synaptic activity (Fig. 5A). In contrast, while baseline

responses were similar in hippocampal slices from knockout mice, LTP was significantly impaired. An induction protocol consisting of 1 Hz stimuli delivered for 15 minutes (900 pulses total) was used to produce LTD in hippocampal slices. As indicated in Fig. 5B, baseline responses were similar and synaptic currents were depressed to equal extents in wild-type and knockout slices in response to this stimulation.

Inhibitory responses in knockout mice

Synaptic activity reflects the balance of excitatory and inhibitory inputs mediated by different neurotransmitter receptors at the postsynaptic membrane. Inhibition in the hippocampus is chiefly mediated by GABA receptors of the A-subtype (GABA_A receptors), which are composed of multiple subunits, including those that bind pregnane steroids which act as agonists of the GABA_A receptor (Belelli and Lambert, 2005). Thus, it was conceivable that cholesterol or 24(S)-hydroxycholesterol binding to a GABA_A receptor subunit might be altered in the knockout mice leading to increased inhibitory input and decreased LTP. To determine if this was the case, we performed LTP experiments in the presence of the GABA_A receptor inhibitor, picrotoxin (Kleschevnikov et al., 2004). This plant toxin increased the magnitude of the LTP response in wild-type slices as would be expected if inhibition were relieved but did not restore LTP in slices from knockout mice (Fig. 7), suggesting that excess inhibition was not the cause of the diminished LTP in the mutant mice.

Metabolic basis of impaired LTP in knockout mice

The 24-hydroxylase knockout mice have two metabolic deficiencies. First, the animals do not synthesize or accumulate 24(*S*)-hydroxycholesterol in the central nervous system, and second, they exhibit an ~50% decrease in *de novo* cholesterol synthesis owing to suppression of the mevalonate pathway ((Lund et al., 2003), see Fig. 1). To explore the role of 24(*S*)-hydroxycholesterol in synaptic plasticity, we measured LTP in hippocampal slices from mice deficient in the liver X receptor (LXR) α and β genes (Repa et al., 2000). 24(*S*)-Hydroxycholesterol is a potent agonist of these nuclear receptors that together regulate numerous aspects of lipid metabolism (Tontonoz and Mangelsdorf, 2003), and it was possible that the absence of the oxysterol caused a decrease in LXR target gene activation and a concomitant reduction in LTP. As shown in Fig. 8, LTP was induced to the same extent in hippocampal slices from wild-type and LXR α/β double knockout mice. In agreement with this finding, microarray experiments and real time PCR measurements of individual mRNAs failed to reveal a difference in LXR target gene expression in the knockout mice (data not shown).

To determine the role of the mevalonate pathway in synaptic plasticity, we measured LTP in wild-type hippocampal slices incubated with compactin, a statin inhibitor of HMG CoA reductase, the rate-limiting enzyme in the pathway. Addition of 12.5 μ M compactin inhibited *de novo* cholesterol synthesis ~80% as assessed by acetate incorporation, and decreased LTP in wild-type slices to an extent similar to that observed in untreated 24-hydroxylase knockout tissue (Fig. 6A).

Mevalonate, the product of HMG CoA reductase, is converted into cholesterol and other biologically relevant end-products, including the isoprenoids farnesyl

diphosphate and geranylgeranyl diphosphate (Fig. 1). To determine whether decreased synthesis of cholesterol or isoprenoids caused loss of LTP, we assessed the effects of these end-products on synaptic plasticity. As shown in Fig. 6B, the addition of cholesterol to compactin-treated hippocampal slices from wild-type mice had no effect on LTP; however, the addition of mevalonate plus cholesterol fully restored LTP. The addition of mevalonate to hippocampal slices from knockout mice restored LTP to levels observed in wild-type tissue (Fig. 6C). In experiments not shown, the addition of cholesterol or compactin to knockout slices had no effect on LTP, and the addition of pyruvate, which is converted into acetate for use in the mitochondrial tricarboxylic acid cycle, did not restore LTP. The 15-carbon isoprenoid farnesol is a direct intermediate in the synthesis of cholesterol, while the 20-carbon isoprenoid geranylgeraniol is synthesized from farnesol but cannot be converted into cholesterol (Kellogg and Poulter, 1997). The data of Fig. 6D show that the addition of geranylgeraniol alone to hippocampal slices from knockout mice restored LTP to levels observed in wild-type slices. A quantitative analysis of the LTP data presented in Fig. 6 appears in Fig. 9.

Discussion

A striking aspect of the current data is that LTP can be suppressed by incubation of hippocampal slices with the HMG CoA reductase inhibitor compactin for only 20 minutes. It is highly unlikely that cholesterol becomes depleted in this short time period. Moreover, LTP is restored by the addition of geranylgeraniol, which cannot be converted to cholesterol. This result is consistent with a previous report of tetanic LTP inhibition after statin treatment (Matthies et al., 1997). In mammalian cells geranylgeraniol is

activated to geranylgeranyl diphosphate by a salvage pathway (Crick et al., 1997). The major product derived from this activated intermediate is the geranylgeranyl group attached to small GTP binding proteins such as Rab, Rac, and Rho (Colicelli, 2004), which regulate vesicular transport and cytoskeletal/membrane interactions (Sinensky, 2000). We therefore hypothesize that one or more of these proteins are crucial for LTP. This protein must require a constant supply of freshly synthesized geranylgeranyl diphosphate, either because the protein turns over rapidly or because the geranylgeranyl group is constantly removed and degraded. Statin treatment interrupts the supply of geranylgeranyl diphosphate and leads to loss of function of the prenylated protein, which in turn disrupts LTP, and presumably behavioral learning in the whole animal. In the 24-hydroxylase knockout mice, the block in cholesterol excretion leads to a slight buildup in neuronal cholesterol, which is expected to decrease transcription of the HMG CoA reductase gene and accelerate degradation of the protein (Goldstein and Brown, 1990; Sever et al., 2003). The decrease in HMG CoA reductase limits the supply of geranylgeranyl diphosphate, reduces the amount of the crucial geranylgeranylated protein, and blocks LTP. This deficit can be reversed in vitro by addition of mevalonate or geranylgeraniol to hippocampal slices.

The LTP experiments reported here measure synaptic activity between pyramidal neurons of the CA3 and CA1 regions of the hippocampus. These cells normally express 24-hydroxylase (Lund et al., 1999; Ramirez et al., 2008), and in the intact animal they are implicated in spatial and associative learning (Sweatt, 2003). A major mechanism by which LTP is established involves the recruitment of new α -amino-3-hydroxy-5-methyl-4-isoxazole propionic acid (AMPA) receptors to the synapse by a calcium-mediated

signaling pathway (Bredt and Nicoll, 2003; Malenka and Bear, 2004; Malinow and Malenka, 2002). The movement of intracellular AMPA receptors to the cell surface involves membrane fusion, which requires several small G proteins that are posttranslationally modified by the addition of geranylgeranyl groups (Park et al., 2004; Zhu et al., 2002). An isoprenoid requirement for AMPA receptor trafficking would presumably be selective for LTP as many aspects of membrane fusion including those at the presynaptic terminal and LTD appear normal in the knockout mice. This hypothesis also cannot explain all of the phenotypes observed in these animals as spatial learning is normal in mice that lack an AMPA receptor subunit required for hippocampal LTP (Zamanillo et al., 1999).

The current data raise the question of why the brain relies on cholesterol excretion to ensure a constant supply of geranylgeraniol rather than regulating the expression of the prenyltransferase enzyme that synthesizes the isoprenoid? This reliance on *de novo* synthesis may reflect the need to coordinate the synthesis of isoprenoids with that of cholesterol to produce adequate amounts of both endproducts. Alternatively, the pathway may be a consequence of the blood brain barrier, which prevents the removal of cholesterol from cells via their interactions with plasma lipoproteins. Learning in the intact mouse may also require both geranylgeraniol and the localized turnover of cholesterol at the synapse or elsewhere by 24-hydroxylase.

Statins are widely prescribed for the treatment of hypercholesterolemia and act by inhibiting the production of mevalonate (Fig. 1). While it is abundantly clear that most of the therapeutic benefit derives from lowering plasma levels of cholesterol (Grundy et al., 2004), it has been suggested that the associated reduction in non-sterol

isoprenoid synthesis may also contribute to the beneficial outcome (Liao, 2002; Topol, 2004). Anecdotal reports of amnesia and memory loss are reported in some patients on statins (Wagstaff et al., 2003), which raises the question of whether this side effect may be caused by inhibition of cholesterol synthesis in the human brain producing an outcome similar to that observed in 24-hydroxylase knockout mice. We think this scenario is unlikely for two reasons. First, the concentration of statin used to inhibit LTP in vitro is much higher than that obtained in therapy. Second, large clinical trials indicate no significant differences in cognitive abilities between placebo- and statin-treated subjects (Group, 2002).

To conclude, cholesterol is typically thought of as an abundant component of membranes that plays a largely structural role in the lipid bilayer. The current studies expand this role and indicate that a constant breakdown of the molecule is required for learning. Hebb postulated in 1949 that learning at the cellular level involved a “growth process or metabolic change” in neurons leading to synaptic strengthening (Hebb, 1949). Geranylgeraniol synthesis appears to be one of the metabolic changes that must occur for learning.

Figure 1. Schematic of the mevalonate pathway. Arrows indicate the flow of intermediates, and brakes indicate pharmacologic and genetic inhibition of the indicated steps. PP, diphosphate.

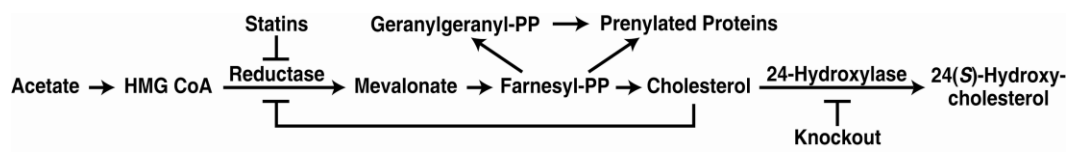


Figure 2. Assessment of behavioral learning. (A) Spatial learning in Morris water maze tests. Mean time to find a submerged platform (latency) is shown as a function of trial day. Data were collected in four different experiments involving 40 wild-type (+/+) and 30 knockout (-/-) mice. Error bars in this and all other experiments represent SEM values. (B) After removal of the platform on the indicated day, the number of times animals of the two genotypes swam across the former location of the platform was determined. (C) Associative learning in cued conditioning fear tests. Percent freezing was measured in response to an auditory cue 1 h after the training period (upper left panel) and 24 h after training period (bottom left panel), or in response to the context in which the training was performed after 1 h (upper right panel) or 24 h (lower right panel). Data were collected in two different experiments involving 30 +/+ mice and 30 -/- mice. (D) Motor learning in rotating rod tests. The mean times mice of the indicated genotypes stayed on the rotating rod are plotted as a function of trial day. Data were collected from 15 (+/+) and 15 (-/-) mice. Behavioral testing experiments were performed by Tiina Kotti and Daphne Head.

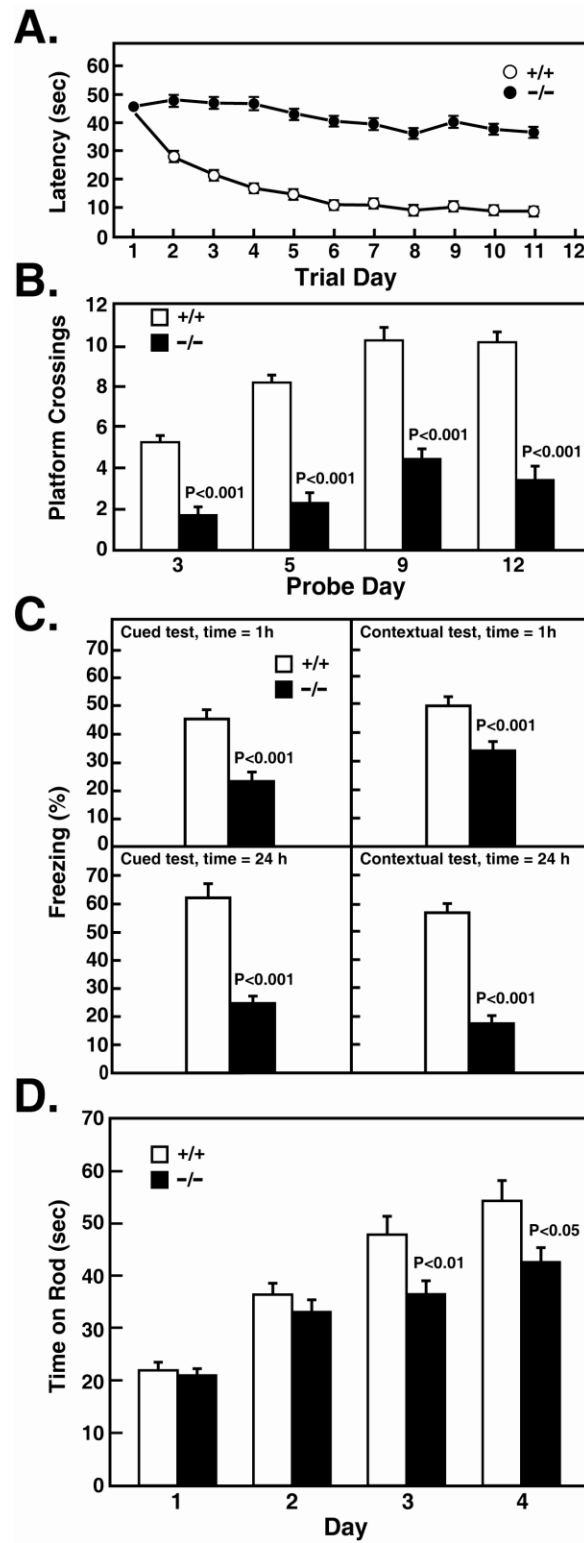


Figure 3. Histology and protein expression in the hippocampus. (A) Hematoxylin and eosin staining of hippocampal sections from wild-type (+/+) and knockout (-/-) mice are shown in the left panels. CA, cornu ammonis; DG, dentate gyrus; bar = 50 μ m. Histochemical staining for cell nuclei (DAPI, blue), and double immunofluorescent staining for MAP2 (antibody AP20, green) and synaptogyrin (antibody P925, red) in the CA1 region of the hippocampus is shown in the middle panels. Bar = 20 μ m. Electron microscopic analyses of synaptic contacts on pyramidal cell dendrites in CA1 stratum radiatum are shown in the right panels. Arrows indicate synaptic clefts. Bar = 400 nm. (B) Protein expression assessed in hippocampal extracts by immunoblotting. The levels of three glutamate receptor subunits (NR1, GluR1, and GluR2/3), a small GTP binding protein (Rab3A), two synaptic vesicle proteins (synaptotagmin and synaptogyrin), glutamic acid decarboxylase (GAD67), and calnexin were determined. H&E staining and assessment of synaptic proteins was performed by Denise Ramirez. Immunofluorescence and electron microscopy were performed by Radha Ram and the Molecular and Cellular Imaging Facility at UT Southwestern, respectively, under the supervision of Denise Ramirez.

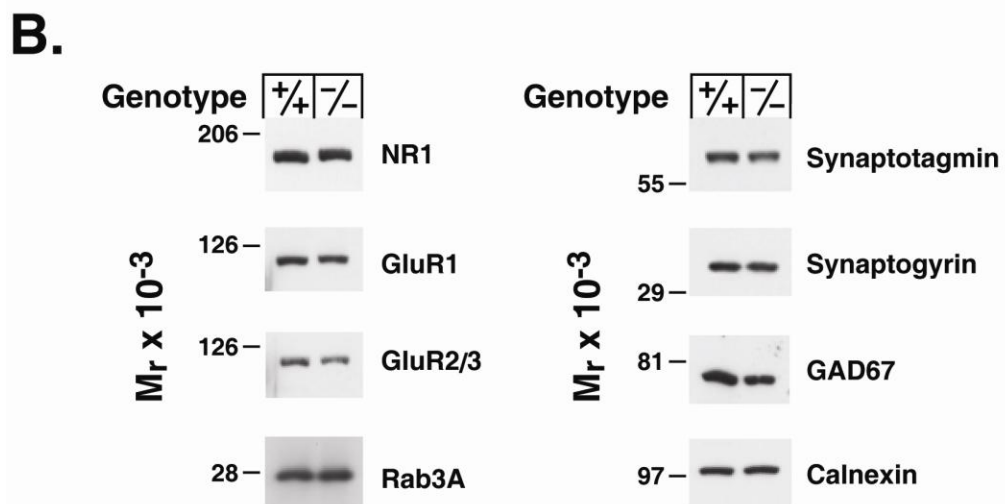
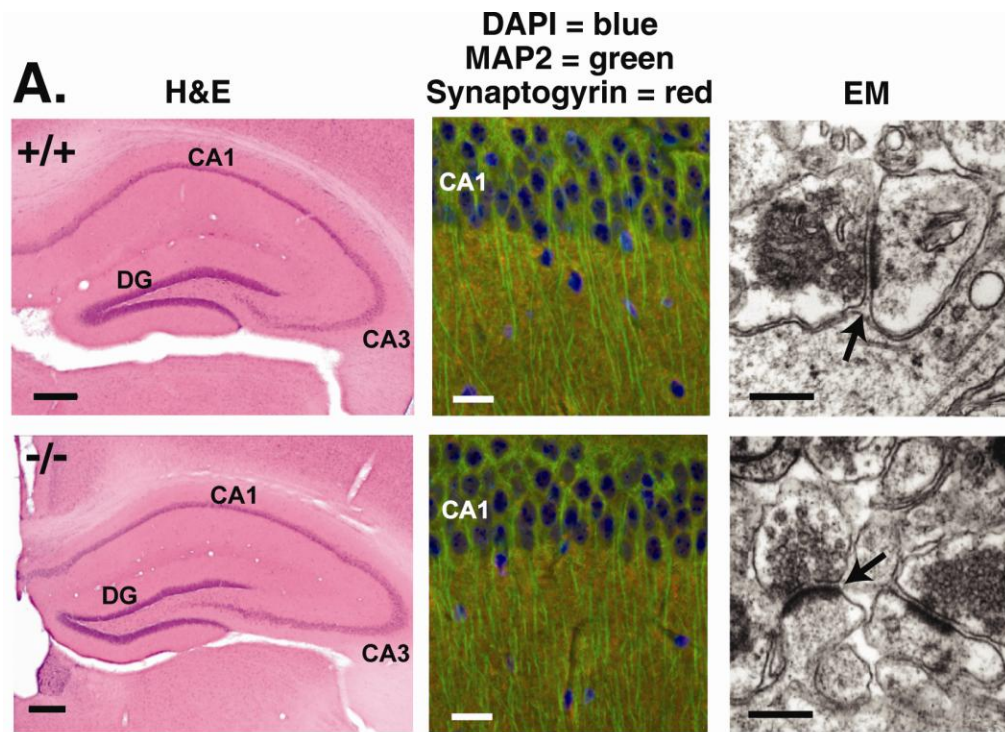


Figure 4. Synaptic transmission in wild-type and 24-hydroxylase knockout mice. (A) The indicated hippocampal membrane fractions from wild-type (+/+) and knockout (-/-) mice were probed for 24-hydroxylase, the GluR1 glutamate receptor subunit, and synaptophysin. (B) Spontaneous miniature synaptic currents in single CA1 pyramidal neurons in the presence of 1 μ M tetrodotoxin. Representative traces from recordings made from 11 +/+ (\circ) and 14 -/- (\bullet) neurons. (C) Input-output curves. Field potentials were determined in wild-type (\circ , n = 14) and knockout slices (\bullet , n = 13) over a stimulus intensity range of 5 to 40 μ A. (D) Short term plasticity assessed by paired-pulse facilitation. Data from two different experiments with 43 +/+ (\circ) and 28 -/- (\bullet) slices. Synaptic fractionation was performed by Denise Ramirez. mEPSC recordings were performed by Brad Pfeiffer in the laboratory of Dr. Kim Huber at UT Southwestern. Input-output curves and paired-pulse facilitation experiments were performed by Tiina Kotti.

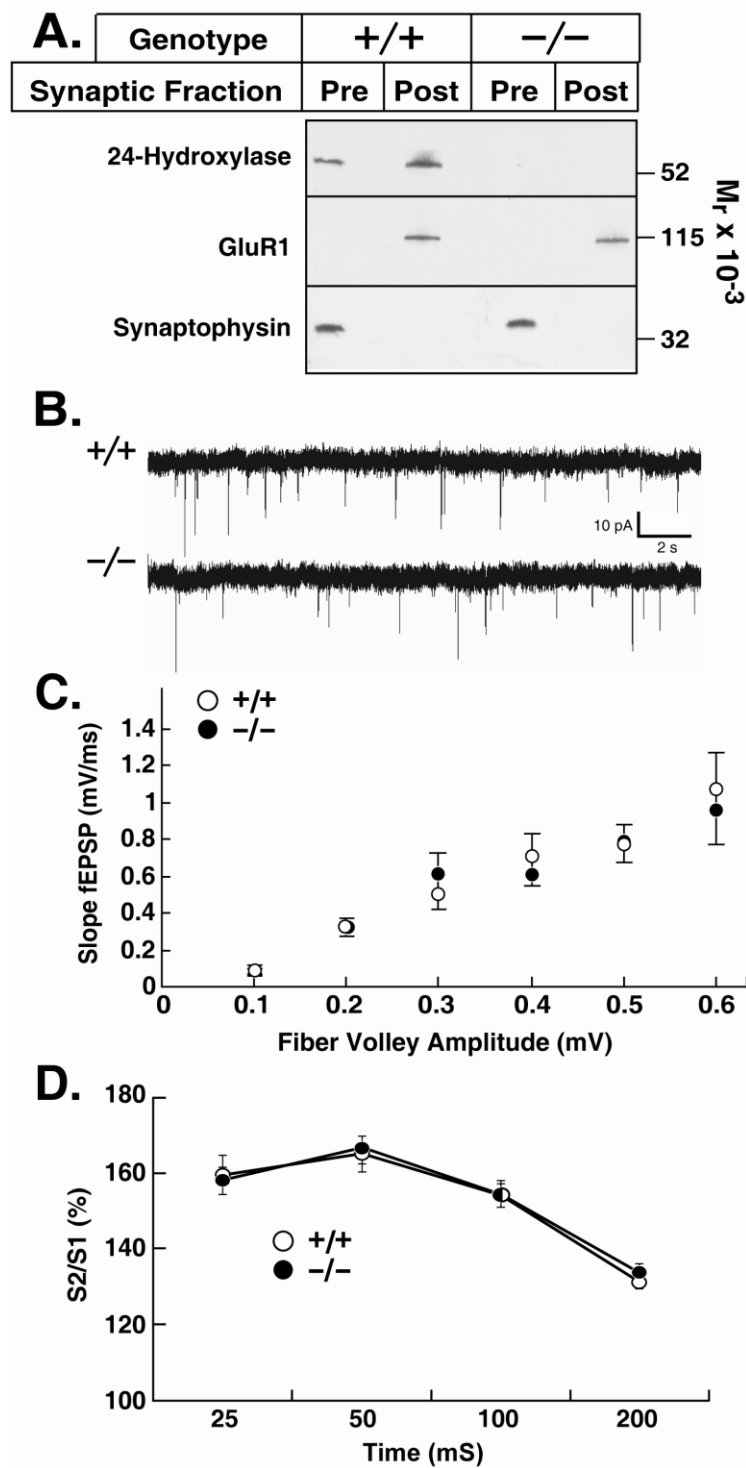


Figure 5. Impaired hippocampal LTP and normal LTD in 24-hydroxylase knockout mice. (A) LTP in hippocampal slices from wild-type (○, n=19) and knockout (●, n=13) mice. The arrow marks the point of high frequency stimulation (theta burst). Insets in this and all subsequent experiments show representative recorded potentials immediately before (dashed lines) and 55 min after tetanization (solid lines). (B) LTD in hippocampal slices from wild-type (○, n=13) and knockout (●, n=10) mice. Experiments shown in this figure were performed by Tiina Kotti.

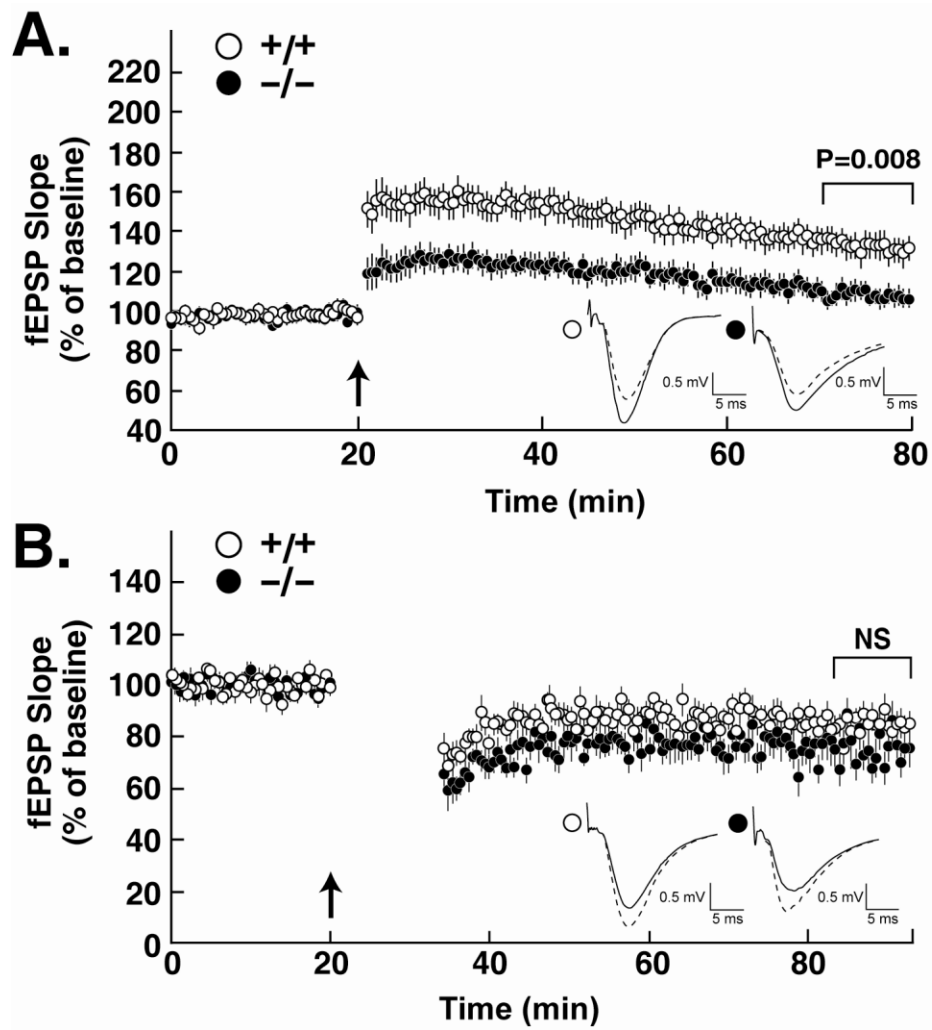


Figure 6. Restoration of LTP by mevalonate and isoprenoids. (A) Hippocampal slices from wild-type mice were incubated beginning at time zero with no additions (\circ , n=11) or 12.5 μ M compactin (statin, \bullet , n=17), and LTP was induced after 20 min. (B) Reversal of compactin mediated LTP inhibition by mevalonate (Mev) but not cholesterol (Chol). Hippocampal slices from wild-type mice were incubated with 12.5 μ M compactin, 0.2 mM mevalonate, and 5 μ g/ml cholesterol (\circ , n=13), or 12.5 μ M compactin and 5 μ g/ml cholesterol (\bullet , n=10). (C) Mevalonate restores LTP in 24-hydroxylase knockout mice. Hippocampal slices were incubated in the absence of additions (\bullet , n=10) or in the presence of 0.2 mM mevalonate (\circ , n=12). (D) Geranylgeraniol (GG) restores LTP to wild type levels. Hippocampal slices from wild-type mice (\circ , n=18) were incubated with no additions. Slices from knockout mice (\bullet , n=12) were incubated with 0.2 mM geranylgeraniol. Experiments shown in this figure were performed by Tiina Kotti.

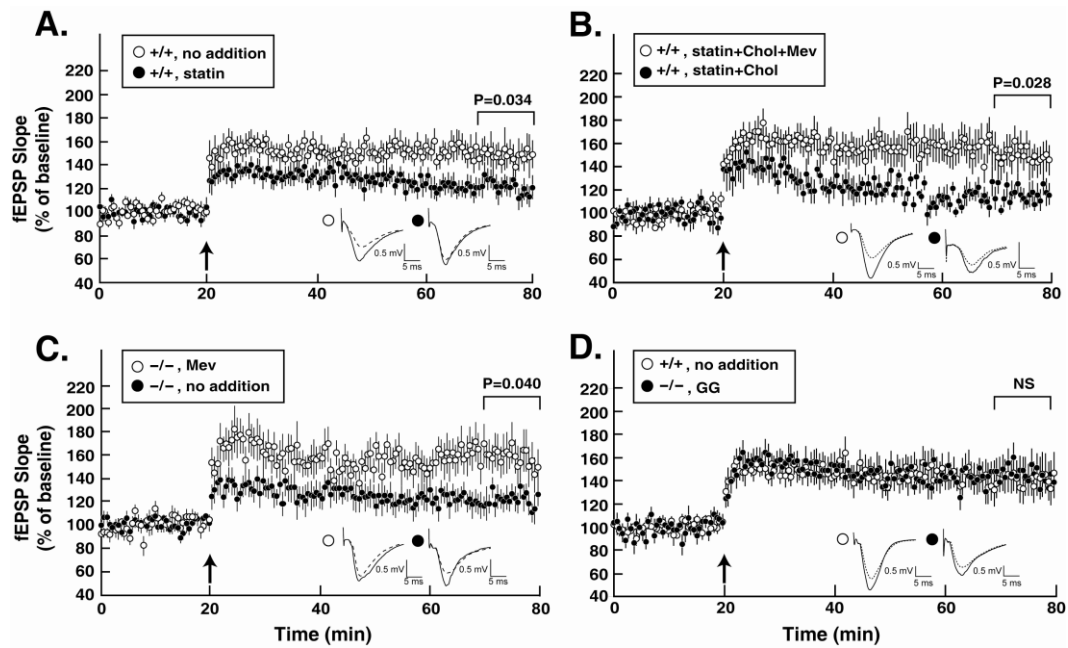


Figure 7. Long-term potentiation (LTP) deficit persists in the absence of γ -aminobutyric acid type A (GABA_A) receptor-mediated inhibition. Hippocampal slices from wild-type (○, $n = 11$) and cholesterol 24-hydroxylase knockout (●, $n = 15$) mice were incubated in the presence of 100 μ M picrotoxin to block inhibitory neural transmission mediated by GABA_A receptors. LTP was induced by high frequency stimulation (arrow) and the resulting increase in synaptic output measured over a period of 60 min. (*Inset*) Representative recorded potentials immediately before (dashed lines) and 55 min after (solid lines) tetanization. Experiments shown in this figure were performed by Tiina Kotti.

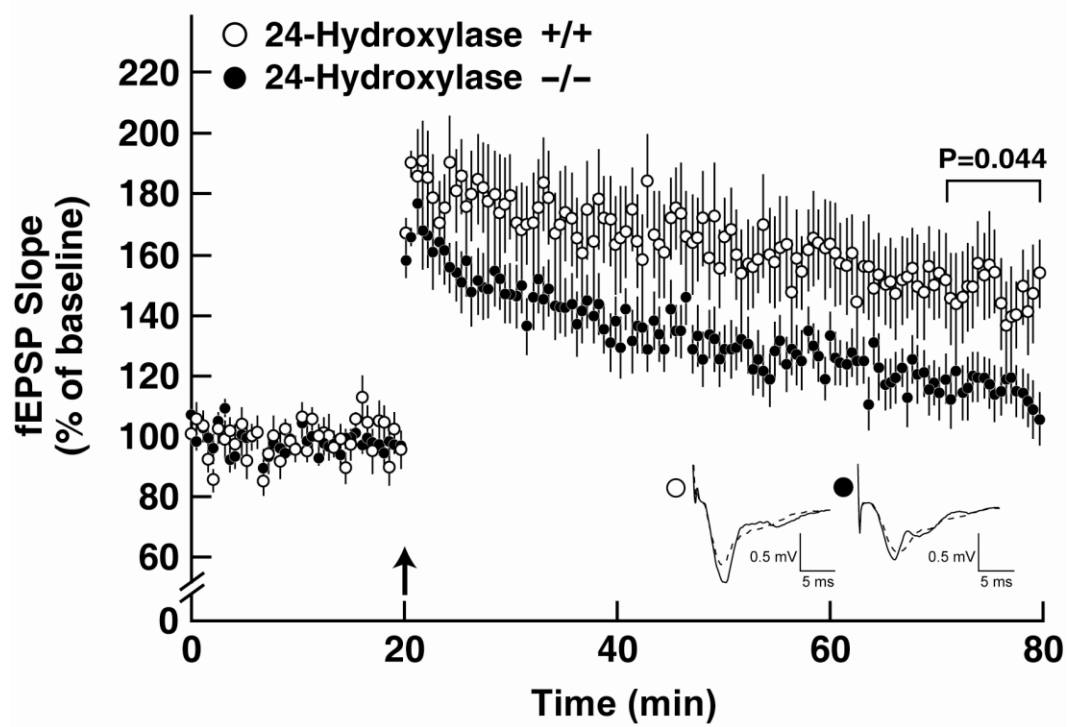


Figure 8. Absence of liver X receptor (LXR) effects in long-term potentiation (LTP). Hippocampal slices from wild-type mice (\circ , $n = 16$) and LXR α , LXR β double knockout mice (\bullet , $n = 16$) were subject to high frequency stimulation (arrow), and LTP was recorded. Experiments shown in this figure were performed by Tiina Kotti.

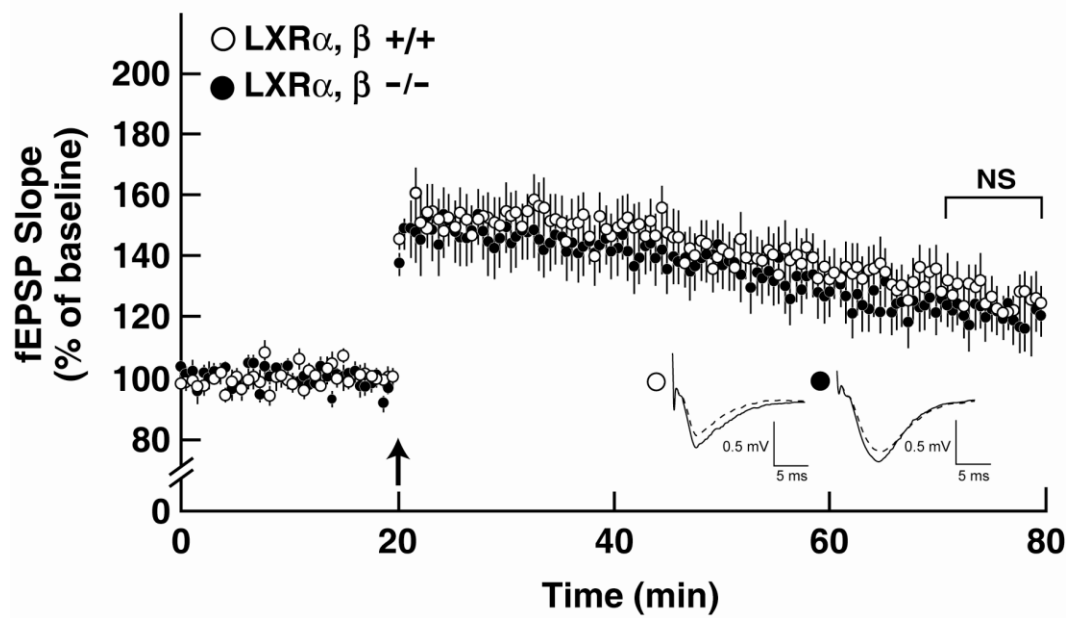
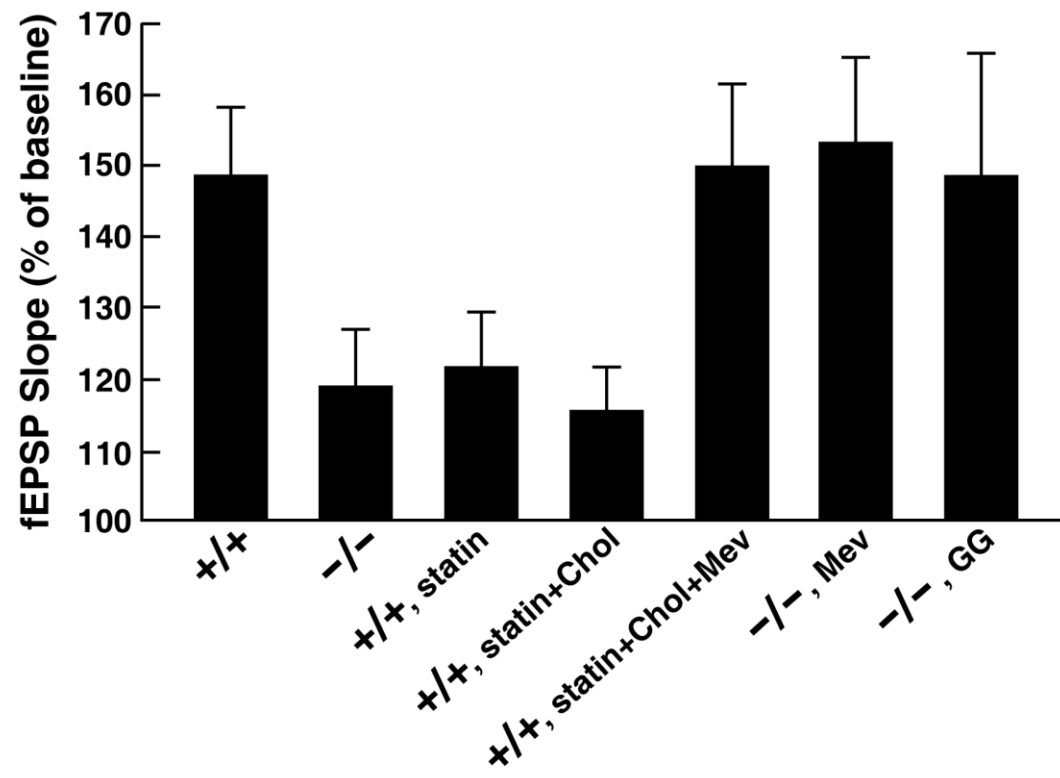


Figure 9. Quantitation of statin, mevalonate, and geranylgeraniol effects on long-term potentiation (LTP). The magnitude of the excitatory postsynaptic field potentials (fEPSP) signals collected between 70 and 80 min in the various experiments shown in Fig. 6 *A–D* was averaged. Error bars represent SEM values. Experiments shown in this figure were performed by Tiina Kotti.



CHAPTER FOUR

Role of Geranylgeraniol in *N*-Methyl-D-Aspartate Receptor Function

Introduction

The role of brain cholesterol turnover and necessity of a specific biosynthetic intermediate (geranylgeraniol; GG) in the induction and maintenance of hippocampal long-term potentiation (LTP), a molecular correlate of learning and memory, have been established by studies presented here (Chapter 2) (Kotti et al., 2006) and elsewhere (Kotti et al., 2008). LTP at Schaffer collateral-CA1 synapses is known to be dependent on the *N*-methyl-D-aspartate (NMDA) subtype of ionotropic glutamate receptor (NMDAR) (Bartlett et al., 2007; Lau and Zukin, 2007; Yashiro and Philpot, 2008). NMDARs are required for LTP induction by virtue of their ability to coincidentally detect presynaptic glutamate release and postsynaptic depolarization, as well as their high permeability to calcium. Postsynaptic calcium influx through NMDAR triggers downstream processes involved in the expression of LTP, such as α -amino-3-hydroxy-5-methyl-4-isoxazole propionic acid (AMPA)-type glutamate receptor (AMPA) insertion into postsynaptic membranes and changes in spine morphology (Kopec et al., 2006; Lau and Zukin, 2007; Park et al., 2006; Yashiro and Philpot, 2008). Further increases in postsynaptic calcium during LTP result from temporary insertion of calcium-permeable AMPARs into the postsynaptic membrane as well as increases in voltage-gated calcium channel (VGCC) activity (Biou et al., 2008; Plant et al., 2006; Raymond and Redman, 2002; 2006).

The kinetics and magnitude of NMDAR-mediated calcium influx are crucial determinants of the direction of synaptic plasticity (synaptic strengthening accompanying

LTP versus weakening accompanying long-term depression (LTD)) and are strongly influenced by the subunit composition of NMDARs (Yashiro and Philpot, 2008). NMDARs are generally believed to exist primarily as di-heteromeric receptors containing two obligatory NR1 subunits and two modulatory NR2 subunits. The predominant NR2 subunits expressed in the forebrain are the NR2A and NR2B subunits, although low levels of the NR2D subunit are also present. NR2C expression is restricted to the cerebellum (Al-Hallaq et al., 2007; Stephenson, 2001). The NR1/NR2A and NR1/NR2B heteromeric receptors (abbreviated here as NR2A or NR2B) differ in many ways, including developmental expression, channel biophysical properties, subcellular localization, posttranslational modification, and intracellular binding partners (Al-Hallaq et al., 2007; Erreger et al., 2005; Lau and Zukin, 2007; Li et al., 2002; Petralia et al., 2005; Sans et al., 2000; Yashiro and Philpot, 2008). While definitive identification of specific NMDAR subtypes important for different types of synaptic plasticity is still debated in the literature, it seems clear that subtype-specific roles for NR2A and/or NR2B are present in LTP and LTD (Bartlett et al., 2007; Bellone and Nicoll, 2007; Erreger et al., 2005; Gardoni et al., 2009; Izumi et al., 2006; Kohr et al., 2003; Kutsuwada et al., 1996; Li et al., 2007; Liu et al., 2004; Morishita et al., 2007; Sakimura et al., 1995; Weitlauf et al., 2005; Yashiro and Philpot, 2008).

Here I report additional mechanistic characterization of the role of GG in hippocampal LTP. Ratiometric calcium imaging measurements of wild-type and 24-hydroxylase knockout cultured embryonic neurons show GG specifically modulates NMDAR function in a subtype-specific manner, without affecting the activity of other ion channels involved in LTP. Neurons cultured from 24-hydroxylase knockout embryos

are more sensitive to the NR2B-specific antagonist, ifenprodil. Biochemical analyses of synaptic and surface NMDAR subunits in wild-type and 24-hydroxylase knockout hippocampal slices show similar NR2B/NR2A ratios in these functional receptor pools isolated from animals of different 24-hydroxylase genotypes, suggesting NMDAR subtype expression and channel assembly are not influenced by GG. Therefore, GG may influence NMDAR subtypes directly and specifically in an as yet unidentified manner.

Materials and Methods

Ratiometric Calcium Imaging

Calcium imaging experiments were performed on mouse embryonic cortical and hippocampal neurons cultured for 11-14 days, using modifications of previously published work (Chen et al., 2005; Tang et al., 2005). Primary neurons were prepared as described in Chapter 3 and plated on poly-D-lysine coated glass coverslips in 24-well plates. On day 1 after plating, the mitotic inhibitor cytosine β -D-arabinofuranoside (AraC; #C1768, Sigma) was added to the medium from a 400 μ M stock to a final concentration of 4 μ M. This treatment generated essentially pure neuronal cultures with only a few astrocytes present as judged by immunocytochemical staining with specific markers for neurons (MAP2) and astrocytes (BLBP) (data not shown). Neurons were loaded with 2 μ M cell-permeant Fura-2 AM ester (#F1225, Invitrogen) for 30 minutes at 37°C in normal artificial cerebrospinal fluid (ACSF) containing the following (in mM): 124 NaCl, 5 KCl, 1.2 NaH₂PO₄, 26 NaHCO₃, 10 dextrose, 2 CaCl₂, and 1 MgCl₂, rinsed once, transferred to fresh ACSF and incubated for an additional 15 minutes at 37°C to allow for ester cleavage. For experiments measuring the responses of voltage-gated

calcium channels, neurons were loaded and imaged in normal ACSF and stimulated with 50 mM KCl in the same fluid. For experiments measuring the responses of calcium-permeable AMPARs, neurons were loaded with Fura-2 and imaged in normal ACSF supplemented with 1 μ M tetrodotoxin (TTX; #T5651, Sigma), 5 μ M nimodipine (#N149, Sigma), and 50 μ M D(-)-2-amino-5-phosphonopentanoic acid (AP5; #A8054, Sigma) and stimulated with either 20 μ M or 40 μ M glutamate (#G8415, Sigma). For experiments measuring the responses of NMDARs, neurons were loaded with Fura-2 and imaged in ACSF lacking $MgCl_2$ and supplemented with 1 μ M TTX, 5 μ M nimodipine, and 40 μ M 6-cyano-7-nitroquinoxaline-2,3-dione (CNQX; #C239, Sigma), and stimulated with 1-80 μ M NMDA plus 10 μ M glycine. Some NMDAR experiments also included 1 μ M ifenprodil (#I2892, Sigma) for the duration of the experiment. For measurement of NMDAR responses in the absence of extracellular calcium, neurons were imaged in calcium-free ACSF prepared as described above but lacking $CaCl_2$ and additionally supplemented with 100 μ M ethylenediamine tetraacetic acid (EDTA; #15575-038, Invitrogen). For measurement of NMDAR responses in the presence of thapsigargin (#T9033, Sigma), 2 μ M thapsigargin was included throughout the experiment. Geranylgeraniol (GG; #G3278, Sigma) was added at 200 μ M GG to supplemented ACSF from a 50 mM stock in absolute ethanol.

After Fura-2 loading and washing, coverslips were mounted onto a recording/perfusion chamber (#RC-26G, Warner Instruments) and placed on the stage of an inverted microscope (IX-70, Olympus). A gravity-fed perfusion system supplied supplemented ACSF to the coverslip during the baseline recordings. Images at 340 nm

and 380 nm excitation wavelengths were acquired using a 40X UApo, 1.35 NA oil-immersion objective every 2 seconds for a period of 50 frames. Baseline images were taken for the first 20 frames of the experiment, ACSF was emptied from the perfusion chamber, the appropriate stimulating agent was added directly into the perfusion chamber (500 μ L total volume), and the perfusion system was stopped. Thirty additional frames were recorded after the addition of stimulating agent.

For data analysis, the change in the 340/380 ratio (ΔR) was calculated for each neuron. Data from multiple experiments and multiple preparations of cultured neurons were averaged to generate average ΔR values as shown in Figures 1-4. ΔR was calculated according to the formula $\Delta R = R_{\text{peak}} - R_{\text{basal}}$. The basal 340/380 ratio (R_{basal}) was calculated as the average ratio from frames 5-19 before stimulation and the peak 340/380 ratio (R_{peak}) was calculated as the average ratio from frames 30-50 after stimulation. For each coverslip, the mean R_{basal} was calculated, and any neuron with an R_{basal} value falling outside one standard deviation of the mean was excluded from ΔR calculations. In Figures 1-4, n = number of individual neurons imaged.

Calcium imaging of HEK-293 cells was performed by seeding cells onto poly-D-lysine coated glass coverslips in 24-well plates at a density of 10,000 cells/well. The cells were transfected two days later using Fugene 6 as described in Chapter 3 with plasmids encoding rat NR1 (pRK7-NR1) and mouse NR2B (pRK5-NR2B). Plasmids were a generous gift of Dr. Joachim Herz, UT Southwestern Medical Center. A total of 0.5 μ g of DNA was transfected per well, at a 2:1 ratio of NR2B plasmid to NR1 plasmid. Four hours after transfection, AP5 was added to 1 mM final concentration to prevent

excitotoxic death of expressing cells. NMDAR expression was verified by immunocytochemistry in some experiments (data not shown). Calcium imaging experiments were performed 20-30 hours post-transfection. Coverslips were loaded in Hank's Balanced Salt Solution (HBSS; #14175, Invitrogen) containing 5 μM Fura-2, 1 mg/ml bovine serum albumin (#37525, Pierce), 0.025% (v/v) Pluronic-F127 (#P6866, Invitrogen), 2 mM CaCl_2 , and 1 mM MgCl_2 for 50 minutes at 37°C. Coverslips were rinsed once, transferred to fresh HBSS supplemented only with 2 mM CaCl_2 and 1 mM MgCl_2 , and incubated at 37°C for an additional 10 minutes to allow for ester cleavage. Coverslips were loaded onto the microscope stage in HBSS containing 1 mM MgCl_2 , but imaging experiments were performed in HBSS lacking magnesium. Baseline images were recorded for 20 frames, and cells were stimulated at frame 20 with 1-100 μM NMDA plus 10 μM glycine in magnesium-free HBSS. Data were processed as for cultured neurons, except the criterion for cell exclusion was a ΔR value of <0.1 (presumably a non-transfected cell) rather than an $R_{\text{basal}} \pm$ one standard deviation.

Preparation of hippocampal synaptoneuroosomes

Synaptoneuroosomes were prepared using a protocol modified from the literature (Quinlan et al., 1999). Adult male wild-type and 24-hydroxylase knockout mice (mixed background; C57Bl/6J;129S6/SvEv) were overdosed with isoflurane and decapitated. Hippocampi were removed and placed immediately into ice-cold Tris-acetate, pH 7.4 buffer containing Complete Protease Inhibitor tablets (#11836170001, Roche Applied Science). Hippocampi from two mice of each genotype were homogenized 2 ml total volume of Tris-acetate buffer in a motorized glass-Teflon homogenizer. An aliquot of

the homogenate was saved for immunoblotting analysis. The homogenate was aspirated through an 18-gauge needle into a 3 mL syringe and filtered through a 100 μm pore size filter (#CMN-105-D, Small Parts) attached with a filter holder (Swinnex; #SX0001300, Millipore) into a fresh tube. The filtration was repeated a second time with a fresh 100 μm filter. The filtrate was passed without excessive force a third time through a 5 μm pore size mesh (#SVLP01300, Millipore). If the 5 μm filter became clogged, a fresh one was used to strain the remainder of the solution. The filtrate was centrifuged at 1000 x g in a microcentrifuge at 4°C for 10 minutes and the supernatant removed and discarded. The pellet containing the synaptoneuroosomes was resuspended in RIPA buffer containing Complete Protease Inhibitors. Protein concentration was determined by BCA assay and 25 μg aliquots of the synaptoneurosome fractions were subjected to immunoblotting as described below. Data quantified in Fig. 5B correspond to three separate experiments from two mice per genotype per experiment.

Preparation of hippocampal Triton-soluble and Triton-insoluble fractions

Triton-soluble and -insoluble fractions were prepared as previously reported (Davies et al., 2007; Davies et al., 2008). Adult wild-type and 24-hydroxylase knockout mice (mixed background; C57Bl/6J;129S6/SvEv) were overdosed with isoflurane and decapitated. Hippocampi were removed and placed immediately into ice-cold Tris-acetate, pH 7.4 buffer containing Complete Protease Inhibitors. Hippocampi from five mice (4 males and 1 female) of each genotype were homogenized in 4 ml total volume of Tris-acetate buffer in a motorized glass-Teflon homogenizer. The homogenate was centrifuged at 900 x g in a tabletop centrifuge (Beckman GS-6R) for 15 minutes at 4°C.

The supernatant (S1) was centrifuged at 10,000 x g in a microcentrifuge for 15 minutes at 4°C to generate the crude mitochondrial pellet (P2). P2 was resuspended in 500 µL homogenization buffer (10 mM Tris, pH 7.4, 1 mM EDTA, 0.5% (v/v) Triton X-100 (Surfact-Amps X-100; #28314, Pierce)) with a motorized Pellet Pestle (#Z359971, Sigma) and incubated on ice for 40 minutes. This material was centrifuged at 32,000 x g for 20 minutes at 4°C in a tabletop ultracentrifuge (Beckman Optima TLX) in a TLA 120.2 rotor. The Triton-soluble supernatant (TxS) was removed to a fresh tube and the Triton-insoluble pellet (TxP) was stored overnight at 4°C in RIPA buffer containing Complete Protease Inhibitors before resuspension. Protein concentration was determined by BCA assay and 25 µg aliquots of the Triton-soluble and -insoluble fractions were subjected to immunoblotting as described below. Data shown in Fig. 6 correspond to one experiment representative of two separate experiments.

Surface biotinylation of proteins in hippocampal slices

Surface proteins from acute hippocampal slices were chemically modified according to a protocol adapted from (Nosyreva and Huber, 2005). Adult, male and female wild-type and 24-hydroxylase knockout mice (mixed background; C57Bl/6J;129S6/SvEv) were anesthetized with isoflurane and decapitated. The brain was removed and incubated in hippocampal dissection buffer (3 mM KCl, 1 mM NaH₂ PO₄, 26 mM NaHCO₃, 5 mM MgCl₂, 0.5 mM CaCl₂) maintained as a partially-frozen slush for 4 minutes. Hippocampi were dissected over ice and quickly placed on the stage of a McIlwain tissue chopper (800 series, Vibratome) modified with craft foam (1/16 inch thickness) to allow for tissue adhesion and complete blade penetration through the

hippocampus. Both hippocampi from one animal were placed end-to-end on the chopper stage and 400 μm slices were made transversely at the slowest speed. Approximately 12 slices were collected per animal. Slices were collected into ice-cold, oxygenated ACSF and placed into separate wells of a six-well tissue culture plate (Costar) containing 100 μm mesh cups (#352360, BD Falcon). ACSF in the wells was aspirated and replaced with 5 ml of ACSF containing 1 mg/ml EZ-Link Sulfo-NHS-SS-biotin (#21331, Pierce). Slices were incubated in biotinylation reagent for 30 minutes at 4°C while gently rotating, and then washed three times with ice-cold Tris-buffered saline (TBS, #T6664, Sigma) to quench the biotinylation reaction. Pools of four slices were homogenized using a motorized Pellet Pestle in 200 μl RIPA buffer containing Complete Protease Inhibitors, sodium orthovanadate (1 mM) and sodium fluoride (5 mM). The homogenates were rotated at 4°C for 10 minutes and centrifuged in a microcentrifuge at 12,000 rpm for 5 minutes at 4°C. The supernatant was subjected to BCA assay to determine protein concentration. Two hundred micrograms of the clarified homogenate was rotated overnight at 4°C with 200 μl of washed NeutrAvidin Agarose Resin (#29201, Pierce) in a total volume of 400 μl RIPA buffer supplemented as above. The beads were washed three times with 1 ml of RIPA containing Complete Protease Inhibitors and surface proteins were eluted by adding 80 μl of a 1:1 mixture of 2X Laemmli sample buffer (#161-0737, Bio-Rad) containing 5% (v/v) β -mercaptoethanol: solubilization buffer (62.5 mM Tris-HCl, pH 6.8, 15% (w/v) sodium dodecyl sulfate, 8 M urea, 10% (v/v) glycerol, 100 mM dithiothreitol) to the beads and incubating for 30 minutes at room temperature. The 80 μl sample of eluted proteins (derived from 200 μg of homogenate) was divided

into 2 x 40 μ l samples and subjected to SDS-PAGE as described below alongside 20 μ g of the starting hippocampal homogenate. The data quantified in Figs. 7B and 7C correspond to five separate experiments from one mouse per genotype per experiment.

Immunoblotting procedures

Protein samples were solubilized with the addition of an equal volume of a 1:1 mixture of 2X Laemmli sample buffer containing 5% (v/v) β -mercaptoethanol: solubilization buffer as described above and incubated at room temperature for 30 minutes. Samples were loaded onto 4-15% Ready Gel Tris-HCl polyacrylamide gradient gels (#161-1158, Bio-Rad) with Kaleidoscope and Precision Plus Blue (#161-0324 and #161-0373, Bio-Rad) molecular weight markers. Gels were electrophoresed at 100 volts for approximately 1.5 hours in 1X Tris-Glycine-SDS (TGS, #161-0772, Bio-Rad) running buffer followed by electrophoretic transfer to nitrocellulose membranes (Hybond-C Extra, GE Healthcare Biosciences, Piscataway, NJ) for 1.25 hours in a tank transfer apparatus (Hoefer TE 22, San Francisco, CA) at 100 volts. Protein transfer was verified by staining with Ponceau S (#P7170, Sigma-Aldrich Inc.) diluted 1:4 in Millipore water. Immunoblotting was performed according to the manufacturer's protocol (Li-Cor Odyssey Infrared Imaging System). Ponceau S was rinsed off the membranes by washing twice in PBS for 10 minutes each. Membranes were then incubated for at least 1 hour at room temperature in blocking buffer (#927-40000, Li-Cor). Primary antibodies were incubated overnight at 4°C and diluted in blocking buffer supplemented with 0.2% (v/v) Tween-20 (Surfact-Amps 20, #28320, Pierce). Primary antibodies used in these studies were directed against the following proteins and diluted

as follows: NR1 (1:2500, #05-432, Upstate Biotechnology), NR2A (1:500, #07-632, Upstate Biotechnology), NR2A (1:200, #612286, BD Biosciences), NR2B (1:1000, #06-600, Upstate Biotechnology), GAD67 (1:2500, #MAB5406, Chemicon), β III tubulin, (1:20,000, #05-559, Upstate Biotechnology), PSD-95 (1:10,000, #05-494, Upstate Biotechnology), synaptogyrin (1:10,000, #P925, gift of Dr. Thomas Sudhof), P450 reductase (1:1000, #OSA-300, Stressgen), NR2D (1:2000, #MAB5578, Chemicon), and phospho-NR2B (1:1000, #M2442, Sigma). The anti-24-hydroxylase monoclonal antibody 1A7 was used as neat hybridoma tissue culture supernatant (containing 20-25 μ g/ml antibody) supplemented with Tween 20 to 0.2% (v/v). The membranes were washed three times for 10 minutes each with PBS-T. IRDye-680-conjugated goat anti-rabbit (#926-32221, Li-Cor) and IRDye-800-conjugated goat anti-mouse secondary antibodies (#926-32210, Li-Cor) were diluted 1:15,000 in blocking buffer supplemented with 0.2% Tween-20 and 0.01% (v/v) sodium dodecyl sulfate (SDS, #SPB1135, Open Biosystems) and incubated with the membranes for 1 hour at room temperature in the dark. The membranes were washed three times for 10 minutes each with PBS-T then once with PBS. Membranes were then scanned on a Li-Cor Odyssey machine using application software, version 3.0. Membranes were scanned at 169 μ m resolution, high quality, and with intensity values of 3-6. Resulting images were exported in both color and grayscale as TIF files and integrated band intensities were quantified and exported to Microsoft Excel using the report feature. Gel images and graphs were imported into Adobe Illustrator for final figure preparation.

Results

Measurement of channel-mediated calcium influx in cultured neurons

Increased intracellular calcium from a variety of sources is necessary for the generation of LTP. In particular, calcium influx through the NMDAR is required for LTP induction, while calcium-permeable AMPARs and voltage-gated calcium channels (VGCCs) contribute additional calcium influx downstream of NMDAR activation (Biou et al., 2008; Raymond, 2007; Yashiro and Philpot, 2008). To determine if calcium channel function was affected in 24-hydroxylase knockout neurons, calcium influx was stimulated under channel-specific conditions and measured using Fura-2 ratiometric imaging as described in Materials and Methods. First, VGCC-mediated calcium influx was stimulated by depolarizing the neurons with 50 mM KCl (Fig. 1A) (Takasu et al., 2002). This treatment produced an equal increase in intracellular calcium in both wild-type and 24-hydroxylase knockout neurons. Next, calcium influx through AMPA-type glutamate receptors was measured (Fig. 1B). Specifically, the responses of AMPARs lacking the GluR2 subunit were measured because GluR2-containing AMPARs are not calcium-permeable (Biou et al., 2008; Friedman et al., 2003). Neurons were stimulated with either 20 μ M or 40 μ M glutamate in the presence of the L-type VGCC inhibitor, nimodipine, the pan-NMDAR inhibitor, AP5, and the voltage-gated sodium channel blocker TTX to inhibit endogenous neuronal activity. Under these conditions, which pharmacologically isolate the calcium-permeable AMPAR response, an equal dose-dependent calcium influx was produced in response to glutamate stimulation in both wild-type and 24-hydroxylase knockout neurons. In experiments for which the data are not shown, AMPAR responses recorded under these conditions were blocked by the

specific AMPAR antagonist, CNQX. In Figure 1C, dose-dependent calcium influx through NMDARs was measured in neurons of different 24-hydroxylase genotypes. NMDAR responses were isolated pharmacologically by incubating the neurons in Mg-free ACSF supplemented with nimodipine, TTX, and the AMPAR inhibitor, CNQX, and by stimulating the neurons with the specific NMDAR co-agonists, NMDA and glycine. Higher concentrations of NMDA produced increased calcium influx through NMDARs in both wild-type and 24-hydroxylase knockout neurons. Responses of similar magnitude were detected in both types of neurons. Together, the results presented in Figure 1 suggested that overall calcium channel function was normal in 24-hydroxylase knockout neurons.

Subtype-specific defect in NMDAR-mediated calcium influx

Due to the importance of NMDARs in LTP induction, additional studies were conducted to further probe the function of specific subtypes of NMDARs in wild-type and 24-hydroxylase knockout neurons. For this purpose, the subtype-specific NR2B antagonist ifenprodil was used (Kew et al., 1996; Neyton and Paoletti, 2006; Paoletti and Neyton, 2007; Williams, 1993). With the addition of ifenprodil to the cocktail of drugs used to isolate NMDAR responses (nimodipine, TTX, and CNQX), NR2B-containing NMDARs are predominantly blocked, whereas NR2A-containing NMDARs are unaffected. Dose-dependent calcium influx through NMDARs was again measured in wild-type and 24-hydroxylase knockout neurons, but in the presence of ifenprodil. As shown in Figure 2A, dose-dependent calcium influx in 24-hydroxylase knockout neurons was more sensitive to ifenprodil than the response in wild-type neurons, suggesting

increased NR2B function or decreased NR2A function in the knockout neurons. Similar results were obtained using another NR2B-specific antagonist, Ro-25691 (data not shown). Interestingly, the dose-response curves at the low end of the scale (0-10 μ M NMDA) showed no differences between the wild-type and 24-hydroxylase knockout, similar to the responses shown in Figure 1C where total NMDAR responses were measured. To investigate the possibility of reduced NR2B-blocking activity of ifenprodil at low NMDA concentrations as described in (Kew et al., 1996), additional experiments were performed in transfected HEK293 cells expressing recombinant NR1/NR2B receptors. As shown in Figure 2B, the responses of transfected HEK293 cells either treated or not with ifenprodil show similar dose-response curves in the low range (1-10 μ M NMDA), but increasing NMDA concentrations cause ifenprodil to inhibit NR2B responses. Therefore, the indistinguishable responses of ifenprodil-treated wild-type and 24-hydroxylase knockout neurons at or below 10 μ M NMDA are due to the fact that no subtype-specific inhibition is taking place. These results provide additional evidence that the total NMDAR response of knockout neurons is unaffected.

Defective NMDAR function in 24-hydroxylase knockout neurons can be restored by geranylgeraniol

If the increased ifenprodil sensitivity observed in 24-hydroxylase knockout neurons is related to the LTP defect in these mice, then decreased calcium influx in the knockout neurons should be reversed by treatment with GG analogous to the LTP rescue seen in hippocampal slices from knockout mice (Kotti et al., 2006). To test this

hypothesis, wild-type and 24-hydroxylase knockout neurons were treated with ifenprodil and stimulated with 40 μM NMDA, 10 μM glycine in the presence or absence of 200 μM GG. Figure 3 shows that GG treatment has no effect on wild-type NMDAR-mediated calcium influx in the presence of ifenprodil, but the knockout responses are increased significantly to the point of being indistinguishable from those in wild-type neurons. The total NMDAR responses in wild-type and 24-hydroxylase knockout neurons in the absence of ifenprodil are also presented for comparison and again show there is little difference between wild-type and knockout levels of calcium influx under these conditions. Furthermore, the percentage decrease of the NMDAR response after ifenprodil treatment in knockout neurons (46.6% decrease) compared to wild-type (26.2% decrease) is abolished upon treatment of wild-type and knockout neurons with GG (15.9% decrease in WT vs. 15.3% decrease in KO). These results imply a direct effect of GG on NMDAR function.

Determination of origin of increased intracellular calcium after NMDA stimulation

We next confirmed the extracellular origin of the increased intracellular calcium after NMDAR stimulation, because release of ER calcium is known to contribute to increased intracellular calcium during some forms of LTP induction (Raymond, 2007; Raymond and Redman, 2002). In the first experiment, NMDAR responses were isolated pharmacologically as before, but the imaging experiment was performed in either normal ACSF containing 2 mM CaCl_2 or in calcium-free ACSF. In Figure 4A, wild-type and 24-hydroxylase knockout neurons were stimulated with 40 μM NMDA and 10 μM glycine in the presence or absence of extracellular calcium. In the presence of extracellular

calcium, robust increases in intracellular calcium were measured in both wild-type and knockout neurons. In contrast, when calcium was omitted from the extracellular solution, no NMDAR responses were measured in either cell type. These results suggest an extracellular origin for the observed increase in intracellular calcium following NMDAR stimulation. In a second type of experiment, the ER calcium store was emptied by pretreatment of wild-type neurons with thapsigargin, a sarco-endoplasmic reticulum calcium ATPase (SERCA) inhibitor. This compound is thought to promote complete depletion of the ER store over time by allowing calcium leakage through unidentified channels (Choi et al., 2006; Foradori et al., 2007). Figure 4B shows wild-type neurons stimulated with 40 μ M NMDA and 10 μ M glycine under NMDAR-isolating conditions with or without thapsigargin pretreatment. Thapsigargin pretreatment had no effect on the NMDAR-mediated increase in intracellular calcium. Therefore, under these experimental conditions, it appears that calcium influx through NMDAR into neurons is being measured.

Biochemical analyses of functional NMDAR pools in wild-type and 24-hydroxylase knockout hippocampus

A possible explanation for the increase in ifenprodil sensitivity observed by calcium imaging in 24-hydroxylase knockout neurons is an increase in the NR2B/NR2A ratio either at the plasma membrane or at the postsynaptic density (Quinlan et al., 1999). To investigate this possibility, I performed several biochemical analyses. In the first set of experiments, synaptoneurosomes, a crude synaptic preparation enriched in presynaptic

and postsynaptic membrane proteins, were isolated from wild-type and 24-hydroxylase knockout hippocampi and immunoblotted with antibodies against NMDAR subunits as described in Materials and Methods. Figure 5A shows the results of a representative immunoblotting experiment. Although the NMDAR subunit proteins NR1, NR2A, and NR2B are enriched in the synaptoneurosome fraction compared to the starting homogenate, there are no differences in the synaptoneurosomal levels of NMDAR subunits between the wild-type and the 24-hydroxylase knockout samples. Blotting with an antibody against β III tubulin showed that equal amounts of protein were present in each sample analyzed. Figure 5B shows quantified data from multiple independent experiments conducted in a similar fashion where the intensities of the NMDAR subunits present in synaptoneurosome fractions were normalized to the intensities of the corresponding homogenates to generate a fold-enrichment factor. While each NMDAR subunit protein analyzed is enriched approximately 2-fold in the synaptoneurosome fraction compared to the homogenate, confirming the synaptoneurosome isolation protocol was successful, there were no differences in wild-type versus knockout levels of NMDAR subunits in the synaptoneurosome fraction.

Differences in the synaptic NR2B/NR2A ratio between wild-type and 24-hydroxylase knockout neurons could be masked by the relative impurity of the synaptoneurosome fraction. To exclude this possibility, Triton-X-100-soluble (TxS) and -insoluble (TxP) fractions were prepared from wild-type and 24-hydroxylase knockout hippocampus. In this type of preparation, the insolubility of the postsynaptic density in the non-ionic detergent Triton-X-100 is exploited to separate the fraction containing presynaptic and extrasynaptic membranes from the postsynaptic density (Davies et al.,

2007; Davies et al., 2008; Gardoni et al., 2009). These two synaptic fractions were immunoblotted with antibodies against NMDAR subunit proteins and other subcellular markers as shown in Figure 6A. The separation of the presynaptic (TxS) and postsynaptic (TxP) membranes by this protocol was good as judged by the nearly exclusive presence of synaptogyrin, a presynaptic vesicle marker, and PSD-95, a structural protein of the postsynaptic density, in the appropriate fractions. 24-hydroxylase protein was detected only in wild-type samples and was present in both presynaptic and postsynaptic membrane fractions, as reported previously (Kotti et al., 2006). A known ER resident protein, P450 reductase, was present only in the presynaptic fractions from wild-type and knockout hippocampi, suggesting the TxP fraction is not extensively contaminated with ER membranes. Levels of the NR1, NR2A, NR2B, and NR2D NMDAR subunits were unchanged between wild-type and knockout hippocampal TxP fractions, suggesting differences in synaptic receptor subunit levels do not underlie the differential ifenprodil sensitivity observed in knockout neurons. The postsynaptic levels of NR1 and NR2B were verified by blotting with additional antibodies against these two proteins (data not shown). Although small amounts of NR1 were present in the TxS fraction composed of both presynaptic and extrasynaptic membranes, there were no differences between wild-type and knockout NR1 levels, nor were appreciable amounts of any NR2 subunits detected in this fraction. For this reason, and due to the small amount of PSD-95 also present in the TxS fraction, it appears this fraction represents predominantly presynaptic membranes with some postsynaptic contamination. Lastly, an antibody that recognizes NR2B phosphorylated on tyrosine-1472 was used to probe the wild-type and 24-hydroxylase knockout TxS and TxP fractions. Tyrosine

phosphorylation of NR2B by Fyn, a Src family kinase, is implicated in hippocampal and amygdaloid synaptic plasticity (Nakazawa et al., 2001; Nakazawa et al., 2006). No differences were found between wild-type and knockout levels of postsynaptic phosphorylated NR2B, in agreement with a recent report showing mutant mice that lack the ability to phosphorylate NR2B on this residue perform normally in hippocampal-dependent learning tests such as the Morris water maze and have normal synaptic plasticity in the hippocampus (Nakazawa et al., 2006). β III tubulin immunoblotting showed equal loading of protein in all samples analyzed. Expression of proteins found in the TxP fraction of wild-type and knockout hippocampus was quantified by normalizing band intensities to that of the PSD marker, PSD-95 (Figure 6B).

Any potential differences in NMDAR subunit composition between wild-type and 24-hydroxylase knockout mice must be expressed in a functional pool of receptors in order for this phenomenon to cause the observed defects in NMDAR-dependent calcium imaging. Synaptic NMDAR levels as determined above represent analysis of one type of functional pool. Another functional pool of receptors is located on the plasma membrane of neurons and was examined in the next set of experiments. Surface receptors were isolated by biotinylation of hippocampal slices followed by avidin-resin precipitation and subjected to immunoblotting using antibodies against the NR1, NR2A, and NR2B NMDAR subunits. Figure 7A shows a representative immunoblot where total homogenates and surface fractions from pooled wild-type and knockout hippocampal slices were immunoblotted with the NMDAR subunit antibodies as well as an antibody against an intracellular protein, glutamic acid decarboxylase of 67kDa (GAD67). GAD67 was localized exclusively to the homogenate in both wild-type and knockout

samples, confirming the biotinylation reagent preferentially labels surface proteins. The expression of all NMDAR subunits in the wild-type and knockout hippocampal homogenates was similar; however, NR1 surface levels appeared to be increased in slices from 24-hydroxylase knockout animals, whereas the surface levels of NR2A and NR2B appeared similar between the wild-type and knockout samples. The data from this and other similar experiments were quantified in Figure 7B. In panel B, surface levels of NR1 were consistently increased ~ 50% in the knockout slices, and this increase reached statistical significance ($p=0.048$). However, surface NR2A and NR2B levels were unchanged in knockout slices. These results suggest an alteration in the surface NR2B/NR2A ratio is not involved in the increased ifenprodil sensitivity demonstrated in the knockout neurons, although knockout neurons may have an increased number of NR1 NMDA receptor subunits in the plasma membrane.

Discussion

Previous studies using 24-hydroxylase knockout mice revealed an essential role for tonic brain cholesterol synthesis in learning and memory. 24-hydroxylase knockout mice have an approximate 50% decrease in the rate of *de novo* cholesterol synthesis in the brain, which suppresses their ability to perform hippocampal-dependent learning tasks and the expression of LTP in acute hippocampal slices (Kotti et al., 2006; Lund et al., 2003). The necessity of brain cholesterol turnover for proper LTP production was subsequently traced to the requirement for a single intermediate in the cholesterol biosynthetic pathway, geranylgeranyl-diphosphate (Kotti et al., 2008; Kotti et al., 2006). These earlier studies did not address the mechanism by which GG influenced LTP and

presumably learning and memory. The results reported here reveal that GG specifically modulates NMDA receptor function, a crucial mediator of LTP induction, but does not affect other calcium channels important in LTP. The observed defect in 24-hydroxylase knockout NMDAR function becomes evident in the presence of the subtype-specific NR2B inhibitor, ifenprodil, suggesting that 24-hydroxylase knockout neurons have either an increase in NR2B activity or a decrease in NR2A activity in the functional pool of NMDA receptors. Biochemical measurements of synaptic and surface NMDAR subunits in wild-type and 24-hydroxylase knockout hippocampus imply that alterations in NR2B/NR2A ratio are not the cause of altered NMDAR function in knockout neurons.

The current studies suggest a role for GG in determining the identity of functional NR2 subunits. Both subcellular localization studies of the 24-hydroxylase enzyme showing a postsynaptic localization and functional studies showing LTP rescue of 24-hydroxylase knockout slices when GG is delivered postsynaptically via the recording electrode suggest that GG has a postsynaptic mode of action, which is consistent with a role in NMDAR function (Kotti et al., 2008; Ramirez et al., 2008). Many studies have proposed that the identity of the modular NR2 NMDAR subunits found at synapses, or the NR2A/NR2B ratio, is an important determinant of the nature of bidirectional synaptic plasticity induction (LTP or LTD) due to differences in their biophysical properties, synaptic localization, and downstream signaling (Lau and Zukin, 2007; Yashiro and Philpot, 2008). A number of studies using both mutant mice and subtype-specific pharmacological inhibitors proposed mutually exclusive roles of NR2A and NR2B in synaptic plasticity, where NR2A was required for LTP and NR2B was required for LTD (Kutsuwada et al., 1996; Liu et al., 2004; Massey et al., 2004; Sakimura

et al., 1995; Sprengel et al., 1998); however, more recent studies have questioned these findings and suggest a less dichotomous view whereby LTP depends on both NR2A and NR2B receptors (Bartlett et al., 2007; Li et al., 2007). Still other studies have reached opposite conclusions, and demonstrate that NR2B is required for LTP and unnecessary for LTD (Barria and Malinow, 2005; Bartlett et al., 2007; Gardoni et al., 2009; Morishita et al., 2007). Some of the discrepancies in the literature may be due to the use of the pharmacological agent NVP-AAM077 (NVP), the single existing NR2A-specific antagonist that was recently shown to exhibit less specificity for the NR2A subunit over the NR2B subunit than was originally reported (Auberson et al., 2002; Neyton and Paoletti, 2006; Weitlauf et al., 2005). Furthermore, even though ifenprodil is a well-characterized and highly specific antagonist for NR2B over NR2A ($IC_{50} = 0.34 \mu\text{M}$ for NR2B versus $146 \mu\text{M}$ for NR2A), use of ifenprodil also has complications because the compound inhibits only ~80% of NR2Bs and produces an increase in the receptor affinity for glutamate (Kew et al., 1996; Neyton and Paoletti, 2006; Williams, 1993). Additional discrepancies in the literature may be accounted for by the species, brain region, and developmental differences in NMDAR subunit expression between the various experimental preparations used.

Although many current studies support the hypothesis that NR2B promotes LTP and NR2A promotes LTD, the analysis of synaptic plasticity in the respective knockout mouse models seems to refute this idea, as LTP is reduced in the NR2A knockout and LTD is abolished in the NR2B knockout (Kutsuwada et al., 1996; Sakimura et al., 1995; Yashiro and Philpot, 2008). Furthermore, patch-clamp recording studies of recombinant NR2A and NR2B receptors and subsequent simulations of synaptic responses have

shown that NR2A receptors are likely to mediate greater charge transfer, and thus calcium influx, after stimulation with LTP-inducing protocols. Similarly, NR2B receptors are likely to mediate increased charge transfer after stimulation patterns often used to induce LTD (Erreger et al., 2005). Activity-dependent trafficking of NR2A into synapses after LTP induction has recently been shown in immature hippocampal slices, although this phenomenon was not recapitulated in adult slices (Bellone and Nicoll, 2007). Therefore, extensive evidence supports an essential role for NR2A in LTP, although NR2B receptors may also be involved.

24-Hydroxylase knockout neurons are more sensitive to the NR2B antagonists, ifenprodil and Ro-25691, as measured by calcium imaging in cultured embryonic neurons reported here, and by NMDAR-mediated field potential recordings in acute hippocampal slices from adult animals (T. Kotti, unpublished observations). Consistent with previous observations, ifenprodil appears to inhibit approximately 20% of NMDAR responses in mature (11-14DIV) cultured embryonic neurons as well as adult (P14-21) wild-type hippocampal slices, demonstrating that the majority of NMDAR responses in these preparations are due to NR2A activation (Bellone and Nicoll, 2007; Kohr et al., 2003). An increase in NR2B antagonist sensitivity suggests an increase in the functional NR2B/NR2A ratio in 24-hydroxylase knockout neurons, commonly manifested as an increase or decrease, respectively, of these receptors expressed synaptically or on the neuronal surface. Extensive biochemical assays reported here do not show changes, at least in the steady-state, in the synaptic or surface NR2B/NR2A ratio in 24-hydroxylase knockout hippocampal slices. Normal NMDAR subunit localization at the synapse and plasma membrane in knockout neurons is consistent with data showing the role of GG in

LTP induction is independent of prenylation of essential trafficking proteins necessary for LTP such as Rab, Rac, or Rho family proteins (Kotti et al., 2008). Furthermore, as NMDAR surface expression is also tightly regulated by quality control checkpoints in the ER, properly localized NMDA receptors in knockout neurons are in agreement with previous demonstrations of normal ER membrane structure and chaperone expression in these neurons (Kenny et al., 2009; Kotti et al., 2006; Ramirez et al., 2008).

Our current and previous studies on the 24-hydroxylase knockout mouse appear to support a specific defect in NR2A function as underlying the severe impairments in hippocampal LTP and spatial learning (Kotti et al., 2006). The phenotype of these mutant mice is reminiscent of those seen in constitutive NR2A knockout mice and mice expressing C-terminally truncated NR2A receptors, which both exhibit reduced CA3-CA1 LTP after tetanic stimulation and impaired hippocampal-dependent learning (Sakimura et al., 1995; Sprengel et al., 1998). Interestingly, it was recently shown that in mutant mice expressing C-terminally truncated NR2A, functionally ablating NR2A, LTP can be restored to wild-type levels in adult slices (postnatal day 42) upon repeated tetanic stimulation. A similar phenomenon was also apparent in slices prepared from young (postnatal day 14) mice, in which the NR2B to NR2A ratio is higher, whereby LTP could be enhanced by repeated tetanic stimulation (Kohr et al., 2003). These results support the essential role of NR2A in normal LTP expression, but show that under certain circumstances NR2B receptors can also support LTP induction. A similar result has been observed in 24-hydroxylase knockout mice, where repeated theta burst stimulations can induce robust LTP similar to that seen in wild-type slices (T. Kotti, unpublished observations). This finding is consistent with the idea that 24-hydroxylase knockout

mice have defective NR2A receptor function but normal NR2B receptor function. This distinction is important, because the phenotype of 24-hydroxylase knockout mice shows no similarity to that of the NR2B knockout. 24-hydroxylase knockout mice have a normal lifespan and do not exhibit defects in hippocampal LTD (Kotti et al., 2006; Lund et al., 2003), as seen in NR2B knockout mice (Kutsuwada et al., 1996). In agreement with this idea, dose-dependent calcium influx through NMDA receptors in the presence of the NR2A antagonist NVP was unchanged between wild-type and 24-hydroxylase knockout cultured neurons (A. Lin, unpublished observations). Although the specificity of this antagonist is likely only ~10-fold greater for NR2A than NR2B (Neyton and Paoletti, 2006), these experiments were carried out without antagonist pretreatment to limit effects on NR2B receptors (Weitlauf et al., 2005) and are consistent with normal NR2B function in 24-hydroxylase knockout neurons.

In the apparent absence of a role for GG in determining NMDAR subunit composition, it may be considered that GG has a more direct effect on NMDAR channel function and perhaps even binds to the NMDAR itself. Our data support a scenario where GG could directly potentiate the activity of NR2A-containing receptors. Precedence for this idea exists in the reported ability of an unsaturated, 20-carbon fatty acid, arachidonic acid, to potentiate NMDAR currents in cerebellar granule cells (Miller et al., 1992). This activity was not dependent on the generation of second messengers, and was confirmed in heterologous cells, consistent with a direct binding of arachidonic acid to NMDAR, or an alteration of the receptor's lipid environment (Miller et al., 1992; Tabuchi et al., 1997). The NMDAR has been shown to be mechanosensitive, and in fact, membrane alteration as a mechanism for arachidonic acid modulation of the NMDAR has

been demonstrated (Casado and Ascher, 1998; Kloda et al., 2007; Paoletti and Ascher, 1994). On the other hand, support for a potential direct binding interaction exists in the description of a putative fatty acid binding motif in the NMDAR amino acid sequence as well as numerous examples of direct activation of various proteins by fatty acid binding (Ordway et al., 1991; Petrou et al., 1993). Furthermore, it was determined that NR2A containing receptors were more sensitive to the potentiating effects of arachidonic acid than NR2B containing receptors (Tabuchi et al., 1997), perhaps favoring the direct binding hypothesis of arachidonic acid action. Polyamines such as spermine are also known to bind the NMDAR and have subunit-specific effects on receptor activity (Kew and Kemp, 1998). Interestingly, allosteric interactions occur between the polyamine and ifenprodil binding sites, such that occupation at one site reduces receptor affinity at the other site (Kew and Kemp, 1998). An alternative scenario that does not require NR2A potentiation by GG could be a similar reduction of NR2B affinity for ifenprodil after GG binding by means of an allosteric interaction. In light of the modest structural similarities of arachidonic acid and spermine to GG, existing work on the modulation of NMDAR activity by long-chain aliphatic compounds engenders speculation that GG may directly interact with the NMDAR. Further studies are ongoing to address this proposal, and will investigate direct binding between GG and recombinant NMDA receptors as well as subtype-specific potentiation of NMDARs by GG in a heterologous system. Analysis of the effect of GG in experimental preparations from NR2A knockout mice and 24-hydroxylase/NR2A double knockout mice will further clarify the subtype-specific actions of GG on the NMDAR.

Figure 1. Calcium channel activity in neurons cultured from wild-type and 24-hydroxylase knockout embryos. Fura-2 ratiometric imaging was used to measure calcium influx through voltage-gated calcium channels (A), GluR2-lacking AMPA receptors (B), and NMDA receptors (C) stimulated by their respective agonists. The function of these three types of channels was not significantly affected in 24-hydroxylase knockout neurons. In panels A and B, n indicates the number of individual neurons analyzed per genotype and treatment. In panel C, 10-122 individual neurons were analyzed per NMDA concentration per genotype.

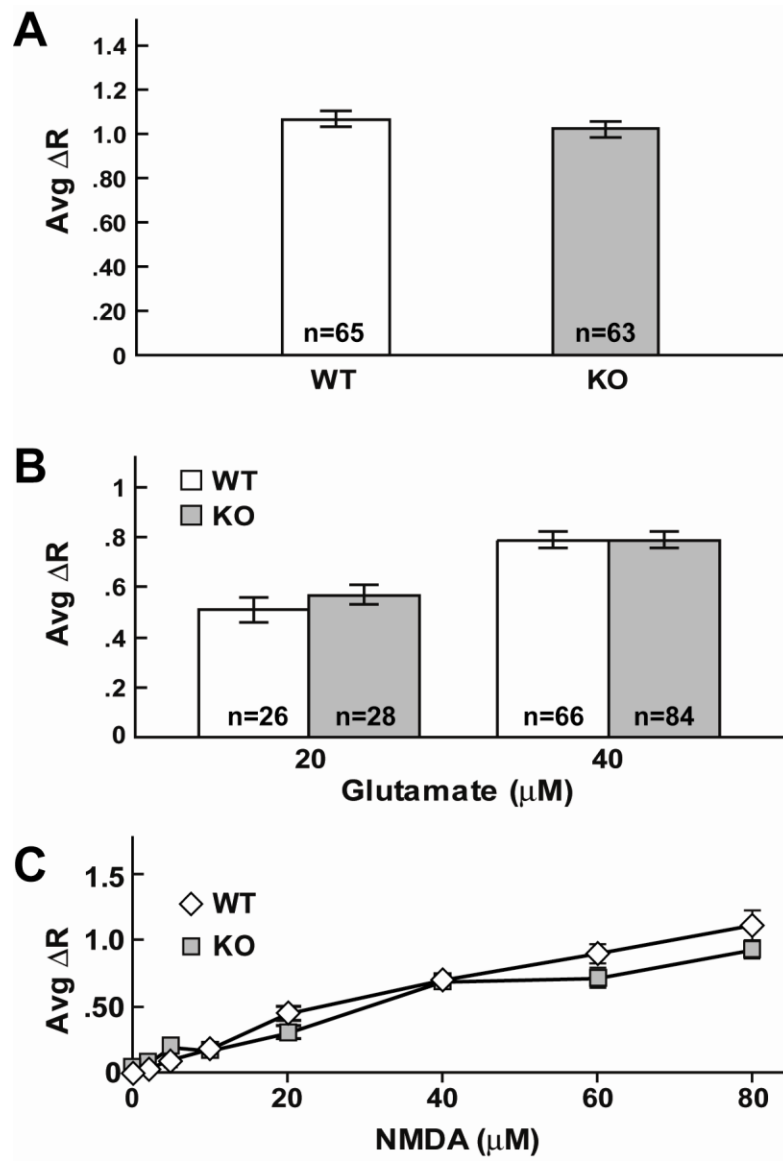


Figure 2. 24-hydroxylase knockout neurons exhibit subtype-specific defects in NMDAR function. A) Dose-dependent calcium influx mediated by NMDA receptors was measured using Fura-2 ratiometric imaging in wild-type and 24-hydroxylase knockout neurons in the presence of the NR2B-specific inhibitor, ifenprodil. Knockout neurons exhibit an increased sensitivity to ifenprodil compared to wild-type neurons at NMDA concentrations $\geq 20 \mu\text{M}$. 6-124 individual neurons were analyzed per NMDA concentration per genotype. B) Dose-dependent calcium influx was measured in transfected HEK-293 cells expressing recombinant NR2B-containing NMDARs either treated or untreated with ifenprodil. At NMDA concentrations $\leq 10 \mu\text{M}$, ifenprodil has little effect on NMDAR function. At 40 and 100 μM NMDA, ifenprodil significantly inhibits NR2B responses. 17-29 individual transfected cells were analyzed per NMDA concentration per treatment.

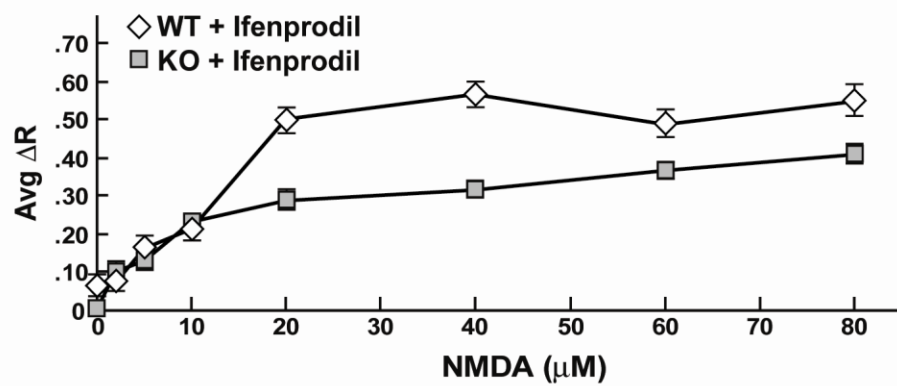
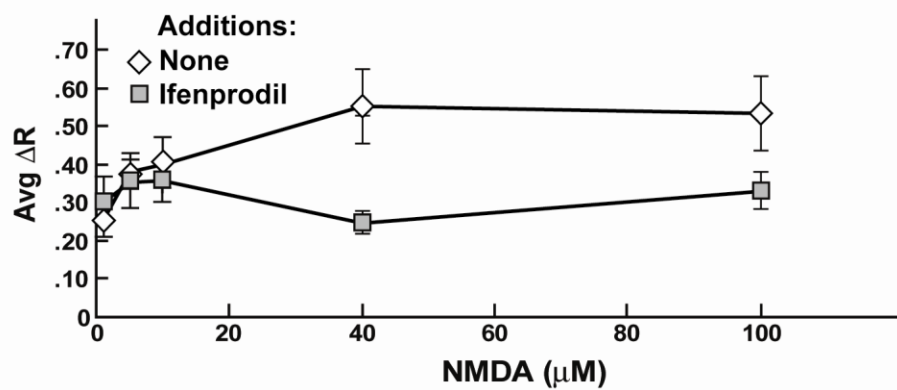
A Neurons**B HEK-293 Cells**

Figure 3. Geranylgeraniol treatment normalizes functional NR2A/NR2B ratio in 24-hydroxylase knockout neurons. Neurons were treated with the NR2B-specific inhibitor ifenprodil in the presence or absence of 200 μ M geranylgeraniol, or left untreated to measure total NMDAR responses upon stimulation with 40 μ M NMDA, 10 μ M glycine. Total NMDAR responses are similar between wild-type and knockout neurons, whereas ifenprodil treatment inhibits knockout NMDAR responses significantly more than those in wild-type neurons. The addition of geranylgeraniol to ifenprodil-treated neurons did not affect the response of wild-type cells, but significantly increased the NMDAR responses in the knockout cells to a level indistinguishable from that of wild-type neurons. n indicates the number of individual neurons analyzed per genotype and treatment.

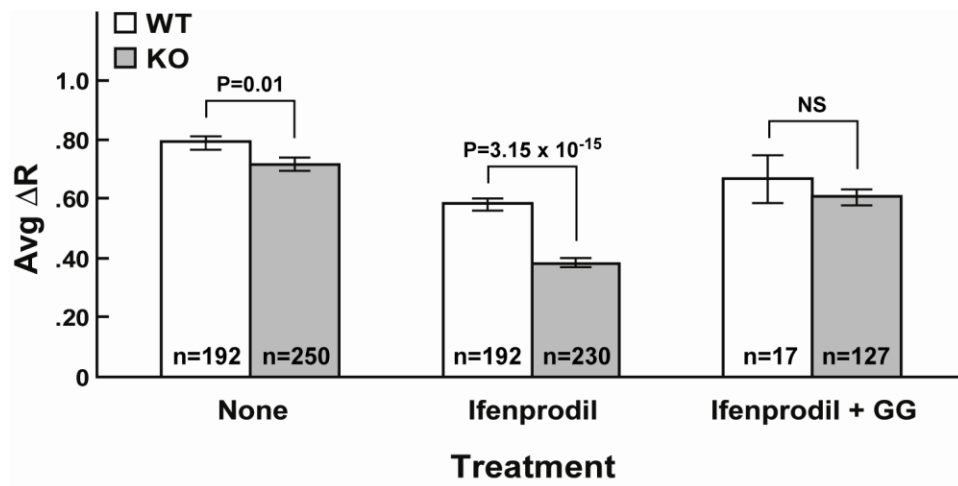


Figure 4. Calcium influx through NMDA receptor has an extracellular origin. A) NMDAR-mediated calcium influx into wild-type and 24-hydroxylase knockout neurons was measured in the presence or absence of extracellular calcium. In the presence of 2 mM extracellular calcium, NMDAR-mediated calcium influx was stimulated in both wild-type and knockout neurons to a similar degree. In the absence of extracellular calcium, no NMDAR-mediated calcium influx was observed. B) NMDAR-mediated calcium influx was stimulated in untreated wild-type neurons or those pretreated with the sarco-endoplasmic reticulum calcium ATPase (SRERCA) inhibitor thapsigargin to deplete the ER calcium store; thapsigargin pretreatment had no effect on NMDAR-mediated calcium influx. In both panels, n indicates the number of individual neurons analyzed per genotype and treatment.

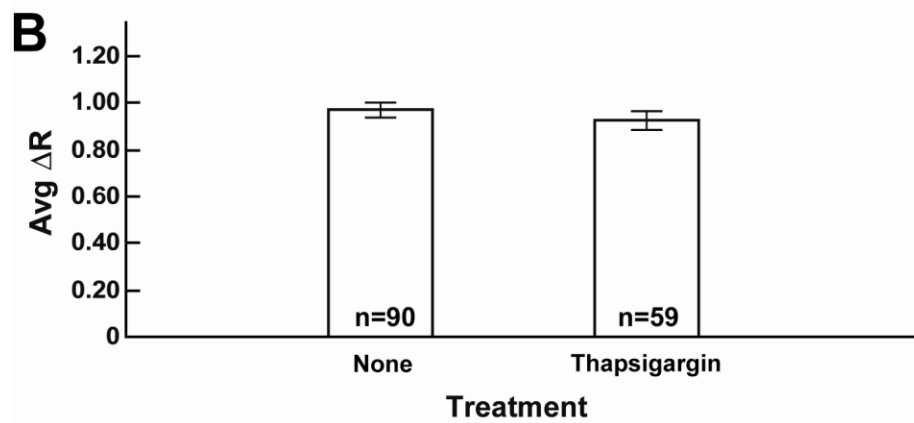
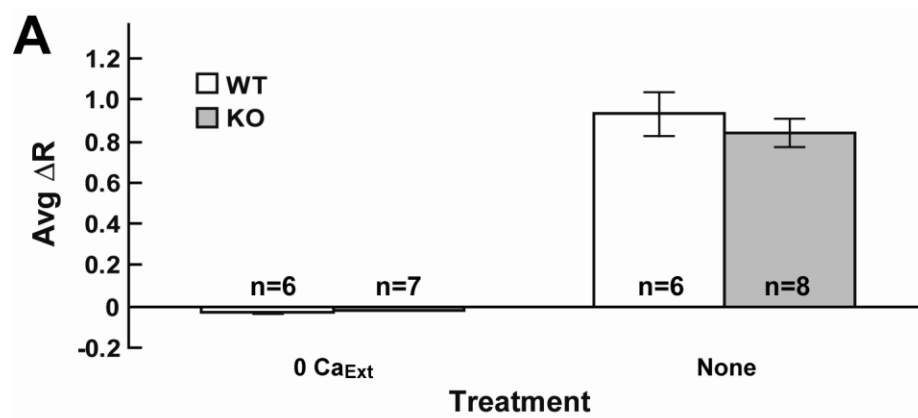


Figure 5. Measurement of synaptic NMDAR levels in wild-type and 24-hydroxylase knockout hippocampal synaptoneuroosomes. A) Representative immunoblot of homogenate, supernatant, and synaptoneurosome fractions from wild-type and knockout hippocampi using antibodies recognizing the NR1, NR2A, and NR2B NMDAR subunits. Although NMDAR subunits are enriched in the synaptoneurosome fraction compared to the homogenate in both wild-type and knockout samples, no differences were observed between wild-type and knockout synaptoneurosomal levels of NMDAR subunits. Concurrent immunoblotting with an antibody against β III tubulin shows that equal amounts of protein were present in each lane. B) The fold-enrichment of synaptoneurosomal NMDAR subunits from wild-type and knockout hippocampus. A 2-fold enrichment is seen for each of the NMDAR subunits in both wild-type and knockout samples. Data were quantified from three independent experiments from two animals per genotype per experiment.

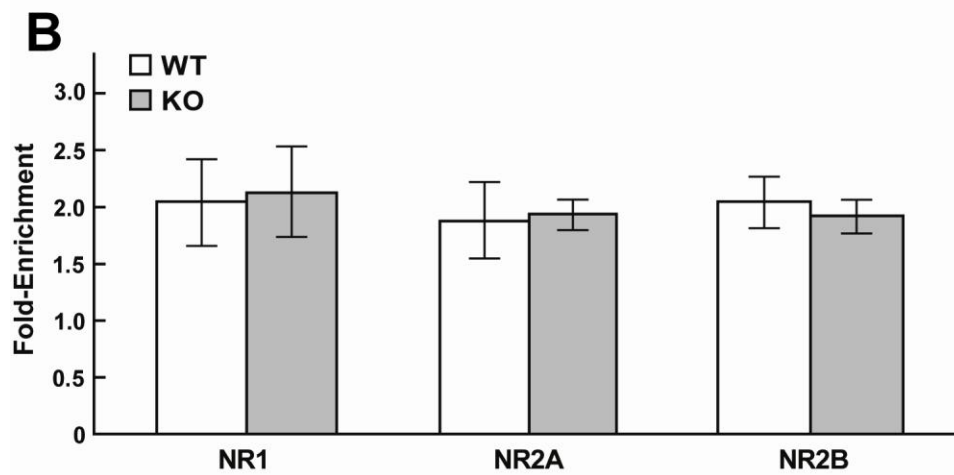
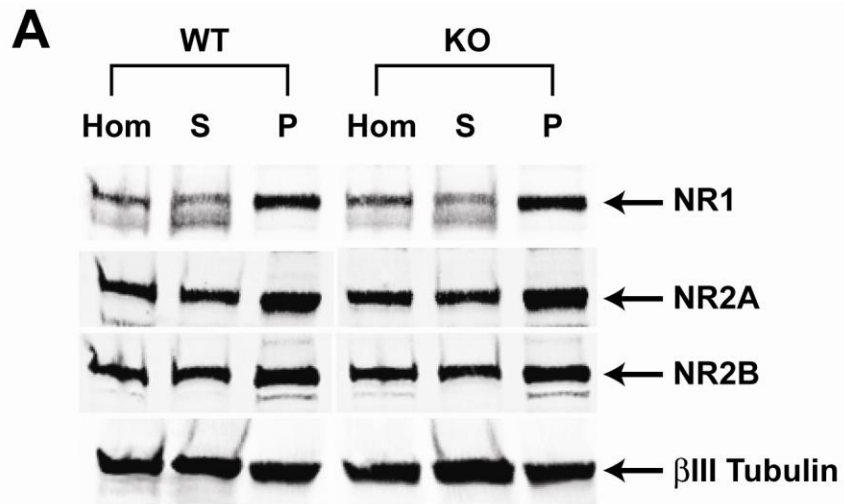


Figure 6. Measurement of synaptic NMDAR levels in wild-type and 24-hydroxylase knockout hippocampal Triton X-100-soluble (TxS) presynaptic and -insoluble (TxP) postsynaptic density fractions. A) Immunoblots of wild-type and 24-hydroxylase knockout TxS (Pre) and TxP (Post) fractions using a variety of antibodies against NMDAR subunits and other subcellular markers. PSD-95, a postsynaptic density marker, and synaptogyrin, a presynaptic marker, are expressed predominantly in the postsynaptic and presynaptic fractions, respectively, indicative of good separation of presynaptic and postsynaptic density membranes. Cholesterol 24-hydroxylase was detected using monoclonal antibody 1A7 and is found in both the presynaptic and postsynaptic membranes of wild-type samples. P450 reductase, an ER resident protein, was detected in both wild-type and knockout presynaptic membranes and shows the lack of ER membrane contamination in the postsynaptic density fraction. The NR1, NR2A, NR2B, phospho-Tyr-1472-NR2B, and NR2D NMDAR subunits were detected exclusively in the postsynaptic density fraction and showed no expression differences between wild-type and 24-hydroxylase knockout samples. β III tubulin was expressed equally in all protein samples. B) Quantification of postsynaptic protein levels in wild-type and 24-hydroxylase knockout TxP fractions. The signal intensities derived from immunoblots of individual synaptic proteins were normalized to that of the postsynaptic density marker protein, PSD-95. Data are quantified from a single experiment and are representative of two separate experiments.

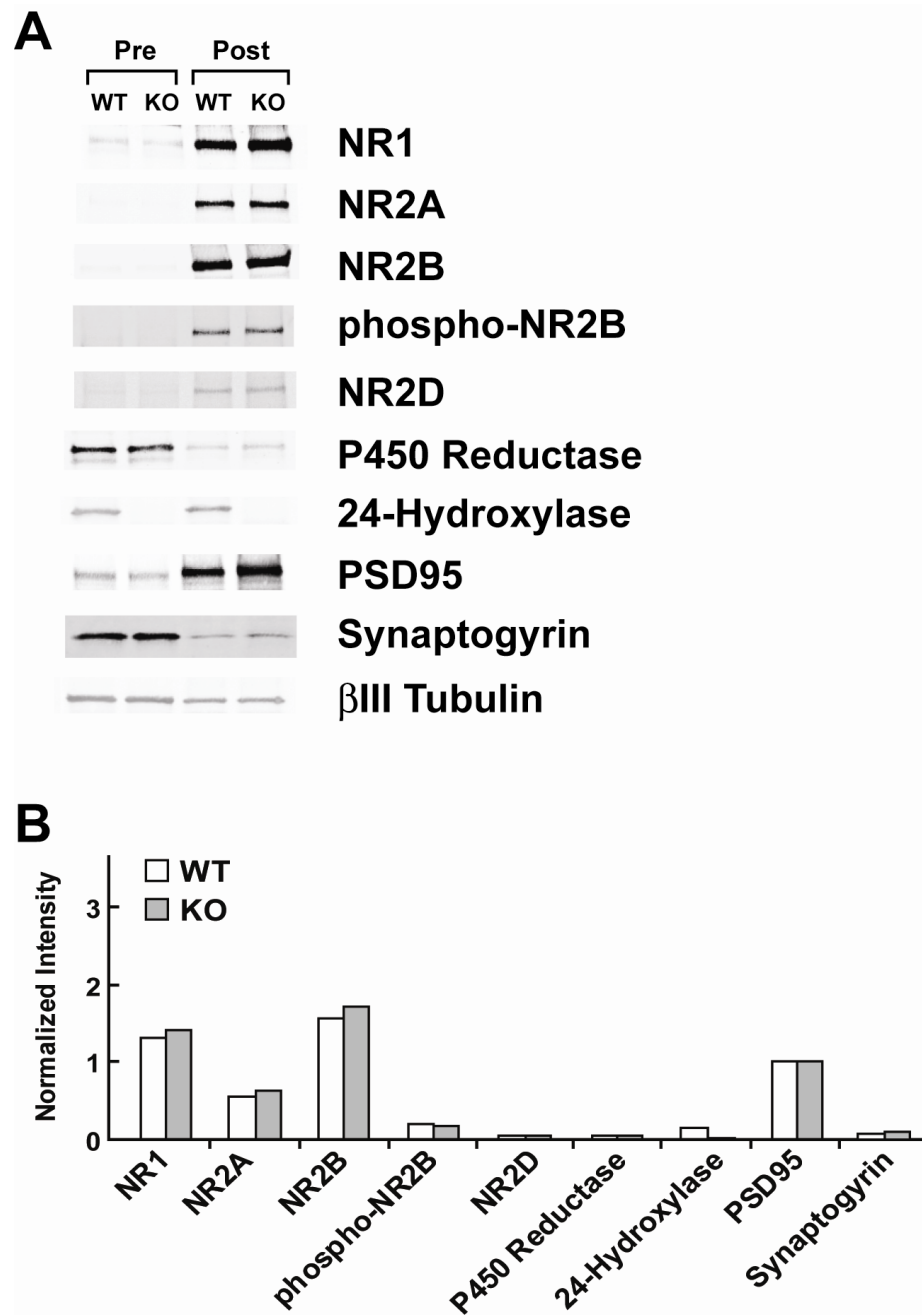
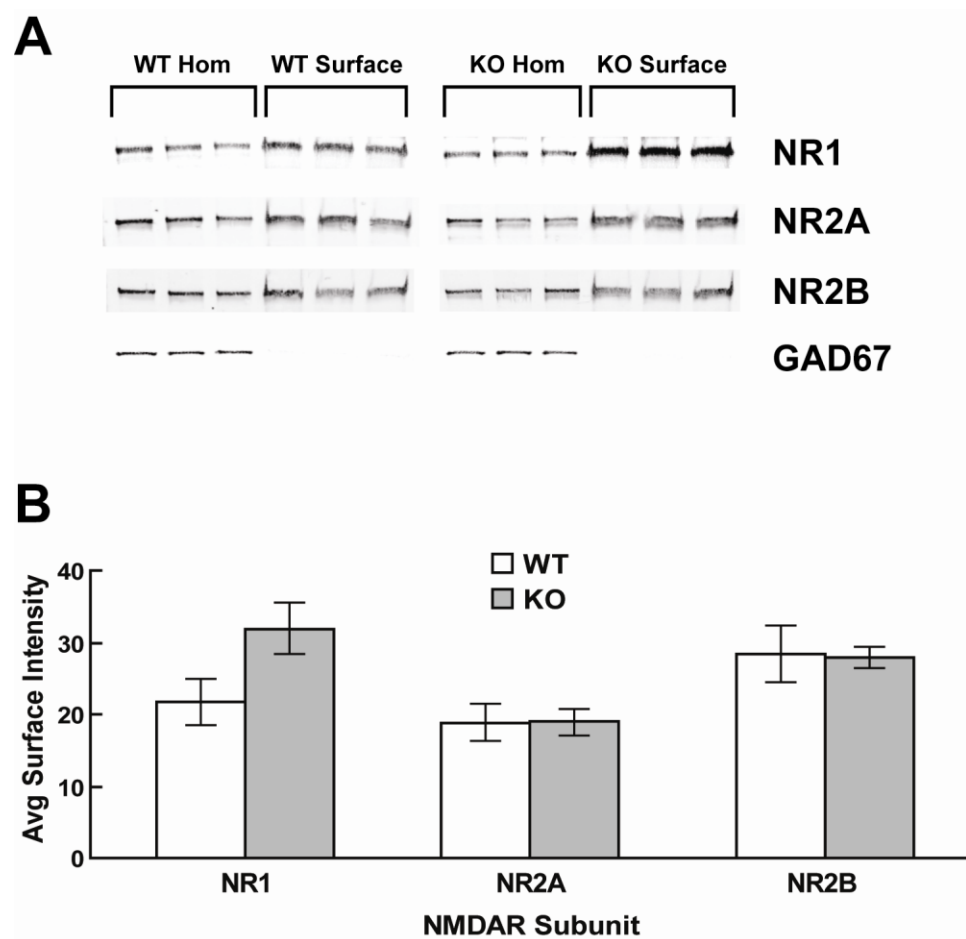


Figure 7. Surface NMDAR subunit levels in wild-type and 24-hydroxylase knockout hippocampal slices. A) Wild-type and 24-hydroxylase knockout surface proteins were isolated by biotinylation and precipitation and subjected to immunoblotting using antibodies against NR1, NR2A, NR2B, and GAD67. Three pools of slices were prepared from one animal per genotype and analyzed individually. GAD67 expression is detected only in the homogenates of wild-type and knockout slices, confirming the specificity of the biotinylation reagent for surface proteins. The wild-type and 24-hydroxylase knockout homogenates have similar levels of NMDAR subunits NR1, NR2A, and NR2B. Surface levels of NR1 are increased in knockout compared to wild-type samples, but this difference is not apparent when comparing NR2A and NR2B expression in knockout samples to those in wild-type samples. B) Quantification of NMDAR subunit levels in surface proteins isolated from wild-type and knockout hippocampal slices. Raw band intensities (integrated) are shown. Expression of NR2A and NR2B on the surface is similar in wild-type and knockout slices, but knockout slices have an increase in surface NR1, which is statistically significantly different from wild-type surface NR1 ($p=0.048$). For panel B, data were quantified from five independent experiments from one animal per genotype per experiment.



CHAPTER FIVE

Concluding Remarks

The human brain contains more cholesterol than any other organ in the body, when normalized to organ weight (Bjorkhem, 2006; Dietschy and Turley, 2004). The majority of brain cholesterol is found in myelin sheaths elaborated by oligodendrocytes that insulate neuronal axons, but some cholesterol is also present in the plasma membranes of neurons and glial cells. While the major, myelin-associated pool of brain cholesterol seems to be static in the adult, neuronal cholesterol is continually turned over by the enzyme cholesterol 24-hydroxylase, which catalyzes the major pathway of cholesterol metabolism in the brain. As neuronal cholesterol is metabolized to 24(*S*)-hydroxycholesterol, which crosses the blood brain barrier and enters the circulation, new cholesterol is synthesized from acetyl-CoA precursors to maintain steady-state levels of brain cholesterol, presumably to maintain myelin function (Kotti et al., 2006; Lund et al., 1999; Lund et al., 2003; Ramirez et al., 2008).

Studies in cholesterol 24-hydroxylase knockout mice demonstrate that proper rates of brain cholesterol synthesis are important for learning and the expression of a specific type of synaptic plasticity in the hippocampus, long-term potentiation (LTP) of Schaffer collateral-CA1 synaptic responses (Kotti et al., 2006). The metabolic defects in 24-hydroxylase knockout mice result in reduced brain cholesterol synthesis as well as a concomitant reduction in the synthesis of the entire complement of intermediates arising from the cholesterol biosynthetic pathway (Lund et al., 2003). A restoration of LTP in 24-hydroxylase knockout hippocampal slices was achieved after treatment with

geranylgeraniol (GG), a non-sterol isoprenoid end product of the cholesterol biosynthetic pathway (Kotti et al., 2006). Control experiments established a specific role for GG among the various isoprenoids produced by the mevalonate pathway in LTP (Kotti et al., 2006), consistent with an early demonstration of LTP defects after statin treatment (Matthies et al., 1997). Although other studies have shown decreased LTP after acute cholesterol depletion with cyclodextrin (Frank et al., 2008; Koudinov and Koudinova, 2001), this is presumably separate from the GG effect as 24-hydroxylase knockout mice have normal brain cholesterol levels and may be due to pre- and postsynaptic effects related to the ability of cholesterol to regulate membrane fluidity or lipid raft stability (Hering et al., 2003; Korade and Kenworthy, 2008; Lund et al., 2003; Ponce et al., 2008; Wasser et al., 2007). Additional studies have confirmed the specificity of GG in LTP at the chemical and genetic levels and a requirement for GG in both LTP induction and maintenance that does not appear to be dependent on protein prenylation (Kotti et al., 2008).

The results presented here provide strong evidence for the essential role of cholesterol turnover in learning and memory and its molecular correlate, LTP, and begin to describe the mechanism by which this occurs. Cholesterol turnover occurs in select neurons of the brain because they express the enzyme cholesterol 24-hydroxylase and can produce the membrane-permeable oxysterol, 24(*S*)-hydroxycholesterol. This process appears to be particularly important in neurons of brain regions important for various types of learning and memory such as the hippocampus, cortex, and cerebellum due to their high levels of 24-hydroxylase expression. Furthermore, cholesterol turnover is restricted to the postsynaptic compartments of neurons as 24-hydroxylase is highly

expressed throughout the endoplasmic reticulum of the soma and dendrites, and found in postsynaptic density biochemical fractions, but is undetectable in axons or presynaptic terminals. Constant cholesterol turnover and continued flow of intermediates through the mevalonate pathway provide a steady supply of GG, which is necessary to induce LTP in acute hippocampal slices and for normal learning ability in mice. Geranylgeraniol appears to modulate the function of the NMDA receptor, which is required for LTP induction, but does not affect the activity of other ion channels involved in LTP maintenance. This outcome is consistent with a variety of evidence presented here and elsewhere (Kotti et al., 2008) suggesting a postsynaptic role of brain cholesterol turnover in LTP. Pharmacological experiments using subtype-specific inhibitors show that GG affects specific subtypes of the NMDAR, though the mechanism of GG action on NMDAR function is still unknown.

Geranylgeraniol may affect NMDAR function and thus LTP by multiple potential mechanisms. Many prenylated proteins, including members of the Rab, Rac, and Rho families, are known to be involved in important cellular processes such as intracellular trafficking and actin dynamics that are also thought to be important in synaptic plasticity (Gerges et al., 2005; O'Kane et al., 2004). Previous studies have not established a possible role for GG in the acute prenylation of proteins involved in LTP induction (Kotti et al., 2008), although another study describes a requirement of protein prenylation in LTP (O'Kane et al., 2004). It is important to note that GG is required both for LTP induction and LTP maintenance at a time point approximately 10-15 minutes after stimulation (Kotti et al., 2008). These results correspond well to the temporal characteristics of glutamate receptor activity during LTP. The period of NMDAR-

mediated calcium entry necessary to induce LTP is on the order of seconds, whereas LTP induction promotes AMPAR insertion into the plasma membrane 15-30 minutes after stimulation (Blitzer, 2005; Malinow and Malenka, 2002), a process dependent on the geranylgeranylated protein Rab8 (Gerges et al., 2004). The present mechanistic studies specifically address the effect of GG on NMDARs, which mediate LTP induction, and do not rule out a possible later effect on prenylation-dependent AMPAR trafficking during LTP maintenance.

A remarkable aspect of the current data is that the NMDAR defect in 24-hydroxylase knockout neurons is only apparent in the presence of NR2B-specific inhibitors. This result implies knockout neurons have either increased NR2B function or decreased NR2A function due to the decreased availability of GG, and is consistent with the specific defect in LTP but not LTD. Current studies support the involvement of NR2B in LTD and NR2A in LTP (Kutsuwada et al., 1996; Liu et al., 2004; Massey et al., 2004; Sakimura et al., 1995; Sprengel et al., 1998), although these roles are likely not mutually exclusive (Bartlett et al., 2007; Li et al., 2007), and some studies contest this idea (Barria and Malinow, 2005; Bartlett et al., 2007; Gardoni et al., 2009; Morishita et al., 2007). Importantly, in wild-type hippocampal slices, the LTP induced by theta burst stimulation that is defective in 24-hydroxylase knockout hippocampal slices is unaffected by the NR2B antagonist, ifenprodil, suggesting a major role of NR2A receptors in this type of synaptic plasticity (T. Kotti, unpublished observation), consistent with previous reports (Bellone and Nicoll, 2007; Kohr et al., 2003).

GG appears to have a subtype-specific effect on NMDARs that is not due to changes in the surface receptor complement, or NR2A/NR2B ratio. Several possibilities

may explain this result. GG may alter the lipid environment of the postsynaptic membrane, which is known to affect membrane-spanning receptors in general (Pucadyil and Chattopadhyay, 2006), and NMDARs in particular (Casado and Ascher, 1998; Kloda et al., 2007; Paoletti and Ascher, 1994). Alterations in the physical characteristics of the membrane could affect both NMDAR activity and lateral exchange between synaptic and extrasynaptic pools of NMDA receptors (Tovar and Westbrook, 2002). Although NR2A and NR2B containing receptors are reported to possess similar mechanosensitive properties (Casado and Ascher, 1998), the lateral mobility of NMDARs depends on the identity of the NR2 subunit (Groc et al., 2009; Groc et al., 2006). Another possibility is the direct binding of GG to either NR2A or NR2B, which may increase or decrease receptor function, respectively. This idea is supported by reports of small molecules, such as arachidonic acid and spermine, binding to and affecting the function of NMDARs in a subtype-specific manner (Kew and Kemp, 1998; Tabuchi et al., 1997). Further studies utilizing available NR2A knockout mice will address subtype-specific effects of GG on NMDAR function.

Another intriguing aspect of the current data is that a possible role of dysfunctional ER-derived calcium in the LTP phenotype of 24-hydroxylase knockout animals is not readily apparent. This finding is surprising due to the exclusive subcellular distribution of 24-hydroxylase in the ER and the known dependence of some forms of LTP on ER calcium release, which amplifies the calcium influx through NMDARs (Rudy, 2008). Moreover, mutant mice lacking the specialized ER of dendritic spines, the spine apparatus, show defects in LTP and spatial learning similar to those described in 24-hydroxylase knockout mice (Deller et al., 2003). The LTP measured here in wild-type

and 24-hydroxylase knockout hippocampal slices was generated by four trains of theta bursts, similar to LTP2 as described by Raymond and Redman. This type of LTP depends on calcium release from inositol 1,4,5-trisphosphate receptors (IP3Rs) in the ER of the dendrite (Raymond, 2007; Raymond and Redman, 2002; 2006). Although the role of ER calcium in the LTP defect seen in 24-hydroxylase knockout slices has not been directly assessed, there was no contribution of ER calcium to NMDAR-mediated calcium influx in cultured neurons from wild-type or knockout embryos. Furthermore, the ER structure and protein expression in neurons from 24-hydroxylase knockout embryos was indistinguishable from those of wild-type neurons, suggesting a normal ER in the absence of 24-hydroxylase. The clear defect in 24-hydroxylase knockout NMDAR function is presumably unrelated to any potential abnormalities in ER function and could be expected to fully account for the lack of LTP in these animals; however, a contribution of ER calcium cannot be ruled out at this point. For instance, in a manner analogous to the endogenous cannabinoid system (Barinaga, 2001), GG could be produced and/or released during LTP and act as a ligand for a metabotropic receptor coupled to phospholipase C in addition to the effects on NMDAR function documented here. In this case, IP3 will be produced and ER calcium will be released, augmenting NMDAR-mediated calcium influx and promoting LTP induction under normal conditions.

The present work describes an essential role of brain cholesterol synthesis and the non-sterol isoprenoid, geranylgeraniol, in LTP and by extension, learning and memory in the intact animal. A specific effect of GG on NMDAR function is seen in cultured embryonic neurons, consistent with the requirement for this glutamate receptor subtype in LTP induction. Further studies will address the apparent NMDAR subunit

specificity of this effect and determine the molecular mechanism by which GG can affect NMDAR activity and therefore LTP.

BIBLIOGRAPHY

- Adams CM, Reitz J, De Brabander JK, Feramisco JD, Li L, Brown MS, Goldstein JL. 2004. Cholesterol and 25-hydroxycholesterol inhibit activation of SREBPs by different mechanisms, both involving SCAP and Insigs. *The Journal of biological chemistry* 279(50):52772-52780.
- Al-Hallaq RA, Conrads TP, Veenstra TD, Wenthold RJ. 2007. NMDA dimeric receptor populations and associated proteins in rat hippocampus. *J Neurosci* 27(31):8334-8343.
- Auberson YP, Allgeier H, Bischoff S, Lingenhoehl K, Moretti R, Schmutz M. 2002. 5-Phosphonomethylquinoxalinediones as competitive NMDA receptor antagonists with a preference for the human 1A/2A, rather than 1A/2B receptor composition. *Bioorganic & medicinal chemistry letters* 12(7):1099-1102.
- Banker G, Goslin K, editors. 2002. *Culturing Nerve Cells*. 2nd ed. Cambridge, MA: MIT Press. 1-666 p.
- Barinaga M. 2001. Neurobiology. How cannabinoids work in the brain. *Science* (New York, NY 291(5513):2530-2531.
- Barria A, Malinow R. 2005. NMDA receptor subunit composition controls synaptic plasticity by regulating binding to CaMKII. *Neuron* 48(2):289-301.
- Bartlett TE, Bannister NJ, Collett VJ, Dargan SL, Massey PV, Bortolotto ZA, Fitzjohn SM, Bashir ZI, Collingridge GL, Lodge D. 2007. Differential roles of NR2A and NR2B-containing NMDA receptors in LTP and LTD in the CA1 region of two-week old rat hippocampus. *Neuropharmacology* 52(1):60-70.
- Belelli D, Lambert JJ. 2005. Neurosteroids: endogenous regulators of the GABA_A receptors. *Nat Rev Neurosci* 6:565-575.
- Bellone C, Nicoll RA. 2007. Rapid bidirectional switching of synaptic NMDA receptors. *Neuron* 55(5):779-785.

- Beltran-Parrazal L, Lopez-Valdes HE, Brennan KC, Diaz-Munoz M, Vellis Jd, Charles AC. 2006. Mitochondrial transport in processes of cortical neurons is independent of intracellular calcium. *Am J Physiol Cell Physiol* 291:C1193-C1197.
- Berasi SP, Huard C, Li D, Shih HH, Sun Y, Zhong W, Paulsen JE, Brown EL, Gimeno RE, Martinez RV. 2006. Inhibition of gluconeogenesis through transcriptional activation of EGR1 and DUSP4 by AMP-activated kinase. *J Biol Chem* 281:27167-27177.
- Berridge MJ. 1998. Neuronal calcium signaling. *Neuron* 21:13-26.
- Biou V, Bhattacharyya S, Malenka RC. 2008. Endocytosis and recycling of AMPA receptors lacking GluR2/3. *Proceedings of the National Academy of Sciences of the United States of America* 105(3):1038-1043.
- Bjorkhem I. 2006. Crossing the barrier: oxysterols as cholesterol transporters and metabolic modulators in the brain. *Journal of internal medicine* 260:493-508.
- Bjorkhem I, Andersson U, Ellis E, Alvelius G, Ellegard L, Diczfalusy U, Sjovall J, Einarsson C. 2001. From brain to bile. Evidence that conjugation and ω -hydroxylation are important for elimination of 24S-hydroxycholesterol (cerebrosterol) in humans. *J Biol Chem* 276:37004-37010.
- Bjorkhem I, Lutjohann D, Breuer O, Sakinis A, Wennmalm A. 1997. Importance of a novel oxidative mechanism for elimination of brain cholesterol. Turnover of cholesterol and 24(S)-hydroxycholesterol in rat brain as measured with $^{18}O_2$ techniques in vivo and in vitro. *The Journal of biological chemistry* 272(48):30178-30184.
- Bjorkhem I, Lutjohann D, Diczfalusy U, Stahle L, Ahlborg G, Wahren J. 1998. Cholesterol homeostasis in human brain: turnover of 24S-hydroxycholesterol and evidence for a cerebral origin of most of this oxysterol in the circulation. *Journal of lipid research* 39(8):1594-1600.
- Bjorkhem I, Meaney S. 2004. Brain cholesterol: long secret life behind a barrier. *Arteriosclerosis, thrombosis, and vascular biology* 24:806-815.

- Bliss TV, Lomo T. 1973. Long-lasting potentiation of synaptic transmission in the dentate area of the anaesthetized rabbit following stimulation of the perforant path. *The Journal of physiology* 232(2):331-356.
- Blitzer RD. 2005. Teaching resources. Long-term potentiation: mechanisms of induction and maintenance. *Sci STKE* 2005(309):tr26.
- Bredt DS, Nicoll RA. 2003. AMPA receptor trafficking at excitatory synapses. *Neuron* 40:361-379.
- Brown J, 3rd, Theisler C, Silberman S, Magnuson D, Gottardi-Littell N, Lee JM, Yager D, Crowley J, Sambamurti K, Rahman MM, Reiss AB, Eckman CB, Wolozin B. 2004. Differential expression of cholesterol hydroxylases in Alzheimer's disease. *The Journal of biological chemistry* 279:34674-34681.
- Brown MS, Goldstein JL. 1980. Multivalent feedback regulation of HMG CoA reductase, a control mechanism coordinating isoprenoid synthesis and cell growth. *J Lipid Res* 21:505-517.
- Caceres A, Payne MR, Binder LI, Steward O. 1983. Immunocytochemical localization of actin and microtubule-associated protein MAP2 in dendritic spines. *Proc Natl Acad Sci U S A* 80:1738-1742.
- Casado M, Ascher P. 1998. Opposite modulation of NMDA receptors by lysophospholipids and arachidonic acid: common features with mechanosensitivity. *The Journal of physiology* 513 (Pt 2):317-330.
- Chang DT, Reynolds IJ. 2006. Differences in mitochondrial movement and morphology in young and mature primary cortical neurons in culture. *Neuroscience* 141:727-736.
- Chen Y, Beffert U, Ertunc M, Tang TS, Kavalali ET, Bezprozvanny I, Herz J. 2005. Reelin modulates NMDA receptor activity in cortical neurons. *J Neurosci* 25(36):8209-8216.
- Choi YM, Kim SH, Chung S, Uhm DY, Park MK. 2006. Regional interaction of endoplasmic reticulum Ca²⁺ signals between soma and dendrites through rapid luminal Ca²⁺ diffusion. *J Neurosci* 26:12127-12136.

- Colicelli J. 2004. Human Ras superfamily proteins and related GTPases. *Sci STKE*(250):re13.
- Colombo S, Longhi R, Alcaro S, Ortuso F, Sprocati T, Flora A, Borgese N. 2005. N-myristoylation determines dual targeting of mammalian NADH-cytochrome b5 reductase to ER and mitochondrial outer membranes by a mechanism of kinetic partitioning. *J Cell Biol* 168:735-745.
- Crick DC, Andres DA, Waechter CJ. 1997. Novel salvage pathway utilizing farnesol and geranylgeraniol for protein isoprenylation. *Biochem Biophys Res Comm* 237:483-487.
- Crook J, Hendrickson A, Robinson FR. 2006. Co-localization of glycine and gaba immunoreactivity in interneurons in Macaca monkey cerebellar cortex. *Neuroscience* 141:1951-1959.
- Custer SK, Garden GA, Gill N, Rueb U, Libby RT, Schultz C, Guyenet SJ, Deller T, Westrum LE, Sopher BL, La Spada AR. 2006. Bergmann glia expression of polyglutamine-expanded ataxin-7 produces neurodegeneration by impairing glutamate transport. *Nature neuroscience* 9(10):1302-1311.
- Davidson AN. 1965. Brain Sterol Metabolism. *Adv Lipid Res* 3:171-196.
- Davies KD, Alvestad RM, Coultrap SJ, Browning MD. 2007. alphaCaMKII autophosphorylation levels differ depending on subcellular localization. *Brain research* 1158:39-49.
- Davies KD, Goebel-Goody SM, Coultrap SJ, Browning MD. 2008. Long term synaptic depression that is associated with GluR1 dephosphorylation but not alpha-amino-3-hydroxy-5-methyl-4-isoxazolepropionic acid (AMPA) receptor internalization. *The Journal of biological chemistry* 283(48):33138-33146.
- de Blas AL. 1984. Monoclonal antibodies to specific astroglial and neuronal antigens reveal the cytoarchitecture of the Bergmann glia fibers in the cerebellum. *J Neurosci* 4(1):265-273.
- Deller T, Korte M, Chabanis S, Drakew A, Schwegler H, Stefani GG, Zuniga A, Schwarz K, Bonhoeffer T, Zeller R, Frotscher M, Mundel P. 2003. Synaptopodin-deficient mice lack a spine apparatus and show deficits in

- synaptic plasticity. *Proceedings of the National Academy of Sciences of the United States of America* 100(18):10494-10499.
- Derkach VA. 2003. Silence analysis of AMPA receptor mutated at the CaM-kinase II phosphorylation site. *Biophysical journal* 84(3):1701-1708.
- Dietschy JM, Turley SD. 2004. Thematic review series: brain Lipids. Cholesterol metabolism in the central nervous system during early development and in the mature animal. *Journal of lipid research* 45:1375-1397.
- Ehlers MD. 2000. Reinsertion or degradation of AMPA receptors determined by activity-dependent endocytic sorting. *Neuron* 28:511-525.
- Endo A. 1992. The discovery and development of HMG-CoA reductase inhibitors. *Journal of lipid research* 33(11):1569-1582.
- Erbel-Sieller C, Dudley CA, Zhou Y, Wu X, Estil SJ, Han T, Diaz-Arrastia R, Brunskill EW, Potter SS, McKnight SL. 2004. Behavioral and regulatory abnormalities in mice deficient in the NPAS1 and NPAS3 transcription factors. *Proc Natl Acad Sci U S A* 101:13648-13653.
- Erreger K, Dravid SM, Banke TG, Wyllie DJ, Traynelis SF. 2005. Subunit-specific gating controls rat NR1/NR2A and NR1/NR2B NMDA channel kinetics and synaptic signalling profiles. *The Journal of physiology* 563(Pt 2):345-358.
- Espenshade PJ, Hughes AL. 2007. Regulation of sterol synthesis in eukaryotes. *Annual review of genetics* 41:401-427.
- Feng L, Hatten ME, Heintz N. 1994. Brain lipid-binding protein (BLBP): a novel signaling system in the developing mammalian CNS. *Neuron* 12:895-908.
- Ferri P, Biagiotti E, Ambrogini P, Santi S, Del Grande P, Ninfali P. 2005. NADPH-consuming enzymes correlate with glucose-6-phosphate dehydrogenase in Purkinje cells: an immunohistochemical and enzyme histochemical study of the rat cerebellar cortex. *Neuroscience research* 51(2):185-197.
- Finn RD, McLaughlin LA, Ronseaux S, Rosewell I, Houston JB, Henderson CJ, Wolf CR. 2008. Defining the in Vivo Role for cytochrome b5 in cytochrome P450 function through the conditional hepatic deletion of

microsomal cytochrome b5. *The Journal of biological chemistry* 283(46):31385-31393.

- Fischer von Mollard G, Mignery GA, Baumert M, Perin MS, Hanson TJ, Burger PM, Jahn R, Sudhof TC. 1990. rab3 is a small GTP-binding protein exclusively localized to synaptic vesicles. *Proceedings of the National Academy of Sciences of the United States of America* 87:1988-1992.
- Flajollet S, Lefebvre B, Rachez C, Lefebvre P. 2006. Distinct roles of the steroid receptor coactivator 1 and MED1 in retinoid-induced transcription and cellular differentiation. *J Biol Chem* 281:20338-20348.
- Fong AY, Stornetta RL, Foley CM, Potts JT. 2005. Immunohistochemical localization of GAD67-expressing neurons and processes in the rat brainstem: subregional distribution in the nucleus tractus solitarius. *J Comp Neurol* 493:274-290.
- Foradori CD, Werner SB, Sandau US, Clapp TR, Handa RJ. 2007. Activation of the androgen receptor alters the intracellular calcium response to glutamate in primary hippocampal neurons and modulates sarco/endoplasmic reticulum calcium ATPase 2 transcription. *Neuroscience* 149(1):155-164.
- Frank C, Rufini S, Tancredi V, Forcina R, Grossi D, D'Arcangelo G. 2008. Cholesterol depletion inhibits synaptic transmission and synaptic plasticity in rat hippocampus. *Experimental neurology* 212(2):407-414.
- Friedman LK, Segal M, Veliskova J. 2003. GluR2 knockdown reveals a dissociation between $[Ca^{2+}]_i$ surge and neurotoxicity. *Neurochemistry international* 43(3):179-189.
- Garcia JA, Zhang D, Estill SJ, Michnoff C, Rutter J, Reick M, Scott K, Diaz-Arrastia R, McKnight SL. 2000. Impaired cued and contextual memory in NPAS2-deficient mice. *Science* 288:2226-2230.
- Gardoni F, Mauceri D, Malinverno M, Polli F, Costa C, Tozzi A, Siliquini S, Picconi B, Cattabeni F, Calabresi P, Di Luca M. 2009. Decreased NR2B subunit synaptic levels cause impaired long-term potentiation but not long-term depression. *J Neurosci* 29(3):669-677.

- Genoux D, Montgomery JM. 2007. Glutamate receptor plasticity at excitatory synapses in the brain. *Clinical and experimental pharmacology & physiology* 34(10):1058-1063.
- Gerges NZ, Backos DS, Esteban JA. 2004. Local control of AMPA receptor trafficking at the postsynaptic terminal by a small GTPase of the Rab family. *The Journal of biological chemistry* 279:43870-43878.
- Gerges NZ, Backos DS, Rupasinghe CN, Spaller MR, Esteban JA. 2006. Dual role of the exocyst in AMPA receptor targeting and insertion into the postsynaptic membrane. *EMBO J* 25:1623-1634.
- Gerges NZ, Brown TC, Correia SS, Esteban JA. 2005. Analysis of Rab protein function in neurotransmitter receptor trafficking at hippocampal synapses. *Methods in enzymology* 403:153-166.
- Goldstein JL, Brown MS. 1990. Regulation of the mevalonate pathway. *Nature* 343(6257):425-430.
- Goldstein ME, Sternberger LA, Sternberger NH. 1983. Microheterogeneity ("neurotypy") of neurofilament proteins. *Proc Natl Acad Sci USA* 80:3101-3105.
- Groc L, Bard L, Choquet D. 2009. Surface trafficking of N-methyl-d-aspartate receptors: Physiological and pathological perspectives. *Neuroscience* 158(1):4-18.
- Groc L, Heine M, Cousins SL, Stephenson FA, Lounis B, Cognet L, Choquet D. 2006. NMDA receptor surface mobility depends on NR2A-2B subunits. *Proceedings of the National Academy of Sciences of the United States of America* 103(49):18769-18774.
- Grosshans DR, Clayton DA, Coultrap SJ, Browning MD. 2002. LTP leads to rapid surface expression of NMDA but not AMPA receptors in adult rat CA1. *Nature neuroscience* 5(1):27-33.
- Group HPSC. 2002. MRC/BHF heart protection study of cholesterol lowering with simvastatin in 20536 high-risk individuals: a randomised placebo-controlled trial. *Lancet* 360:7-22.

- Gruart A, Munoz MD, Delgado-Garcia JM. 2006. Involvement of the CA3-CA1 synapse in the acquisition of associative learning in behaving mice. *J Neurosci* 26(4):1077-1087.
- Grundy SM, Cleeman JI, Merz CNB, Brewer JHB, Clark LT, Hunninghake DB, Pasternak RC, Smith JSC, Stone NJ. 2004. Implications of recent clinical trials for the national cholesterol education program adult treatment panel III guidelines. *Circulation* 110:227-239.
- Harris AZ, Pettit DL. 2007. Extrasynaptic and synaptic NMDA receptors form stable and uniform pools in rat hippocampal slices. *The Journal of physiology* 584(Pt 2):509-519.
- Harris AZ, Pettit DL. 2008. Recruiting extrasynaptic NMDA receptors augments synaptic signaling. *Journal of neurophysiology* 99(2):524-533.
- Hebb DO. 1949. *The Organization of Behavior; a neuropsychological theory*. New York: Wiley Press.
- Hell JW, Jahn R. 1998. Bioenergetic characterization of gamma-aminobutyric acid transporter of synaptic vesicles. *Methods Enzymol* 296:116-124.
- Hering H, Lin CC, Sheng M. 2003. Lipid rafts in the maintenance of synapses, dendritic spines, and surface AMPA receptor stability. *J Neurosci* 23:3262-3271.
- Horton AC, Ehlers MD. 2003. Dual modes of endoplasmic reticulum-to-Golgi transport in dendrites revealed by live-cell imaging. *J Neurosci* 23:6188-6199.
- Horton AC, Ehlers MD. 2004. Secretory trafficking in neuronal dendrites. *Nat Cell Biol* 6:585-591.
- Horton JD, Goldstein JL, Brown MS. 2002. SREBPs: activators of the complete program of cholesterol and fatty acid synthesis in the liver. *The Journal of clinical investigation* 109(9):1125-1131.
- Ikonen E, Fiedler K, Parton RG, Simons K. 1995. Prohibitin, an antiproliferative protein, is localized to mitochondria. *FEBS Lett* 358:273-277.

- Izumi Y, Auberson YP, Zorumski CF. 2006. Zinc modulates bidirectional hippocampal plasticity by effects on NMDA receptors. *J Neurosci* 26(27):7181-7188.
- Johnston PA, Jahn R, Sudhof TC. 1989. Transmembrane topography and evolutionary conservation of synaptophysin. *J Biol Chem* 264:1268-1273.
- Jones VC, McKeown L, Verkhratsky A, Jones OT. 2008. LV-pIN-KDEL: a novel lentiviral vector demonstrates the morphology, dynamics and continuity of the endoplasmic reticulum in live neurones. *BMC neuroscience* 9:10.
- Kandel ER, Schwartz, James H., and Jessell, Thomas M., editor. 1991. *Principles of Neural Science*. 3rd ed. Norwalk, Connecticut: Appleton & Lange.
- Kellogg BA, Poulter CD. 1997. Chain elongation in the isoprenoid pathway. *Curr Opin Chem Biol* 1:570-578.
- Kenny AV, Cousins SL, Pinho L, Stephenson FA. 2009. The integrity of the glycine co-agonist binding site of N-methyl-D-aspartate receptors is a functional quality control checkpoint for cell surface delivery. *The Journal of biological chemistry* 284(1):324-333.
- Kerchner GA, Nicoll RA. 2008. Silent synapses and the emergence of a postsynaptic mechanism for LTP. *Nat Rev Neurosci* 9(11):813-825.
- Kew JN, Kemp JA. 1998. An allosteric interaction between the NMDA receptor polyamine and ifenprodil sites in rat cultured cortical neurones. *The Journal of physiology* 512 (Pt 1):17-28.
- Kew JN, Trube G, Kemp JA. 1996. A novel mechanism of activity-dependent NMDA receptor antagonism describes the effect of ifenprodil in rat cultured cortical neurones. *The Journal of physiology* 497 (Pt 3):761-772.
- Kleschevnikov AM, Belichenko PV, Villar AJ, Epstein CJ, Malenka RC, Mobley WC. 2004. Hippocampal long-term potentiation suppressed by increased inhibition in the Ts65Dn mouse, a genetic model of Down syndrome. *J Neurosci* 24:8153-8160.
- Kloda A, Lua L, Hall R, Adams DJ, Martinac B. 2007. Liposome reconstitution and modulation of recombinant N-methyl-D-aspartate receptor channels

- by membrane stretch. *Proceedings of the National Academy of Sciences of the United States of America* 104(5):1540-1545.
- Kohr G. 2006. NMDA receptor function: subunit composition versus spatial distribution. *Cell and tissue research* 326(2):439-446.
- Kohr G, Jensen V, Koester HJ, Mihaljevic AL, Utvik JK, Kvello A, Ottersen OP, Seeburg PH, Sprengel R, Hvalby O. 2003. Intracellular domains of NMDA receptor subtypes are determinants for long-term potentiation induction. *J Neurosci* 23(34):10791-10799.
- Kopec C, Malinow R. 2006. Neuroscience. Matters of size. *Science (New York, NY)* 314:1554-1555.
- Kopec CD, Li B, Wei W, Boehm J, Malinow R. 2006. Glutamate receptor exocytosis and spine enlargement during chemically induced long-term potentiation. *J Neurosci* 26(7):2000-2009.
- Korade Z, Kenworthy AK. 2008. Lipid rafts, cholesterol, and the brain. *Neuropharmacology* 55(8):1265-1273.
- Kosik KS, Finch EA. 1987. MAP2 and tau segregate into dendritic and axonal domains after the elaboration of morphologically distinct neurites: an immunohistochemical study of cultured rat cerebrum. *J Neurosci* 7:3142-3153.
- Kotti T, Head DD, McKenna CE, Russell DW. 2008. Biphasic requirement for geranylgeraniol in hippocampal long-term potentiation. *Proceedings of the National Academy of Sciences of the United States of America* 105(32):11394-11399.
- Kotti TJ, Ramirez DM, Pfeiffer BE, Huber KM, Russell DW. 2006. Brain cholesterol turnover required for geranylgeraniol production and learning in mice. *Proceedings of the National Academy of Sciences of the United States of America* 103:3869-3874.
- Koudinov AR, Koudinova NV. 2001. Essential role for cholesterol in synaptic plasticity and neuronal degeneration. *Faseb J* 15(10):1858-1860.
- Kutsuwada T, Sakimura K, Manabe T, Takayama C, Katakura N, Kushiya E, Natsume R, Watanabe M, Inoue Y, Yagi T, Aizawa S, Arakawa M,

- Takahashi T, Nakamura Y, Mori H, Mishina M. 1996. Impairment of suckling response, trigeminal neuronal pattern formation, and hippocampal LTD in NMDA receptor epsilon 2 subunit mutant mice. *Neuron* 16(2):333-344.
- Lan JY, Skeberdis VA, Jover T, Grooms SY, Lin Y, Araneda RC, Zheng X, Bennett MV, Zukin RS. 2001. Protein kinase C modulates NMDA receptor trafficking and gating. *Nature neuroscience* 4(4):382-390.
- Lange Y, Ye J, Strebel F. 1995. Movement of 25-hydroxycholesterol from the plasma membrane to the rough endoplasmic reticulum in cultured hepatoma cells. *Journal of lipid research* 36(5):1092-1097.
- Lau CG, Zukin RS. 2007. NMDA receptor trafficking in synaptic plasticity and neuropsychiatric disorders. *Nat Rev Neurosci* 8(6):413-426.
- Lee MK, Tuttle JB, Rebhun LI, Cleveland DW, Frankfurter A. 1990. The expression and posttranslational modification of a neuron-specific beta-tubulin isotype during chick embryogenesis. *Cell Motil Cytoskeleton* 17:118-132.
- Li-Hawkins J, Lund EG, Bronson AD, Russell DW. 2000. Expression cloning of an oxysterol 7 α -hydroxylase selective for 24-hydroxycholesterol. *J Biol Chem* 275:16543-16549.
- Li B, Chen N, Luo T, Otsu Y, Murphy TH, Raymond LA. 2002. Differential regulation of synaptic and extra-synaptic NMDA receptors. *Nature neuroscience* 5(9):833-834.
- Li R, Huang FS, Abbas AK, Wigstrom H. 2007. Role of NMDA receptor subtypes in different forms of NMDA-dependent synaptic plasticity. *BMC neuroscience* 8:55.
- Liao JK. 2002. Isoprenoids as mediators of the biological effects of statins. *J Clin Invest* 110:285-288.
- Liu L, Wong TP, Pozza MF, Lingenhoehl K, Wang Y, Sheng M, Auberson YP, Wang YT. 2004. Role of NMDA receptor subtypes in governing the direction of hippocampal synaptic plasticity. *Science (New York, NY)* 304(5673):1021-1024.

- Longart M, Liu Y, Karavanova I, Buonanno A. 2004. Neuregulin-2 is developmentally regulated and targeted to dendrites of central neurons. *J Comp Neurol* 472:156-172.
- Lund EG, Guileyardo JM, Russell DW. 1999. cDNA cloning of cholesterol 24-hydroxylase, a mediator of cholesterol homeostasis in the brain. *Proceedings of the National Academy of Sciences of the United States of America* 96:7238-7243.
- Lund EG, Xie C, Kotti T, Turley SD, Dietschy JM, Russell DW. 2003. Knockout of the cholesterol 24-hydroxylase gene in mice reveals a brain-specific mechanism of cholesterol turnover. *The Journal of biological chemistry* 278:22980-22988.
- Lutjohann D, Breuer O, Ahlborg G, Nennesmo I, Siden A, Diczfalusy U, Bjorkhem I. 1996. Cholesterol homeostasis in human brain: evidence for an age-dependent flux of 24S-hydroxycholesterol from the brain into the circulation. *Proceedings of the National Academy of Sciences of the United States of America* 93(18):9799-9804.
- Malenka RC, Bear MF. 2004. LTP and LTD: an embarrassment of riches. *Neuron* 44:5-21.
- Malinow R, Malenka RC. 2002. AMPA receptor trafficking and synaptic plasticity. *Annual review of neuroscience* 25:103-126.
- Man HY, Sekine-Aizawa Y, Huganir RL. 2007. Regulation of α -amino-3-hydroxy-5-methyl-4-isoxazolepropionic acid receptor trafficking through PKA phosphorylation of the Glu receptor 1 subunit. *Proceedings of the National Academy of Sciences of the United States of America* 104(9):3579-3584.
- Martone ME, Zhang Y, Simpliciano VM, Carragher BO, Ellisman MH. 1993. Three-dimensional visualization of the smooth endoplasmic reticulum in Purkinje cell dendrites. *J Neurosci* 13:4636-4646.
- Massey PV, Johnson BE, Moulton PR, Auberson YP, Brown MW, Molnar E, Collingridge GL, Bashir ZI. 2004. Differential roles of NR2A and NR2B-containing NMDA receptors in cortical long-term potentiation and long-term depression. *J Neurosci* 24(36):7821-7828.

- Mast N, Norcross R, Andersson U, Shou M, Nakayama K, Bjorkhem I, Pikuleva IA. 2003. Broad substrate specificity of human cytochrome P450 46A1 which initiates cholesterol degradation in the brain. *Biochem* 42:14284-14292.
- Matthies H, Jr., Schulz S, Hollt V, Krug M. 1997. Inhibition by compactin demonstrates a requirement of isoprenoid metabolism for long-term potentiation in rat hippocampal slices. *Neuroscience* 79(2):341-346.
- McIntosh TJ, Simon SA. 2006. Roles of bilayer material properties in function and distribution of membrane proteins. *Annual review of biophysics and biomolecular structure* 35:177-198.
- Meaney S, Bodin K, Diczfalusy U, Bjorkhem I. 2002. On the rate of translocation in vitro and kinetics in vivo of the major oxysterols in human circulation: critical importance of the position of the oxygen function. *Journal of lipid research* 43(12):2130-2135.
- Mezgrahani A, Courageot J, Mani JC, Pugnieri M, Bastiani P, Miquelis R. 2000. Protein-disulfide isomerase (PDI) in FRTL5 cells. pH-dependent thyroglobulin/PDI interactions determine a novel PDI function in the post-endoplasmic reticulum of thyrocytes. *J Biol Chem* 275:1920-1929.
- Miller B, Sarantis M, Traynelis SF, Attwell D. 1992. Potentiation of NMDA receptor currents by arachidonic acid. *Nature* 355(6362):722-725.
- Morishita W, Lu W, Smith GB, Nicoll RA, Bear MF, Malenka RC. 2007. Activation of NR2B-containing NMDA receptors is not required for NMDA receptor-dependent long-term depression. *Neuropharmacology* 52(1):71-76.
- Morris R. 1984. Developments of a water-maze procedure for studying spatial learning in the rat. *Journal of neuroscience methods* 11(1):47-60.
- Nakazawa T, Komai S, Tezuka T, Hisatsune C, Umemori H, Semba K, Mishina M, Manabe T, Yamamoto T. 2001. Characterization of Fyn-mediated tyrosine phosphorylation sites on GluR epsilon 2 (NR2B) subunit of the N-methyl-D-aspartate receptor. *The Journal of biological chemistry* 276(1):693-699.

- Nakazawa T, Komai S, Watabe AM, Kiyama Y, Fukaya M, Arima-Yoshida F, Horai R, Sudo K, Ebine K, Delawary M, Goto J, Umemori H, Tezuka T, Iwakura Y, Watanabe M, Yamamoto T, Manabe T. 2006. NR2B tyrosine phosphorylation modulates fear learning as well as amygdaloid synaptic plasticity. *The EMBO journal* 25(12):2867-2877.
- Neyton J, Paoletti P. 2006. Relating NMDA receptor function to receptor subunit composition: limitations of the pharmacological approach. *J Neurosci* 26(5):1331-1333.
- Norris PJ, Hardwick JP, Emson PC. 1994. Localization of NADPH cytochrome P450 oxidoreductase in rat brain by immunohistochemistry and in situ hybridization and a comparison with the distribution of neuronal NADPH-diaphorase staining. *Neuroscience* 61(2):331-350.
- Nosyreva ED, Huber KM. 2005. Developmental switch in synaptic mechanisms of hippocampal metabotropic glutamate receptor-dependent long-term depression. *J Neurosci* 25(11):2992-3001.
- O'Kane EM, Stone TW, Morris BJ. 2004. Increased long-term potentiation in the CA1 region of rat hippocampus via modulation of GTPase signalling or inhibition of Rho kinase. *Neuropharmacology* 46(6):879-887.
- Oh MC, Derkach VA, Guire ES, Soderling TR. 2006. Extrasynaptic membrane trafficking regulated by GluR1 serine 845 phosphorylation primes AMPA receptors for long-term potentiation. *The Journal of biological chemistry* 281(2):752-758.
- Ordway RW, Singer JJ, Walsh JV, Jr. 1991. Direct regulation of ion channels by fatty acids. *Trends in neurosciences* 14(3):96-100.
- Paoletti P, Ascher P. 1994. Mechanosensitivity of NMDA receptors in cultured mouse central neurons. *Neuron* 13(3):645-655.
- Paoletti P, Neyton J. 2007. NMDA receptor subunits: function and pharmacology. *Current opinion in pharmacology* 7(1):39-47.
- Park M, Penick EC, Edwards JG, Kauer JA, Ehlers MD. 2004. Recycling endosomes supply AMPA receptors for LTP. *Science* 305:1972-1975.

- Park M, Salgado JM, Ostroff L, Helton TD, Robinson CG, Harris KM, Ehlers MD. 2006. Plasticity-induced growth of dendritic spines by exocytic trafficking from recycling endosomes. *Neuron* 52:817-830.
- Petralia RS, Sans N, Wang YX, Wenthold RJ. 2005. Ontogeny of postsynaptic density proteins at glutamatergic synapses. *Molecular and cellular neurosciences* 29(3):436-452.
- Petrou S, Ordway RW, Singer JJ, Walsh JV, Jr. 1993. A putative fatty acid-binding domain of the NMDA receptor. *Trends in biochemical sciences* 18(2):41-42.
- Pfeffer S, Aivazian D. 2004. Targeting Rab GTPases to distinct membrane compartments. *Nat Rev Mol Cell Biol* 5:886-896.
- Pikuleva IA. 2006. Cholesterol-metabolizing cytochromes P450. *Drug metabolism and disposition: the biological fate of chemicals* 34:513-520.
- Plant K, Pelkey KA, Bortolotto ZA, Morita D, Terashima A, McBain CJ, Collingridge GL, Isaac JT. 2006. Transient incorporation of native GluR2-lacking AMPA receptors during hippocampal long-term potentiation. *Nature neuroscience* 9(5):602-604.
- Ponce J, de la Ossa NP, Hurtado O, Millan M, Arenillas JF, Davalos A, Gasull T. 2008. Simvastatin reduces the association of NMDA receptors to lipid rafts: a cholesterol-mediated effect in neuroprotection. *Stroke; a journal of cerebral circulation* 39(4):1269-1275.
- Pucadyil TJ, Chattopadhyay A. 2006. Role of cholesterol in the function and organization of G-protein coupled receptors. *Progress in lipid research* 45(4):295-333.
- Quan G, Xie C, Dietschy JM, Turley SD. 2003. Ontogenesis and regulation of cholesterol metabolism in the central nervous system of the mouse. *Brain research* 146:87-98.
- Quinlan EM, Philpot BD, Haganir RL, Bear MF. 1999. Rapid, experience-dependent expression of synaptic NMDA receptors in visual cortex in vivo. *Nature neuroscience* 2(4):352-357.

- Ramirez DM, Andersson S, Russell DW. 2008. Neuronal expression and subcellular localization of cholesterol 24-hydroxylase in the mouse brain. *The Journal of comparative neurology* 507(5):1676-1693.
- Raymond CR. 2007. LTP forms 1, 2 and 3: different mechanisms for the 'long' in long-term potentiation. *Trends in neurosciences* 30:167-175.
- Raymond CR, Redman SJ. 2002. Different calcium sources are narrowly tuned to the induction of different forms of LTP. *Journal of neurophysiology* 88(1):249-255.
- Raymond CR, Redman SJ. 2006. Spatial segregation of neuronal calcium signals encodes different forms of LTP in rat hippocampus. *The Journal of physiology* 570(Pt 1):97-111.
- Repa JJ, Turley SD, Lobaccaro J-MA, Medina J, Li L, Lustig K, Shan B, Heyman RA, Dietschy JM, Mangelsdorf DJ. 2000. Regulation of absorption and ABC1-mediated efflux of cholesterol by the RXR heterodimers. *Science* 289:1524-1529.
- Riederer BM, Zagon IS, Goodman SR. 1986. Brain spectrin (240/235) and brain spectrin (240/235E): two distinct spectrin subtypes with different locations within mammalian neural cells. *J Cell Biol* 102:2088-2097.
- Ritter LM, Vazquez DM, Meador-Woodruff JH. 2002. Ontogeny of ionotropic glutamate receptor subunit expression in the rat hippocampus. *Brain research* 139(2):227-236.
- Rosahl TW, Geppert M, Spillane D, Herz J, Hammer RE, Malenka RC, Sudhof TC. 1993. Short-term synaptic plasticity is altered in mice lacking synapsin I. *Cell* 75:661-670.
- Rousselot P, Heintz N, Nottebohm F. 1997. Expression of brain lipid binding protein in the brain of the adult canary and its implications for adult neurogenesis. *J Comp Neurol* 385:415-426.
- Rudy JW. 2008. *The Neurobiology of Learning and Memory*. Sunderland, MA: Sinauer Associates, Inc.
- Sakimura K, Kutsuwada T, Ito I, Manabe T, Takayama C, Kushiya E, Yagi T, Aizawa S, Inoue Y, Sugiyama H, et al. 1995. Reduced hippocampal LTP

and spatial learning in mice lacking NMDA receptor epsilon 1 subunit. *Nature* 373(6510):151-155.

- Sannerud R, Marie M, Nizak C, Dale HA, Pernet-Gallay K, Perez F, Goud B, Saraste J. 2006. Rab1 defines a novel pathway connecting the pre-Golgi intermediate compartment to the cell periphery. *Mol Biol Cell* 17:1514-1526.
- Sans N, Petralia RS, Wang YX, Blahos J, 2nd, Hell JW, Wenthold RJ. 2000. A developmental change in NMDA receptor-associated proteins at hippocampal synapses. *J Neurosci* 20(3):1260-1271.
- Schimanski LA, Nguyen PV. 2004. Multidisciplinary approaches for investigating the mechanisms of hippocampus-dependent memory: a focus on inbred mouse strains. *Neuroscience and biobehavioral reviews* 28(5):463-483.
- Sever N, Song B-L, Yabe D, Goldstein JL, Brown MS, DeBose-Boyd RA. 2003. Insig-dependent ubiquitination and degradation of mammalian 3-hydroxy-3-methylglutaryl-CoA reductase stimulated by sterols and geranylgeraniol. *J Biol Chem* 278:52,479-452, 490.
- Shen AL, O'Leary KA, Kasper CB. 2002. Association of multiple developmental defects and embryonic lethality with loss of microsomal NADPH-cytochrome P450 oxidoreductase. *The Journal of biological chemistry* 277(8):6536-6541.
- Sheng M, Cummings J, Roldan LA, Jan YN, Jan LY. 1994. Changing subunit composition of heteromeric NMDA receptors during development of rat cortex. *Nature* 368(6467):144-147.
- Shukla K, Kim J, Blundell J, Powell CM. 2007. Learning-induced glutamate receptor phosphorylation resembles that induced by long term potentiation. *The Journal of biological chemistry* 282(25):18100-18107.
- Sinensky M. 2000. Functional aspects of polyisoprenoid protein substituents: roles in protein-protein interaction and trafficking. *Biochim Biophys Acta* 1529:203-209.
- Smith LL, Ray DR, Moody JA, Wells JD, Van Lier JE. 1972. 24-hydroxycholesterol levels in human brain. *Journal of neurochemistry* 19(3):899-904.

- Sottile V, Li M, Scotting PJ. 2006. Stem cell marker expression in the Bergmann glia population of the adult mouse brain. *Brain research* 1099(1):8-17.
- Spacek J, Harris KM. 1997. Three-dimensional organization of smooth endoplasmic reticulum in hippocampal CA1 dendrites and dendritic spines of the immature and mature rat. *J Neurosci* 17:190-203.
- Sprengel R, Suchanek B, Amico C, Brusa R, Burnashev N, Rozov A, Hvalby O, Jensen V, Paulsen O, Andersen P, Kim JJ, Thompson RF, Sun W, Webster LC, Grant SG, Eilers J, Konnerth A, Li J, McNamara JO, Seeburg PH. 1998. Importance of the intracellular domain of NR2 subunits for NMDA receptor function in vivo. *Cell* 92(2):279-289.
- Stenius K, Janz R, Sudhof TC, Jahn R. 1995. Structure of synaptogyrin (p29) defines novel synaptic vesicle protein. *J Cell Biol* 131:1801-1809.
- Stephenson FA. 2001. Subunit characterization of NMDA receptors. *Current drug targets* 2(3):233-239.
- Sternberger LA, Sternberger NH. 1983. Monoclonal antibodies distinguish phosphorylated and nonphosphorylated forms of neurofilaments *in situ*. *Proc Natl Acad Sci USA* 80:6126-6130.
- Sweatt JD. 2003. *Mechanisms of Memory*. Amsterdam: Elsevier.
- Tabuchi S, Kume K, Aihara M, Ishii S, Mishina M, Shimizu T. 1997. Lipid mediators modulate NMDA receptor currents in a *Xenopus* oocyte expression system. *Neuroscience letters* 237(1):13-16.
- Takasu MA, Dalva MB, Zigmond RE, Greenberg ME. 2002. Modulation of NMDA receptor-dependent calcium influx and gene expression through EphB receptors. *Science (New York, NY)* 295(5554):491-495.
- Tang TS, Slow E, Lupu V, Stavrovskaya IG, Sugimori M, Llinas R, Kristal BS, Hayden MR, Bezprozvanny I. 2005. Disturbed Ca²⁺ signaling and apoptosis of medium spiny neurons in Huntington's disease. *Proceedings of the National Academy of Sciences of the United States of America* 102(7):2602-2607.

- Tang YP, Shimizu E, Dube GR, Rampon C, Kerchner GA, Zhuo M, Liu G, Tsien JZ. 1999. Genetic enhancement of learning and memory in mice. *Nature* 401(6748):63-69.
- Terasaki M, Slater NT, Fein A, Schmidek A, Reese TS. 1994. Continuous network of endoplasmic reticulum in cerebellar Purkinje neurons. *Proc Natl Acad Sci USA* 91:7510-7514.
- Tontonoz P, Mangelsdorf DJ. 2003. Liver X receptor signaling pathways in cardiovascular disease. *Mol Endocrinol* 17:985-993.
- Topol EJ. 2004. Intensive statin therapy - a sea change in cardiovascular prevention. *N Engl J Med* 350:1562-1564.
- Tovar KR, Westbrook GL. 1999. The incorporation of NMDA receptors with a distinct subunit composition at nascent hippocampal synapses in vitro. *J Neurosci* 19(10):4180-4188.
- Tovar KR, Westbrook GL. 2002. Mobile NMDA receptors at hippocampal synapses. *Neuron* 34(2):255-264.
- Wagstaff LR, Mitton MW, Arvik BM, Doraiswamy PM. 2003. Statin-associated memory loss: analysis of 60 case reports and review of the literature. *Pharmacotherapy* 23:871-880.
- Wasser CR, Ertunc M, Liu X, Kavalali ET. 2007. Cholesterol-dependent balance between evoked and spontaneous synaptic vesicle recycling. *The Journal of physiology* 579(Pt 2):413-429.
- Weitlauf C, Honse Y, Auberson YP, Mishina M, Lovinger DM, Winder DG. 2005. Activation of NR2A-containing NMDA receptors is not obligatory for NMDA receptor-dependent long-term potentiation. *J Neurosci* 25(37):8386-8390.
- Whitlock JR, Heynen AJ, Shuler MG, Bear MF. 2006. Learning induces long-term potentiation in the hippocampus. *Science (New York, NY)* 313:1093-1097.
- Williams JM, Guevremont D, Mason-Parker SE, Luxmanan C, Tate WP, Abraham WC. 2007. Differential trafficking of AMPA and NMDA

- receptors during long-term potentiation in awake adult animals. *J Neurosci* 27(51):14171-14178.
- Williams K. 1993. Ifenprodil discriminates subtypes of the N-methyl-D-aspartate receptor: selectivity and mechanisms at recombinant heteromeric receptors. *Molecular pharmacology* 44(4):851-859.
- Winston J. 1978. Loss of hippocampal theta rhythm results in spatial memory deficit in the rat. *Science (New York, NY)* 201:160-163.
- Xie C, Lund EG, Turley SD, Russell DW, Dietschy JM. 2003. Quantitation of two pathways for cholesterol excretion from the brain in normal mice and mice with neurodegeneration. *Journal of lipid research* 44(9):1780-1789.
- Yashiro K, Philpot BD. 2008. Regulation of NMDA receptor subunit expression and its implications for LTD, LTP, and metaplasticity. *Neuropharmacology* 55(7):1081-1094.
- Zamanillo D, Sprengel R, Hvalby O, Jensen V, Burnashev N, Rozov A, Kaiser KMM, Koster HJ, Borchardt T, Worley P, Lubke J, Frotscher M, Kelly PH, Sommer B, Andersen P, Seeburg PH, Sakmann B. 1999. Importance of AMPA receptors for hippocampal synaptic plasticity but not for spatial learning. *Science* 284:1805-1811.
- Zhang J, Akwa Y, el-Etr M, Baulieu EE, Sjoval J. 1997. Metabolism of 27-, 25- and 24-hydroxycholesterol in rat glial cells and neurons. *The Biochemical journal* 322 (Pt 1):175-184.
- Zhu H, Larade K, Jackson TA, Xie J, Ladoux A, Acker H, Berchner-Pfannschmidt U, Fandrey J, Cross AR, Lukat-Rodgers GS, Rodgers KR, Bunn HF. 2004. NCB5OR is a novel soluble NAD(P)H reductase localized in the endoplasmic reticulum. *J Biol Chem* 279:30316-30325.
- Zhu JJ, Qin Y, Zhao M, Aeist LV, Malinow R. 2002. Ras and rap control AMPA receptor trafficking during synaptic plasticity. *Cell* 110:443-455.